Role of NF-κB in autophagy-controlled inflammatory responses and in intestinal epithelial cell fate decisions

DISSERTATION

zur Erlangung des akademischen Grades

Doctor of Philosophy
(Ph.D.)
im Fach Biologie
eingereicht an der

Lebenswissenschaftlichen Fakultät
der Humboldt-Universität zu Berlin
von
Master of Science, Cristina Brischetto

Präsident (komm.) der Humboldt-Universität zu Berlin
Prof. Dr. Peter A. Frensch

Dekan der Lebenswissenschaftlichen Fakultät
Prof. Dr. Christian Ulrichs

Gutachter/innen: 1. Prof. Dr. Claus Scheidereit

2. Prof. Dr. Thomas Sommer

3. Prof. Dr. Michael Naumann

Tag der mündlichen Prüfung: 01.07.2022

TABLE OF CONTENTS

ZUSAMMENFASSUNG

Die zelluläre Homöostase wird durch eine strenge Regulierung sowohl des NF-κB-Signalwegs als auch des Autophagie-Prozesses gewährleistet. Das Zusammenspiel von NF-κB-Signalen und Autophagie soll Entzündungen in verschiedenen zellulären Kontexten und als Reaktion auf unterschiedliche Stimuli regulieren. Die Beeinträchtigung dieses Zusammenspiels bestimmt das Zellschicksal und wird häufig mit verschiedenen Entzündungskrankheiten und der Tumorentstehung in Verbindung gebracht. Der molekulare Mechanismus, durch den diese beiden Signalwege bei der Regulierung der Entzündungsreaktion zusammenwirken, ist jedoch nach wie vor ungeklärt. Mithilfe biochemischer Analysen und bildgebender Verfahren haben wir zum ersten Mal die Interaktion zwischen dem endogenen Autophagie-Marker LC3 und der p65 Untereinheit von NF-κB als Reaktion auf verschiedene Stressbedingungen untersucht. Wir konnten zeigen, dass die Akkumulation von LC3 im Zellkern nach der NF-κB-Aktivierung stark mit p65 kolokalisiert ist, was darauf hindeutet, dass p65 ein Ziel für den Abbau der nukleären Autophagie bei stressinduzierten Entzündungen sein könnte. Mechanistisch gesehen haben wir gezeigt, dass die Interaktion zwischen LC3 und p65 durch die Ubiquitinierung desselben p65-Proteins gefördert wird, das von dem Cargo-Rezeptor p62 erkannt wird. Zusammengenommen zeigen diese Daten eine neue Rolle von p62 beim Transport von nuklear ubiquitiniertem p65 in einer zeitabhängigen Weise zum Abbau in Autophagosomen. Dies ist als zelluläre Reaktion auf Stress zur Kontrolle der entzündungsbedingten NF-κB-Hyperaktivierung zu sehen. Dementsprechend stabilisiert die Hemmung der Autophagie durch die Deletion des wichtigen Autophagie-Gens ATG16L1 selektiv das nukleäre p65, was wiederum die NF-κB-getriebene Expression mehrerer pro-inflammatorischer Zytokine verstärkt. Unsere Ergebnisse zeigen einen neuen molekularen Mechanismus, der die NF-κB-Entzündungsreaktion durch die Sequestrierung der NF-κB/p65-Untereinheit durch Autophagie-Proteine moduliert. Diese Erkenntnisse sind von großer Bedeutung für die Entwicklung neuer therapeutischer Strategien gegen Krankheiten, die mit einer gestörten Autophagie und konstitutiver NF-κB-Aktivität einhergehen.

Der zweite Teil der Arbeit beschreibt eine neue Rolle von NF-κB in intestinalen zellulären Differenzierungsprozessen. Der Dünndarm (SI) von Säugetieren besteht aus einem sich selbst erneuernden einschichtigen Epithel, das in Krypten-Villus-Strukturen organisiert ist. Intestinale Stammzellen innerhalb der Darmkrypta sorgen für die ständige Regeneration des Darmepithels. Mehrere Signalwege wie WNT, Notch und EGF sind für die Erhaltung und Differenzierung von Darmstammzellen von wesentlicher Bedeutung.

Obwohl die Rolle der NF-κB-Signalübertragung in der intestinalen Homöostase im Zusammenhang mit Entzündungen und der Tumorentstehung eingehend untersucht wurde, ist eine physiologische Funktion von NF-κB bei der Regeneration des Darmepithels noch weitgehend unbekannt. Durch die Verwendung von NF-κB-Reporterlinien haben wir eine hohe NF-κB-Aktivität in Paneth-Zellen, in +4/+5 sekretorischen Vorläuferzellen sowie in gelegentlichen Lgr5+ kolumnaren Stammzellen der Krypten der Kryptenbasis (SI) beobachtet. Daher beschlossen wir, die physiologische Rolle von NF-κB bei der Aufrechterhaltung der intestinalen Epithelhomöostase genauer zu untersuchen. Wir konnten zeigen, dass bei Mäusen mit ubiquitärer Unterdrückung der NF-κB-Aktivität (ΔN-Mäuse) die Proliferation und das Absterben von Darmepithelzellen (IEC) unverändert bleiben, während die Zahl der Becherzellen auf Kosten der Paneth-Zellen zunimmt, die unreif und nicht vollständig differenziert erscheinen. Diese Ergebnisse wurden auch durch Daten aus der Transmissionselektronenmikroskopie (TEM) bestätigt. In ähnlicher Weise weisen SI-Organoide von ΔN-Mäusen ein verringertes Wachstum, eine Zunahme der Becherzellen und einen Verlust an Paneth-Zellen auf. Diese Daten deuten darauf hin, dass dieser Phänotyp nicht durch das Immunkompartiment vermittelt wird, sondern vielmehr dem Epithel innewohnt. Zusammenfassend lässt sich sagen, dass unsere Ergebnisse eine neuartige IEC-immanente Rolle von NF-κB bei Entscheidungen über das Zellschicksal und die Differenzierung aufzeigen, die über die Regulierung der Wnt-Signalübertragung und der Sox9-Expression stromabwärts von NF-κB erfolgt. Die hier beschriebenen Ergebnisse verbessern unser Verständnis der NF-κB-Funktionen in der Stammzellbiologie, die, wenn sie dereguliert sind, auch Auswirkungen auf die Entzündung des Darms und die Tumorentstehung haben.

SUMMARY

Cellular homeostasis is ensured by tight regulation of both the NF-κB pathway and the autophagy process. The interplay between NF-κB signaling and autophagy has been suggested to regulate inflammation in different cellular contexts and in response to different stimuli. The impairment of this crosstalk determines cell fate and is frequently associated with different inflammatory diseases and tumorigenesis. However, the molecular mechanism by which these two pathways interact to regulate the inflammatory response remains elusive. By using biochemical analysis and imaging techniques, we characterized for the first time the interaction of endogenous autophagic marker LC3 and NF-κB/p65 subunit in response to different stress conditions. We demonstrated that accumulation of LC3 within the nucleus strongly co-localized with p65 following NF-κB activation, suggesting that p65 may be a target for nuclear autophagy degradation upon stress-induced inflammation. Mechanistically, we showed that LC3-p65 interaction is promoted by ubiquitination of the same p65 protein, which is recognized by the cargo receptor p62. Together, these data identify a novel role for p62 in trafficking nuclear-ubiquitinated p65 to autophagosomes for degradation in a time-dependent manner in response to stress to control inflammation-driven NF-κB hyperactivation. Accordingly, inhibition of autophagy by depletion of an essential autophagy gene *ATG16L1* selectively stabilizes nuclear p65, which in turn enhanced the expression of several pro-inflammatory cytokines, bona fide targets of NF-κB. Our results revealed a novel molecular mechanism modulating the NF-κB inflammatory response through nuclear sequestration of the NF-κB/p65 subunit by autophagy proteins. These findings are of great importance for the development of novel therapeutic strategies against diseases that involve defective autophagy and constitutive NF-κB activity.

The second part of the thesis describes a new role for NF-κB in intestinal epithelial cell fate decisions. The mammalian small intestine (SI) consists of a self-renewing single-layered epithelium organised in crypt-villus structures. Intestinal stem cells within the intestinal crypt ensure the constant regeneration of the intestinal epithelium. Several signaling pathways, such as WNT, Notch and EGF are essential for intestinal stem cell maintenance and differentiation. Although the role of NF-κB signaling in intestinal homeostasis has been extensively studied in context of inflammation and of tumorigenesis, a physiological function of NF-κB in intestinal epithelial regeneration remains largely unknown. By using NF-κB reporter lines, we observed high NF-κB activity in Paneth cells, in +4/+5 secretory progenitors as well as in occasional Lgr5+ crypt base columnar stem cells (CBCs) of SI crypts. Therefore, we decided to closely

examine the physiological role of NF-κB in sustaining intestinal epithelial homeostasis. We demonstrated that while intestinal epithelial cell (IEC) proliferation and death are unaltered in mice with ubiquitous suppression of NF-κB activity (*ΔN* mice), goblet cell numbers increase at the expense of Paneth cells, which appeared immature and not fully differentiated. These results were further supported by transmission electron microscopy (TEM) data. Similarly, SI organoids derived from *ΔN* mice have reduced growth, an increase in goblet cells, and a loss of Paneth cells. These data indicated that this phenotype is not mediated by the immune compartment but rather is intrinsic to the epithelium. In summary, our results revealed a novel IEC-intrinsic role of NF-κB in cell fate decisions and differentiation which occur via regulation of Wnt signaling and Sox9 expression downstream of NF-κB. The findings described here improve our understanding of NF-κB functions in stem cell biology which, when deregulated, also have an impact in intestinal inflammation and tumorigenesis.

1. INTRODUCTION

1.1 The importance of being NF-κB

Discovered for the first time in 1986 in B lymphocytes as an immunoglobulin κ-chain enhancer-binding protein, the nuclear factor-κB (NF-κB) represents one of the most extensively studied proteins involved in the regulation of multiple physiological functions (1,2). During the last decades, transcription factor NF-κB was not only found to play a central role in modulating the immune and inflammatory response, but also in contributing to a wide range of essential biological processes like proliferation, differentiation, organ development, stem cell biology, cell adhesion, cell death and many other cellular stress responses (3,4). Therefore, it is not surprising that much scientific interest is given to understanding the signaling pathways, which control NF-κB activation. Indeed, in line with its physiological importance, deregulation of NF-κB activity is implicated in many pathological conditions including chronic inflammatory diseases and cancer (5,6).

1.2 The NF-κB signaling pathway

A complex network of activating and inhibiting components strictly regulates NF-κB signaling and the transcriptional responses correlated with it. Depending on the upstream signaling factor, NF-κB activation can be divided into a canonical (classical) or non-canonical (alternative) pathway which has different kinetics and functions in inducing a specific gene expression program and allowing the cell to adapt to environmental changes (7). When inactive, NF-κB proteins are held in the cytoplasm by associating with inhibitory IκB proteins (IκBα, IκBβ, and IκBε). In order to translocate into the nucleus and exert their transcriptional functions, NF-κB proteins need to be released from IκB proteins in a stimulus-dependent manner. This is triggered by the upstream IκB kinase (IKK) complex that phosphorylates IκB proteins, triggering their ubiquitination and proteasomal degradation (8).

1.2.1 The NF-κB/Rel Subunits

The NF-κB family of proteins consists of five inducible transcription factors: RelA (also called p65), RelB, and c-Rel, as well as p50 and p52 that are proteolytic products of their

respective precursors p105 and p100 (Fig.1-1). NF-κB proteins only function as either homo- or heterodimers that are able to recognize κB-specific DNA binding sites (5′ GGGPuNNPyPyCC-3′) in the regulatory promoter regions of their target genes. Their ability to form dimers and make contact with DNA is given by the conserved N-terminal Rel homology domain (RHD; Fig. 1-1). The amino-terminal domain (NTD) of the RHD mediates specific DNA binding to the NF-κB consensus sequence, while the carboxy-terminal part of the RHD includes a dimerization domain (DiD) and a nuclear localization signal (NLS) and is responsible for interaction with IκBs. Although only p65, RelB and c-Rel have a C-terminal transactivation domain (TAD) for initiation of transcription, p52 and p50 regulate transcription through heterodimerization with TAD-containing proteins. Moreover, p50 and p52 homodimers have been found to compete with TAD-containing dimers for binding to κB sites, thereby inhibiting transcription (9). The p105 and p100 precursors possess additional C-terminal ankyrin repeats that are characteristic for the IκB protein family. The ankyrin repeats inhibit nuclear localization and thus transcriptional activity of the NF-κB proteins which are associated with them (10,11).

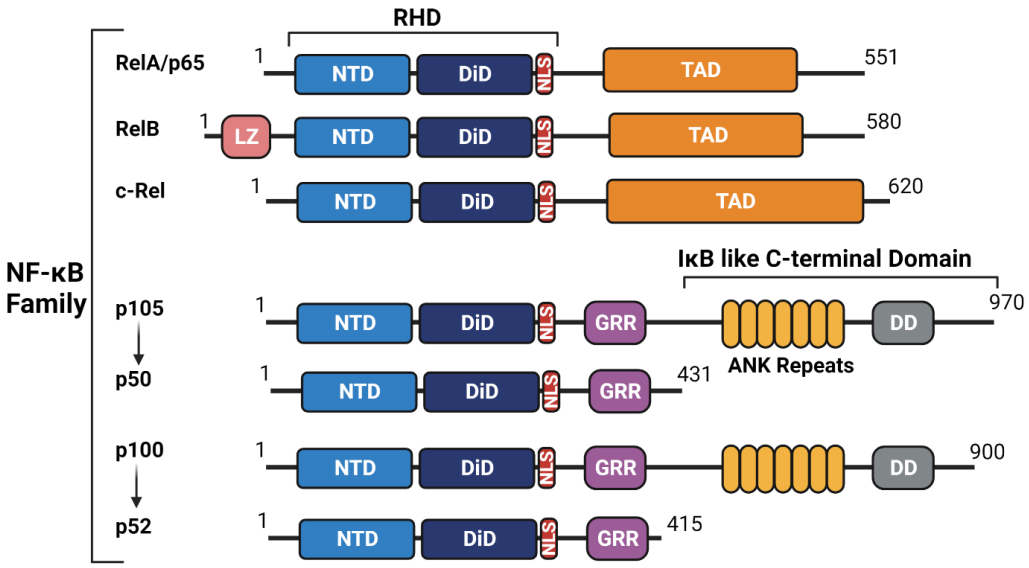

Figure 1-1: Members of the NF-κB family. All five proteins of the NF-κB family share a conserved Rel Homology Domain (RHD) that is essential for dimer formation, DNA binding and interaction with IκB proteins. The subunits p65, RelB and c-Rel have a transactivation domain (TAD), which mediates target gene transcription. A leucine zipper (LZ) domain is present in the N-terminus of RelB and is required for its transcriptional capacity. The subunits p105 and p100 are inactive precursors and require proteasomal processing for generation of the active subunits p50 and p52. Similar to IκBα, β and ε, the C-terminus of p100 and p105 contains ankyrin (ANK) repeats, which mediate their inhibitory functions. In addition, the

inactive precursors present a death domain (DD) that exerts its effects via self-association and/or interaction with death domain of other proteins. Their glycine-rich region (GRR) is essential for terminating proteasomal proteolysis to produce p50 and p52.

1.2.2 The Canonical NF-κB Pathway

A variety of stimuli, including growth factors, inflammatory cytokines, radiation, stress signals and certain pathogens can activate the rapid canonical NF-κB pathway (4,11). Upon ligand recognition, cytokine receptors such as the TNF receptor (TNFR) and IL-1 receptor (IL-1R), or pattern recognition receptors (PRRs) such as Toll-like receptor 4 (TLR4), lead to signaling cascades that culminate in the activation of the IKK complex that consists of two catalytic subunits, IKKβ and IKKα, and the regulatory protein NEMO (also known as IKKγ). Activated IKKβ induces the phosphorylation of IκB proteins, such as IκBα, on critical N-Terminal serine residues. Consequently, IκBs are ubiquitinated by the E3 ubiquitin ligase SCFβTrCP and degraded by the 26S proteasome. Only then heterodimeric NF-κB transcription factors, such as p50:p65 or p50:c-Rel, are released from IκB inhibition and enter the nucleus to activate transcription of NF-κB target genes (see Fig. 1-2; (12,13)). The signaling events upstream of the IKK complex involve signaling-specific adaptor molecules, ubiquitin ligases, and other protein kinases (14), depending on the initial stimulus. The presence of sufficient IκBs, as well as the nature of post-translational modifications (PTMs) targeting the NF-κB subunits both influence the kinetics of NF-κB dimer binding to and release from the DNA (15).

1.2.3 Activation of canonical NF-κB by proinflammatory cytokines and microbial components.

Proinflammatory cytokines and microbial components mediate activation of canonical NF-κB by transmembrane receptors. Binding of TNFα to its receptor TNFR1, drives the recruitment of TRADD at the cytoplasmic domain of the receptor (death domain; DD) and enables assembly of the E3 ubiquitin ligases cIAP1/2, as well as TRAF2 with the protein kinase RIP1 (16,17). The cIAPs mediate the ubiquitination of RIP1, TRAFs and the cIAPs themselves. They are also responsible for the recruitment of the linear ubiquitin chain assembly (LUBAC) complex, which is required for efficient activation of the IKK complex (see Fig. 1-2; (18,19)). Furthermore, the K63-linked polyubiquitination of RIP1 and TRAF2 cooperates in the recruitment of the transforming growth factor β-activating

kinase 1 (TAK1)-TAK1-binding protein (TAB) 1/2/3 complex and the IKK kinase complex, which results in IKK activation (20,21) (Fig. 1-2).

Another important class of receptors able to induce canonical NF-κB signaling is the family of pattern recognition receptors (PRRs), which have an essential role in recognizing specific components of microorganisms and in triggering efficient immune cell responses (22). TLRs (Toll-like receptors) are among the most well-characterized PRRs expressed on the plasma membrane of innate immune cells, such as macrophages, monocytes, neutrophils, and DCs (dendritic cells) (23,24). Upon binding of bacterial LPS to TLR4, TIRAP (Toll/interleukin-1 (IL-1) receptor adaptor protein) and TRAM (TRIF-related adaptor molecule, also known as TICAM2) are recruited, which mediate the MyD88-dependent NF-κB activation pathway through the recruitment of IRAK1 and IRAK4 (IL-1 receptor-associated kinase 1 and 4), TAK1 (TGF-β-activated kinase 1) and TRAF6. TRAF6 acts as an E3 ubiquitin ligase to mediate autoubiquitination, which further forms a complex with TAB2 (TAK1 binding protein 2), TAB3 and TAK1, leading to auto-phosphorylation and activation of TAK1. These events result in activation of the IKK complex concomitant with downstream canonical NF-κB activation (Fig. 1-2; (25,26)).

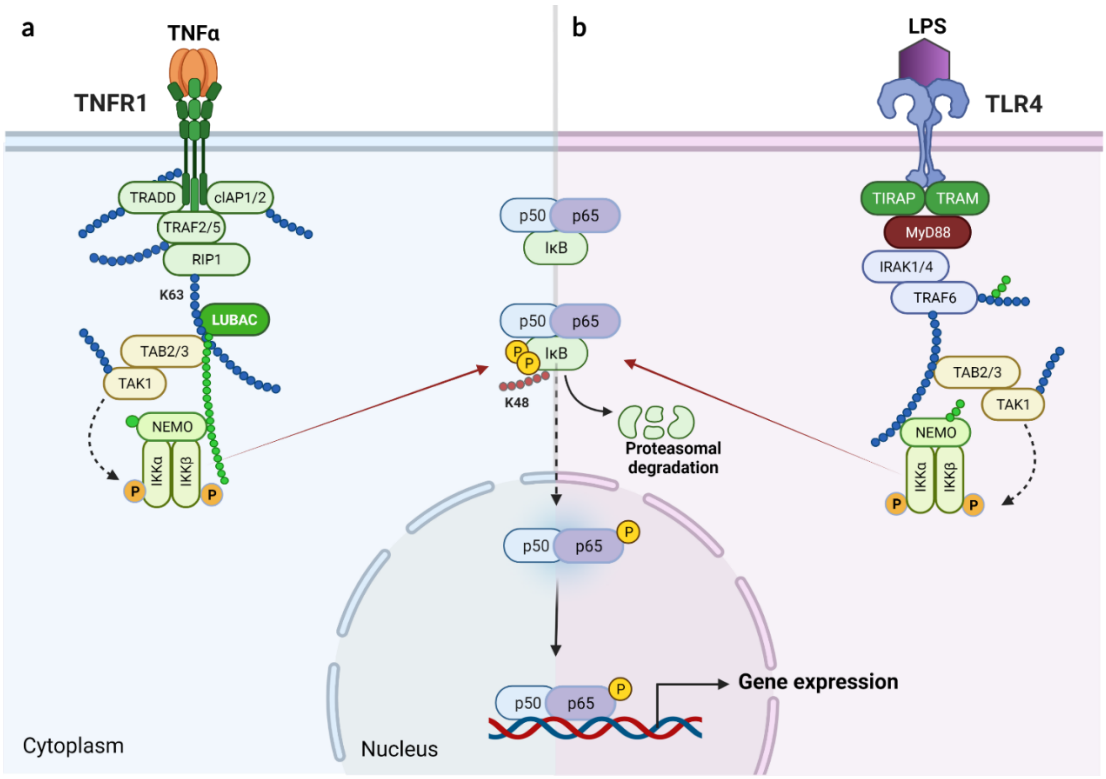

Figure 1-2: Activation and regulation of the canonical NF-κB signalling pathway. (a) TNFα ligand binding to the TNFR receptor leads to the recruitment of TRADD and interaction with the E3 ubiquitin ligases cIAP1/2 and TRAF2 with the protein kinase RIP1. This enables recruitment of the LUBAC complex, which subsequently mediates ubiquitination of several signaling proteins. Subsequently, RIP1 is K63-ubiquitinated and recruits NEMO, which results in the formation of the TAK1-IKK complex. TAK1 phosphorylates and activates the IKK complex. The IKK complex then phosphorylates the ubiquitous and canonical inhibitor IκBα, which leads to its ubiquitination (K48-ubiquitination; red) and proteasomal degradation. This allows the canonical dimers p65:p50 to translocate to the nucleus, where they bind to κB sites in the DNA and induce target gene expression. **(b)** TLR4 mediates signal transduction through MyD88 that is recruited by TIRAP and TRAM. MyD88 then induces the recruitment of IRAK1 and IRAK4, which further recruit TRAF6 to activate the TAK complex and subsequently the IKK complex as described in main text. Ubiquitin chains are represented in green and blue.

1.2.4 DNA damage-induced NF-κB activation

DNA double-strand breaks (DSB) are one of the most lethal types of genomic lesion. Environmental exposure to ultraviolet (UV) or ionizing radiation (IR), as well as endogenous agents like reactive oxygen species generated by cell metabolism can induce DSB (27). Recruitment of sensor proteins to the genomic lesion activates a complex network of cellular responses known as DNA damage response (DDR) that can lead to apoptosis or permanent cell cycle arrest (senescence) in order to maintain genomic integrity (28,29). Deregulated DDR increases the chance of genetic mutations that are often associated with cancer development and progression. Among others, activation of canonical NF-κB signaling was shown to also play a critical role in modulating the cancer cell response to DNA damage following radiation or chemotherapy, as well as in cancer progression and metastasis (30,31).

In contrast to the receptor-ligand initiated NF-κB signaling pathways, DNA damage-induced NF-κB activation is activated in the nucleus where the DNA damage sensor proteins ATM and Poly (ADP-Ribose) Polymerase 1 (PARP1) play essential roles (Fig. 1-3; (32)). In response to DNA damage, PARP1 is activated at the DNA lesions and catalyzes its own poly-ADP-ribosylation (PAR) (33). PARylated PARP1 induces a transient nuclear signalosome complex with IKKγ, ATM, and PIASy (protein inhibitor of activated STATγ) (34). Upon DNA damage, a small fraction of NEMO (IKKγ) dissociates from the IKK complex (IKKα/β) and translocates into the nucleus to interact with the SUMO (small ubiquitin modifier) E3 ligase PIASy through the PARP1 signalosome (34). PIASy sequentially SUMOylates IKKγ enhancing its association with ATM. This interaction leads ATM-dependent phosphorylation and subsequent cIAP1-dependent monoubiquitination of IKKγ (35,36). IKKγ and ATM are then exported from the nucleus

in the cytoplasm in a Ca2+ and Ran-GTP-dependent way, triggering K63-linked autoubiquitination of TRAF6 and linear ubiquitin chains on IKKγ by the LUBAC protein complex (35). Similar to the canonical NF-κB pathway (Fig.1-2), the K63-linked polyubiquitin chains attached to TRAF6 and the linear ubiquitin chains on IKKγ lead to TAK1/TAB1/TAB2 complex formation. Subsequent TAK1-dependent DNA damage-induced IKK complex activation leads to NF-κB gene expression (Fig. 1-3; (35)).

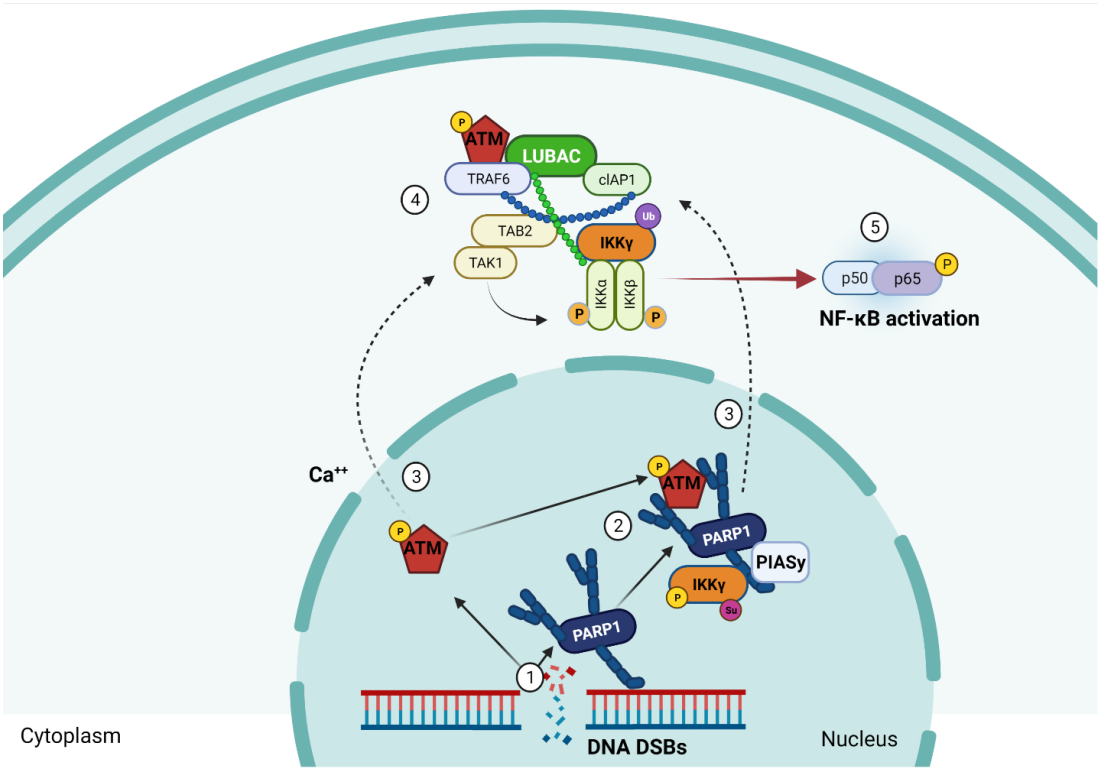

Figure 1-3: Mechanistic insights into the DNA damage-induced NF-κB signaling pathway. (1) PARP1 and ATM are activated by DSBs. PARP1 catalyzes its own covalent attachment of poly-ADP-ribose (PAR) chains. **(2)** PARylated PARP1 dissociates from the DNA and forms a transient nuclear signalosome complex with PIASy, IKKγ, and activated ATM. IKKγ is then phosphorylated by ATM and SUMOylated by PIASy in the PARP1 signalosome complex. **(3)** IKKγ and ATM are exported from the nucleus in a Ran-GTP and Ca2+ dependent manner. **(4)** In the cytoplasm, ATM triggers K63-linked autoubiquitination of TRAF6. Linear ubiquitin chains are synthesized by the LUBAC protein complex. Together with the K63-linked polyubiquitin chains of TRAF6, they create a docking platform for Tak1/Tab1/Tab2 and the IKK complex. Formation of high-molecular-weight protein complexes leads to TAK1 autoactivation and subsequent TAK-1 dependent activation of the IKK complex. **(5)** DNA damage-induced activation of the IKK complex results in downstream signaling events, such as IKK-dependent phosphorylation and degradation of IκBα, which are identical to those in canonical NF-κB signaling.

1.3 Post-translational modifications regulating the activity and function of RelA/p65

Functions of nuclear NF-κB subunits are highly regulated by multiple post-translational modifications (PTMs) that can affect DNA binding, protein interactions as well as the termination of the NF-κB response. The analysis of modifications of the NF-κB subunits is extremely limited and reflects the complexity of its nuclear regulation. Furthermore, many modifications are likely to differ between cell types and the nature of the NF-κB-inducing stimulus (37,38).

1.3.1 Phosphorylation of RelA/p65

Multiple RelA/p65 phosphorylation sites, for example, have a modulatory role in its transcriptional activity. In response to many inflammatory stimuli, phosphorylation of Ser-529 and Ser-536 can stimulate the nuclear translocation and transactivation of p65 (39). Among others, CK2 (Casein kinase 2) and the IKK complex have been described as inducers of NF-κB DNA binding through phosphorylation of p65 at these two sites respectively (40,41). Upon TNF, IL-1β and T-cell stimulation, Ser-468 is also phosphorylated and has been described as a target for GSK3β, IKKε and IKKβ to both stimulate and inhibit p65 transactivation (42–44). Within the RHD of p65, either TNF or LPS stimulation leads to Ser-276 phosphorylation by protein kinase A (PKAc) in the cytoplasm or by MSK1 kinase in the nucleus, which drives p65 transcriptional activation. However, Ser-276 in p65 is also important for determining whether p65 can form homodimers or heterodimers (39,45).

1.3.2 Acetylation of RelA/p65

Acetylation represents another important post-translation modification with different effects on p65 activity, which occurs at lysines 122, 123, 218, 221 and 310. The transcriptional co-activators p300 and CBP can acetylate Lys-218, -221 and -310 stimulating transcriptional activity and enhancing DNA binding of p65. By contrast, p65 acetylation at Lys-122 and Lys-123 has an inhibitory effect (46). It is interesting to note that Ser-276 and Ser-536 phosphorylation have been shown to increase p300 binding and therefore enhance p65 acetylation at Lys-310, which implies a functional relationship between phosphorylation and acetylation (47).

1.3.3 Ubiquitination of RelA/p65

Ubiquitination of p65 can participate in the termination of the NF-κB response. Many regulators of p65 ubiquitination have been identified, including E3 ligases and deubiquitinases, as well as numerous lysine acceptor sites on p65 (48). Ubiquitination of p65 occurs predominantly in the nucleus where it appears to control DNA binding of only a specific fraction of nuclear p65, which ensures limited expression of specific NF-κB target genes (49). Multiple ubiquitin linkages have been proposed with proteasomal dependent- or independent functions. For example, while ING4 and PPARγ were reported to mediate K48 polyubiquitination and proteasome-dependent degradation of p65, TRAF7 protein was found to promote Lys-29-linked polyubiquitination of p65 for lysosome degradation (50–52). Moreover, ubiquitinated p65 at K28, K56, K62, K79, K123, K195, K310 and K315 has been reported (53). However, it is currently unknown whether p65 is ubiquitinated on multiple sites simultaneously by several E3 ligases, or modification at an individual lysine residue occurs in isolation by distinct E3 ligases in the event of different stimuli or as such in different cell types. Interestingly, a number of the ubiquitin acceptor sites identified by mass spectrometry studies were found to overlap with known acetylation sites on p65, suggesting that cross-talk between several post-translational modifications may be important for regulating p65 and controlling transcription in a gene-specific manner (Fig.1-4; (48)). Future studies not only would offer more insight into the role of PTMs in the regulation of p65 but also could result in novel NF-κB based therapeutic agents for the treatment of cancer and inflammatory diseases.

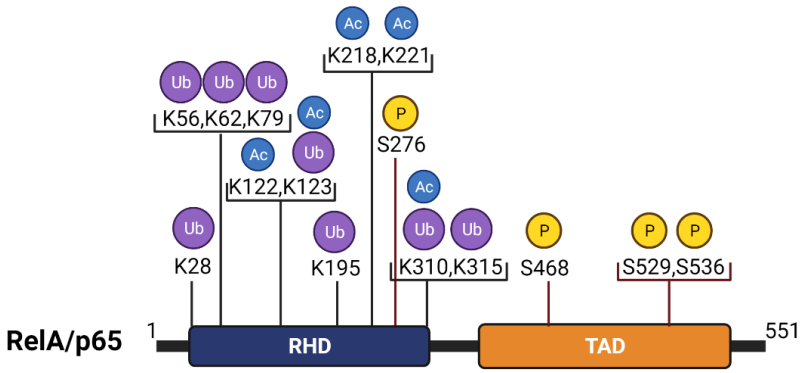

Figure 1-4: Post-translational modifications of RelA/p65. Schematic representation of PTMs of p65 that are known to regulate transcriptional activity, DNA binding and termination of NF-κB signaling. RHD: REL homology domain, TAD: transactivating domain, K: Lysine, S: Serine, P: phosphorylation, Ub: ubiquitination, Ac: acetylation.

1.4 NF-κB activation in inflammation and cancer

Chronic infections and inflammation represent approximately 25% of all cancer-causing factors (54). Activation of canonical NF-κB plays a central role in coordinating inflammatory responses, which is essential for host homeostasis. Consistent with this particular NF-κB function, numerous studies have implicated NF-κB in the development of many different inflammatory disorders and cancer (14). It was shown that NF-κB is highly activated at sites of inflammation in diverse diseases and can induce transcription of proinflammatory cytokines, chemokines, adhesion molecules, MMPs, Cox-2, and inducible nitric oxide (iNOS) (55).

The inflammatory microenvironment inside a tumor increases mutation rates mainly in a ROS- (reactive oxygen species) and RNI- (reactive nitrogen intermediates) dependent manner, promoting tumor growth (5,56). In tumor-associated macrophages (TAMs) and other innate immune cells, activation of canonical NF-κB supports tumor proliferation through expression of cytokines such as TNF-α, IL-1β, and IL-6 (57). In the tumor microenvironment canonical NF-κB also promotes angiogenesis, thereby facilitating tumor invasion (58). Moreover, activation of NF-κB together with other transcription factors induces expression of chemokines that recruit more immune cells, which increases the local inflammatory response and expression of anti-apoptotic genes. Together this promotes the survival of tumor cells and thus cancer progression (59,60).

1.4.1 The central role of NF-κB in tumor-associated macrophage (TAM) function

Solid tumors consist of both malignant and nonmalignant cells that together represent the tumor microenvironment. Among the nonmalignant cells, macrophages have emerged as important drivers of tumor growth, angiogenesis, and metastasis (61,62). Based on the physiological context and environmental signals, two main macrophage phenotypes have been described: “classically” activated or M1 macrophages and “alternatively” activated or M2 macrophages. Exposure to proinflammatory cytokines (TNF-α, IL-1β) and microbial products (LPS, IFN-γ) polarized macrophages into the pro-inflammatory M1 phenotype, which is characterized by increased production of their own pro-inflammatory cytokines, iNOS, ROS, RNI and high microbicidal/tumoricidal activity. In contrast, anti-inflammatory molecules (IL-4, IL-10), as well as apoptotic cells and immune complexes induce the immunosuppressive M2 phenotype, which produces anti-inflammatory cytokines that support angiogenesis, tissue repair, and remodeling (63). A

mixed expression of markers for both classic and alternative activation has been observed in TAMs in murine and human tumors (64).

As mentioned above, molecular analysis of TAMs revealed that activation of IKK/NF-κB signaling plays a tumor-promoting role that is linked to production of pro-inflammatory cytokines such as TNFα and IL-6 within tumors (65). However, the role of NF-κB in regulating TAM functions may be complex and act at many levels that are context- and gene-dependent. For example, although it was shown that genetic inhibition of NF-κB signaling pathway components in murine TAM reduced growth of colon and liver cancer (56,57), TAM with defective NF-κB activity were associated with tumor progression in a model of fibrosarcoma (66,67). The diversity of TAM phenotypes identified in different tumor types and stages could be some reasons for this contradiction (68). Nevertheless, blocking the tumor-promoting roles of TAM by targeting NF-κB, thereby restoring their intrinsic antitumor activity could be a promising therapeutic strategy for many types of cancer. Thus, future studies that focus on the temporal regulation of NF-κB in TAM during different stages of tumor growth and the contribution of different NF-κB members in regulating the TAM phenotype will be important for the development of new therapeutic approaches in cancer therapy in addition to existing therapies (69).

1.5 The mechanism of autophagy and its cellular function

Autophagy is an evolutionarily conserved catabolic cellular degradation pathway involved in the maintenance of cellular homeostasis upon starvation or other stress conditions. There are three different types of autophagy in most cell types: microautophagy, chaperon-mediated autophagy (CMA) and macroautophagy. The term “autophagy” usually indicates macroautophagy, which is the best-characterized form of autophagy.

The autophagic process begins with the isolation of a double membrane (phagophore assembly site; PAS) where proteins of the UNC51-like kinase (ULK) complex (ULK1 or ULK2 and ATG13, FAK family kinase interacting protein of 200 kDa (FIP200) and ATG101) assemble to initiate autophagosome formation (70). Further nucleation of the isolation membrane is induced by activating the ULK complex that targets a class III PI3K complex (Beclin1, vacuolar protein sorting 15 (VPS15), VPS34 and ATG14) to promote specific autophagosome production of a pool of phosphatidylinositol 3-phosphate effectors (71). The expanding double membrane (phagophore) phagocytizes large amounts of cytoplasmic components such as unfolded proteins, protein aggregates, and

organelles. The phagophore membrane is subsequently elongated by two specialized ubiquitin-like conjugation systems. The first (ATG7 and ATG10) produces a ATG5–ATG12 conjugate that forms a multimeric complex with ATG16L, whereas the second results in the conjugation of phosphatidylethanolamine (PE) to LC3 (the microtubule-associated protein 1 light chain 3, homologue of yeast Atg8) upon ATG4-dependent proteolytic maturation (72,73). PE-conjugated LC3 (LC3–PE) is required for the expansion of autophagic membranes, their ability to recognize autophagic cargoes and the fusion of autophagosomes with lysosomes (74–76). This elongated double membrane encloses to form a dense cytosolic, double-membraned vacuole termed autophagosome. The mature autophagosome binds to a lysosome forming an autolysosome, where the autophagosome's contents are released into the lysosomal lumen and degraded by resident hydrolases (Fig. 1-5; (77)).

The autophagic pathway is a very complex process, involving more than 34 known proteins (Atg proteins) to assemble the machinery described above. Additional kinases like mTOR and AMPK (AMP-activated protein kinase) are also able to regulate autophagy by sensing energy and nutrient stress. In nutrient-rich conditions the mammalian target of rapamycin complex 1 (mTORC1) suppresses initial autophagosome formation by catalyzing the inactivating phosphorylation of ATG13 and ULK1 (78). In contrast, in nutrient-limiting conditions mTORC1 is inactivated by AMPK, which responds to reduced ATP levels, concomitant with AMP accumulation (79). AMPK also catalyzes activating phosphorylation events of ULK1 and Beclin1 (80,81).

Autophagy can be either non-selective or selective. Whereas non-selective autophagy, cellular response to nutrient deprivation, typically involves random uptake of cytoplasm, selective autophagy is responsible for specifically removing certain cellular components (82). This implicates a multitude of types of autophagy that play an important role in different catabolic and anabolic cellular processes. Indeed, defects of the autophagy process may be responsible for many human diseases, including cancer (83,84).

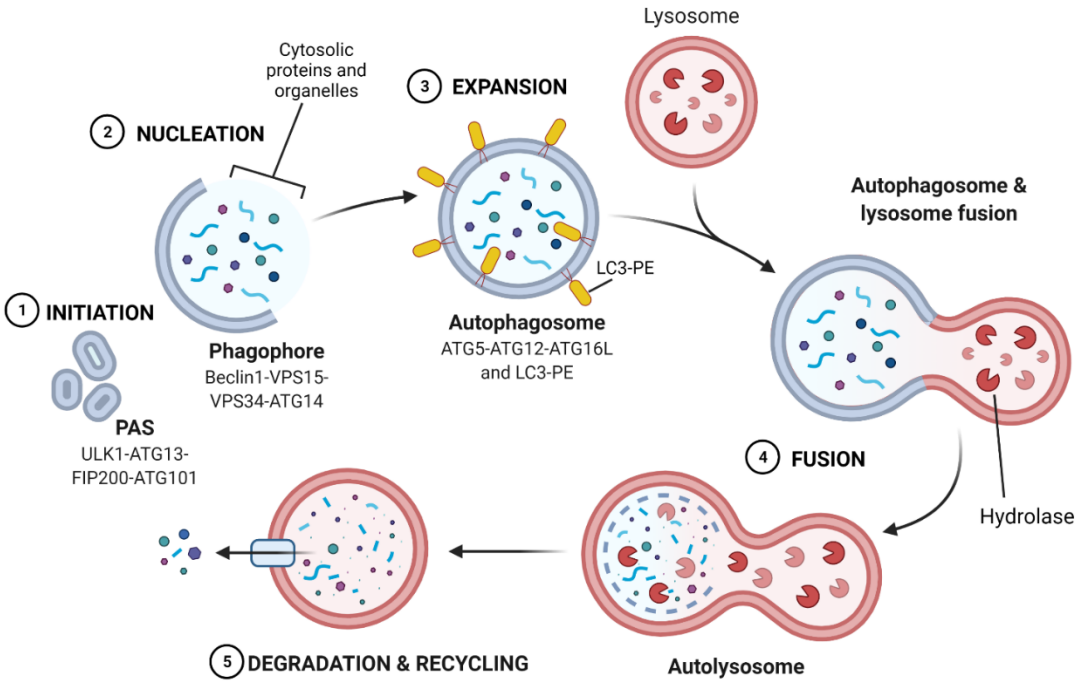

Figure 1-5: Overview of the autophagy pathway. (1) The initiation step begins with the formation of the phagophore assembly site (PAS) mediated by the ULK complex (ULK proteins, ATG13, FIP200, ATG101). **(2)** The membrane nucleation step requires the class III PI3K complex (VPS34, ATG14L, VPS15 and beclin1). **(3)** Phagophore membrane expansion and autophagosome completion involves two ubiquitin-like conjugation pathways which produce the ATG5–ATG12-ATG16L complex and the conjugation of phosphatidylethanolamine (PE) to LC3. **(4)** The resulting autophagosome fuses with endocytic and lysosomal compartments, ultimately leading to formation of the autolysosome. **(5)** The autophagic content is degraded via lysosomal hydrolases and the degraded product is recycled as source of energy or building blocks for the synthesis of macromolecules.

1.5.1 Selective autophagy and cargo receptors

Autophagy either can degrade cytoplasmic material 'in bulk' or selectively degrade some components, such as mitochondria, ER, Golgi, peroxisomes, nuclei, protein aggregates or pathogens (Fig. 1-6). Depending on the cellular stresses, selective autophagy requires sequestration of the specific cargo into autophagosomal membranes. Selectivity is mediated by autophagy cargo receptors, which bind cargos tagged with degradation signals (ubiquitin) via their ubiquitin-binding domain (UBD) and LC3 proteins on the autophosomal membrane by their LC3-interacting regions (LIR motifs) (82). For example, the autophagy cargo receptors p62 (also known as SQSTM1), NBR1 (next to BRCA1 gene 1 protein) and optineurin (OPTN) promote the autophagic clearance of protein aggregates in a process known as aggrephagy (85). In addition to protein aggregates, selective autophagy is involved in the clearance of damaged organelles. For example, autophagic degradation of defective mitochondria is mediated by ubiquitin-

mediated mitophagy. Briefly, PTEN-induced kinase 1 (PINK1) mediates the recruitment of Parkin, an E3 ubiquitin ligase, on dysfunctional mitochondria, which induces poly-ubiquitination of several outer mitochondrial membrane (OMM) proteins that are subsequently recognized by p62 for autophagic degradation (86).

Selective autophagy receptors often cooperate with each other in selecting a specific cargo: the autophagic receptor NBR1 interacts with p62 for sequestration and degradation of aggregated proteins, midbody rings and peroxisomes (87–89). On the other hand, p62 cooperates with OPTN and NDP52 to facilitate the removal of bacteria and mitochondria (90–92). Thus, autophagy is a highly selective cellular clearance pathway for maintenance of cellular and tissue homeostasis. Autophagy can also mediate the availability of carbohydrates, lipids and nucleic acids by means of three main cellular processes: glycophagy, lipophagy and RNAutophagy or DNAutophagy, respectively (93–95).

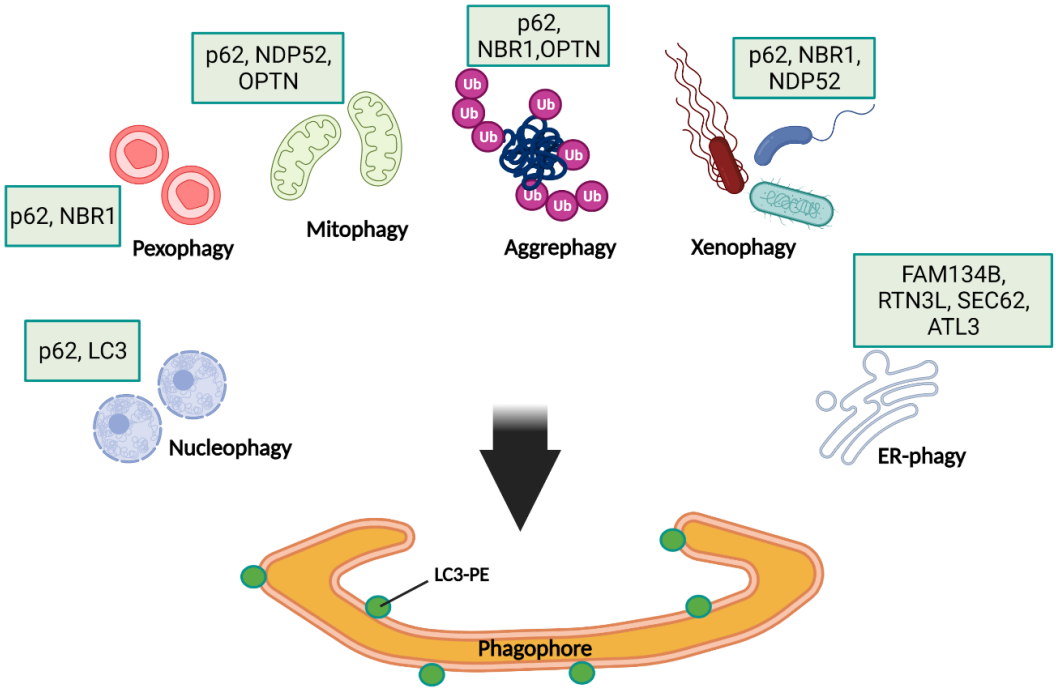

Figure 1-6: Subtypes of selective autophagy and their cargo receptors. Selective autophagy can be divided into many subtypes based on the specific cargos involved. These subtypes can target parts of the nucleus (nucleophagy), peroxisomes (pexophagy), mitochondria (mitophagy), protein aggregates (aggrephagy), pathogens (xenophagy), the endoplasmic reticulum (ER) (ER-phagy) etc. Specific autophagy cargo receptors (listed within the rectangles) are responsible for recognizing and binding of the cargo to LC3 on the autophagosome membrane for degradation. LC3-PE: phosphatidylethanolamine (PE) to LC3.

1.6 The role of autophagy in inflammation and cancer

In addition to its role in maintaining cellular homeostasis, autophagy is critical to pathological processes, such as inflammation and cancer. Several evidence supports reciprocal interconnections between autophagy and inflammation. Interestingly, many of the signaling pathways that control inflammation during tumorigenesis are also known regulators of autophagy (96). Depending on the cellular context, cytokine signaling was found to either inhibit or enhance the autophagy process (97,98). Autophagy itself can also modulate inflammatory cytokine production and secretion in the tumor microenvironment and in cells adjacent to the tumor via diverse mechanisms that result in cancer progression (99,100). Accordingly, autophagy has been reported as both a tumor suppressor and a tumor promoter, which suggests that the role of autophagy in cancer is context-dependent (101,102). In this regard, defective autophagy represents a cell-intrinsic mechanism that is able to create the damaging, inflammatory environment that predisposes to cancer (103,104).

Recent studies suggest that toxicity and tissue damage resulting from defective autophagy is partly due to the aberrant accumulation of p62, which is sufficient to generate high levels of ROS, activation of the DNA damage response, and cell death. Thus, persistent p62 accumulation in autophagy-defective tumor cells enhances tumorigenesis, while limiting p62 accumulation by efficient autophagy is an important factor that would contribute to tumor suppression (105,106).

Nevertheless, cancer cells are more autophagy-dependent than healthy cells, probably due to the increased metabolic and biosynthetic demands imposed by deregulated proliferation. For example, it was shown that cancer cells upregulate autophagy to survive under hypoxic conditions, and RAS-transformed cancer cells require autophagy for their growth, survival, tumorigenesis, invasion, and metastasis (107–109). In addition, autophagy exerts its tumor-supporting function by increasing the resistance of cancer cells not only to stressful conditions (i.e., loss of attachment, hypoxia, and nutrient deprivation) but also to therapy-induced senescence (110).

1.6.1 Autophagy and Tumor-associated macrophage

As previously described (see 1.4.1 paragraph), macrophages represent one of the most abundant immune cells in the tumor microenvironment, which derive from either tumor-

resident macrophages or monocyte-derived macrophages. The differentiated macrophages then switch to tumor-associated macrophages, which play a crucial role in tumor initiation, progression, evasion, and resistance to chemotherapy (see 1.4.1). Thus, characterization of molecular mechanisms involved in macrophage polarization within the tumor microenvironment is essential for improving our understanding of cancer biology (111).

Autophagy is an important component of innate immunity, and increasing evidence supports its role in all steps of TAM generation (112). In the tumor microenvironment, autophagy has a paradoxical function in acting as a tumor suppressor and a tumor promoter. It was shown that TLR signaling modulates macrophage function by autophagy (113). Studies using Toll-like receptor 2-deficient mice revealed that the consequential reduction of autophagy flux and macrophage infiltration increased carcinogenesis and progression of hepatocellular carcinoma (HCC), which suggests a tumor suppressor role of autophagy in macrophages (114). Moreover, autophagy plays a significant role in macrophage polarization by tumor-derived factors IL6 and CCL2 within the tumor microenvironment. Indeed, treatments with autophagy inhibitors or lysosomal protease inhibitors were shown to significantly reduce M2-type macrophage polarization (115). In addition, recent findings highlight that the TSC2-mTOR pathway, the major regulator of autophagy, is critical for the differentiation of monocytes into the M2-TAM phenotype that promotes angiogenesis (116). Increasing knowledge of the mechanisms regulating macrophage autophagy during cancer progression and the pathways involved in tumor fate decisions due to the activation of autophagy will certainly open new insights into tumor biology and potentially provide novel therapeutic targets for cancer therapy.

1.7 The interplay between NF-κB and autophagy signaling pathways

Cellular homeostasis is ensured by tight regulation of both the NF-κB pathway and the autophagy process. Increasing evidences indicate the reciprocal crosstalk between NF-κB and autophagy in a stimulus- and context-dependent manner (117,118). Stress-dependent activation of NF-κB can orchestrate a wide spectrum of transcriptional responses including autophagy. In fact, it was shown that NF-κB might trigger autophagy by directly inducing the expression of genes involved in the autophagosome machine, such as Beclin 1, ATG5, and LC3 (119,120). Interestingly, studies revealed that IKK is also able to induce autophagy, independently of NF-κB signaling (121,122). However, NF-κB is also able to inhibit autophagy by either inducing autophagy repressors, like

A20, Bcl-2 family members, phosphatase and tensin homolog/mammalian target of rapamycin (PTEN/mTOR) and nitric oxide (NO), or by suppressing autophagy inducers, such as BCL-2 interacting protein 3 (BNIP3), JNK1, p53 and ROS (123,124).

In turn, it was reported that autophagy might also influence NF-κB activity by degradation of NF-κB pathway components (125). In response to distinct stimuli, specific cargo receptors, like Kelch-like ECH-associated protein 1 (KEAP1), E3 ubiquitin ligase Ro52 and S-phase kinase-associated protein 2 (SKP2) were shown to induce IKKβ ubiquitination and autophagic degradation (126,127). In addition, recent studies suggest that inhibition of heat shock protein 90 (Hsp90) is sufficient to induce autophagic degradation of the IKK complex and NF-kappa B-inducing kinase (NIK), which leads to the inhibition of NF-κB activity (128,129). In response to TNFα, autophagy appears to be required for prolonged transcriptional activity of NF-κB by autophagic degradation of IκBα, which suggests that degradative systems other than the 26S proteasome may sustain long-term NF-κB activation (130). Further evidences suggest that the autophagy cargo receptor SQSTM1/p62 modulates NF-κB activity at the level of IKK in a mouse model of Ras-induced lung adenocarcinoma (131). These observations indicate that NF-κB and autophagy are intimately interconnected via a complex network of transcriptional and transcription-independent signals.

1.8 NF-κB in developmental biology

In addition to its role in modulating the immune and inflammatory response, NF-κB signalling is essential in other biological contexts such as developmental processes (132). RelA-, IKKβ- or IKKγ-deficient mice are embryonic lethal mainly due to strongly increased hepatocyte apoptosis in the liver, while IKKα-deficient mice die shortly after birth and is required for development of the epidermis (133–135). The first strong evidence showing *in vivo* NF-κB activity during mammalian embryonic development was performed by Schmidt-Ullrich et al. (1996) by using a transgenic reporter mouse line, which expresses the gene of the β-galactosidase enzyme under control of the NF-κB consensus binding site in the Igκ light chain enhancer or in the p105 promotor. The NF-κB activity was observed in the developing brain, thymus, blood vessels, and in the developing hair follicles (HFs) (132). However, the generation of mice with ubiquitously suppressed NF-κB activity (here referred as *ΔN* mice) made it possible to study intrinsic NF-κB functions in tissues independently of any aberrant immune reactions that would affect cell viability. *ΔN* mice are viable and are characterized by macrophage dysfunction and lack of secondary lymphoid organs. Moreover, NF-κB suppression induces severe

defects in the early steps of the development of epidermal appendices, such as hair follicles, sweat glands, and tear (136). Since then, several progresses are made in the roles of NF-κB in embryonic development and tissue regeneration (3,137,138).

1.9 The role of NF-κB signaling in the small intestine

The role of NF-κB signaling in intestinal homeostasis has been extensively studied in the context of diseases, such as cancer and inflammatory bowel disease (IBD) (139,140). Several evidence reported that IKK/NF-κB is required for mucosal innate immunity, immune resistance to the intestinal microbiome, as well as for the formation of Peyer's patches, which are part of the gut associated lymphoid tissue (GALT) in the small intestine (136,141,142). Mice lacking IKKβ or IKKγ/NEMO in intestinal epithelial cells (IECs) are susceptible to chemically induced colitis or develop spontaneous intestinal inflammation, respectively (143,144). Mice with IEC-specific deletion of RelA/p65 also displayed altered IEC proliferation and apoptosis and are susceptible to dextran sulfate sodium (DSS)-induced colitis (145). In addition, high incidence of colitis and spontaneous inflammation-associated tumor formation (CAC, colitis-associated colorectal cancer) was significantly enhanced in mice with constitutively active IKK/NF-κB in IECs (146,147). These studies highlight the importance of well-balanced and strictly controlled intestinal NF-κB activation in order to prevent inflammation and subsequent development of inflammatory bowel disease (IBD) and colon carcinoma. However, the physiological role of NF-κB in intestinal epithelial regeneration remains largely unknown.

1.10 The Small intestine: functions and crypt-villus structure

The mammalian small intestine consists of a self-renewing single-layered epithelium organised in crypt-villus structures whose main functions are the uptake of nutrients and water, and the protection against pathogens. Villi are finger-like protrusions into the intestinal lumen with high absorptive capacity by their excellent connection to the circulatory system. Each villus is covered by a simple postmitotic epithelium of differentiated specialized cell types with a short lifetime (3 - 5days) to minimize its exposure to a harmful environment. The base of each villus is surrounded by multiple epithelial invaginations, called crypts of Lieberkühn. Inside of each crypt, intestinal stem cells (ISC) continuously divide into progenitor cells (or transit amplifying cells) that proliferate and ultimately differentiate into the specialized intestinal epithelial cell types: absorptive (enterocytes and M cell) and secretory (Paneth, goblet, enteroendocrine and tuft cell) cell lineages. Absorptive enterocytes represent the most abundant cell type on

the villus for nutrient uptake and the microfold (M) cells reside in the specialized epithelium that overlies the Peyer's patches (lymphoid accumulations for mucosal immunity) (148). Goblet and enteroendocrine cells secrete mucus and a variety of hormones, respectively, whereas tuft cells are involved in immune regulation (149,150). These differentiated cells migrate along the crypt-villus axis until they reach the tip of the villus and eventually undergo apoptosis. In contrast, mature Paneth cells are the only secretory cell type that settles in the bottom of crypts and thus escapes the upward migration. Paneth cells ensure innate mucosal immunity and antibacterial defense by secreting bactericidal defensin peptides and lysozymes ((151); Fig.1-7). However, Paneth cells are also required for the maintenance of the intestinal stem cell niche (see below; (152)).

1.11 Insights into the small intestinal crypt

Cheng and Leblond described the first evidence of continuously cycling cells at the bottom of the crypt in 1974. However, the toolset of the time was not sophisticated enough to provide formal proof that the crypt base columnar (CBC) cells are stem cells. Only decades later, the advent of the genetic lineage tracing tool brought final proof of CBC cell stemness by identification of the CBC marker Lgr5 (Leucine-rich repeat-containing G-protein coupled receptor 5). *Lgr5* is a direct WNT target gene, but is also required to enhance Wnt signalling (153). LGR5+ CBC cells are able to generate multiple specialised cell lineages and show long-term self-renewal, both of which are criteria for stemness. In addition to CBCs, another stem cell population designated as "+4" has been described, which is located between the LGR5+ stem cell zone and the progenitor-zone. Several studies identified multiple genetic markers of +4 cells including Bmi1, Tert, Hopx and Lgr1, which are partially also detectable in CBC cells (154–157). Given the high resistance to radiation, +4 cells are generally considered as slow-cycling reserve stem cells that are able to replenish the pool of the continuously cycling CBC cells when needed (158). At the bottom of the crypt, every CBC cell is in direct contact with at least one Paneth cell. This organization ensures CBC cell maintenance by Paneth cells that provide WNT ligands, as well as essential epidermal growth factor (EGF) and Notch stimuli within the stem cell niche (159). Moreover, production of lysozyme, α-defensins and phospholipase A by Paneth cells is also essential for protecting CBC cells from enteric pathogens (152).

1.11.1 Signaling pathways in the small intestine

The complex dynamic observed in intestinal crypts is ensured by key signals that regulate intestinal fate determination. The WNT pathway is essential for stem cell maintenance and differentiation. The pivotal role of the WNT pathway in the intestine has been established by several experiments showing that the absence of key elements of this pathway (Tcf4 or β-catenin), as well as overexpression of the WNT inhibitor Dkk1 leads to a complete loss of intestinal stem cells (160,161). Increased WNT activity, on the other hand, results in excessive growth of the intestinal epithelium and loss of differentiation, which ultimately causes spontaneous occurrence of adenomas (162,163). Paneth cells produce WNT ligand in the form of WNT3, which binds to WNT Frizzled receptors on the surfaces of intestinal stem cells. Interestingly, when stem cells start to differentiate and leave the stem cell zone, the amount of surface-bound WNT3 is reduced which creates a gradient from the bottom of the crypt, where WNT is abundant, toward the top of the crypt, where it is gradually lost. The decreased WNT abundance in turn reduces proliferation of stem cells and enables them to differentiate into the different IEC (intestinal epithelial cell) lineages.

Besides the WNT pathway, Notch presents another highly conserved short-range signalling mechanism that plays an important role in cell fate decisions (164). Notch signaling is activated by membrane Notch ligands (DLL1 and DLL4) that bind to its receptors (such as NOTCH1) on the membrane of a nearby cell. Upon receptor activation, the subsequent expression of the basic loop helix transcription factor HES1 represses the transcription of another basic loop helix transcription factor, ATOH1. The absence of ATOH1 in the signal-receiving cell represses its own ability to express Notch ligands such as DLL1. This mechanism is known as lateral inhibition. In the intestine, Paneth cells also provide DLL4 and DLL1 ligands for stem cells to block the formation of secretory lineages and instead to differentiate into enterocytes (165). Secretory progenitor cells also express DLL1 in the transit amplifying (TA) zone, thereby regulating the ratio of secretory to absorptive progeny (166). In addition to the initial lineage decisions, studies showed that Notch can also determine multiple differentiation choices along the crypt-villus axis such as goblet cell versus enteroendocrine cell (167).

While WNT and Notch signaling are both required to maintain stem cell identity, EGF signaling controls the rate of IEC (intestinal epithelium cell) turnover. The receptor tyrosine kinase ERBB1 is highly expressed in CBC cells, whereas Paneth cells produce the ligands such as EGF and transforming growth factor-α (TGFα). Because overactive

EGF signaling is known to increase stem cell proliferation and neoplastic growth, the activity of this pathway is tightly regulated (168).

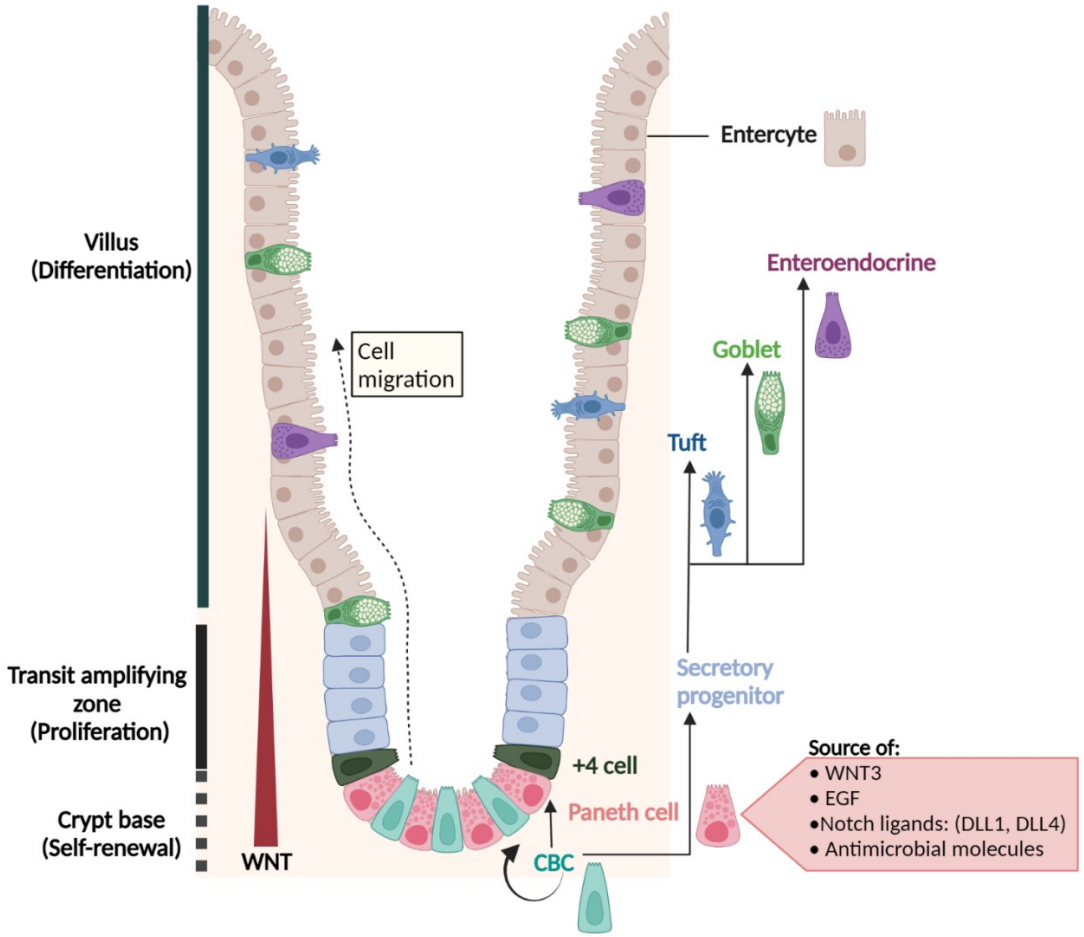

Figure 1-7: Architecture of the small-intestinal epithelium and its regulatory signals. The epithelium of the small intestine is organised in units of crypts (proliferation sites) and villi (differentiation sites). Crypt-base columnar (CBCs) cells are the stem cells intercalated between Paneth cells, the latter providing WNT3 and Notch ligands (DLL1/4) essential for stemness, and epidermal growth factor (EGF) to support their proliferation. Paneth cells also produce antimicrobial molecules (such as lysozyme) to protect the crypt base from bacterial infiltration. The high level of WNT signals is gradually lost when stem cell daughter cells migrate up from the crypt bottom towards the villus. The transit-amplifying (TA) zone connects the crypt base to the villus and consists of progenitor cells that proliferate multiple times before differentiation. +4 stem cells are situated between the CBCs and the TA-zone, and are considered a reserve stem cell mobilized upon tissue damage. In the transit amplifying zone, progenitor cells terminally differentiate into absorptive (enterocyte) or secretory lineages (Tuft, goblet, enteroendocrine and Paneth cells).

2. AIMS OF THE STUDY

Aim 1. To investigate the functional interplay between autophagy and NF-κB signaling in the regulation of inflammation.

Tight regulation of both NF-κB signaling and the autophagy process is necessary for maintenance of cellular homeostasis. Interestingly, genome-wide association studies suggested a connection between autophagy-related gene polymorphisms and many inflammatory disorders, including cancer, in which NF-κB is constitutively activated. The interplay between autophagy and NF-κB has been observed in different cellular contexts and in response to different stimuli. The impairment of this crosstalk determines cell fate and is frequently associated with tumorigenesis and tumor cell resistance to cancer therapies. Therefore, the main goal of this study was to provide a more detailed molecular dissection of the functional interplay between autophagy and NF-κB signaling, which may help to improve the effectiveness of cancer therapies. Previous proteomic studies revealed autophagy-protein interaction patterns within the nucleus, suggesting autophagy-mediated control of nuclear activity. In order to understand if autophagy influences the transcription activity of NF-κB, biochemical analysis, and imaging techniques were used to characterize the molecular interaction between autophagic proteins and p65/NF-κB subunit under different stress conditions. Moreover, to investigate the role of their physical interaction, functional assays were performed either in autophagy-deficient cells or following genetic downregulation of essential components of the autophagic machinery.

Aim 2. To analyze the physiological role of NF-κB in cell fate decisions and stem cell maintenance in the small intestinal epithelium.

Several studies highlighted the critical role of NF-κB in intestinal inflammation and tumor formation. However, nothing is known about its physiological function in sustaining intestinal epithelial homeostasis beyond inflammation. Previous *in vivo* analysis performed in our laboratory revealed strong NF-κB activity in the crypts of the small intestinal epithelium. Therefore, the main goal of this second study was to analyze the role of NF-κB signaling in intestinal epithelial regeneration by using ubiquitous NF-κB suppression (here referred to as *ΔN*), as well as NF-κB reporter mice to study the *in vivo* localization of NF-κB activity in intestinal epithelial cells (IECs). To prove that simultaneous suppression of NF-κB in IECs and surrounding tissues does not result in

inflammation and cell death, I analyzed *in vivo* IEC proliferation, apoptosis, and expression of pro-inflammatory cytokines. However, the major aim of this study was to examine the role of NF-κB in IEC-fate determination, which was evaluated *in vivo*, but also *ex-vivo* by using small 3D intestinal organoids. A further focus was the signaling crosstalk of NF-κB with other known signals known to regulate cell fate decisions in the small intestinal epithelium. For instance, tight regulation of the WNT signaling pathway is essential for homeostasis of the intestinal epithelium. Therefore, to better understand how loss of NF-κB activity alters the IEC-composition, key elements of WNT signaling together with potential NF-κB target genes required for intestinal stem cell maintenance and secretory lineage differentiation were analyzed.

3. MATERIALS

3.1 Instruments and Equipment

137-Cs source for γ-irradiation	STS OB 29, 137Cs- Quelle
Agarose gel camera GelDoc2000	Herolab Transilluminator
Agarose gel electrophoresis chambers	Bio-Rad, self-made
Bacterial Incubators	Memmert
Bioanalyzer	Agilent
Cell culture flasks	TPP
Cell culture plates	TPP
	Sarstedt
Cell lifter	Corning
Centrifuges	Eppendorf 5417 R
	Eppendorf 5810 R
	Beckman Coulter J6-MI
	Beckman Coulter Avanti J-26XP
	IEC MicroMax
CFX96 RealTime PCR Machine	Bio-Rad
CO_2 incubators	Binder
Confocal Laser Scanning Microscope	Zeiss LSM 800
Cryo Box	Nalgene
Cryogenic Vials	CORNING 430488
Dark Reader Transilluminator	Clare Chemical Research
Filter	GE Healthcare Whatmann FP30/0.45 and 0.70 CA-S
Flow Cytometer	BD Biosciences LSR II and Fortessa
Freezers and Fridges	Forma Scientific
	Binder
	Liebherr
Fusion Solo	Vilber Lourmat
Heat block	Techne DRI-Block, DB3
	Eppendorf Thermomixer 5436 and 5437

Incubation shaker	Infors HT - Multitron
Intelli-mixer	NeoLab
LUNA™ Automated Cell Counter	Logos Biosystems
LUNA™ Cell Counting Slides	Logos Biosystems
Magnetic stand	Dynal MPC-P-12
Magnetic stirrer	Heidolph MR3000 and 3001
Microcentrifuge	NeoLab
Microscope (cell culture)	Zeiss TELAVAL 31
Microseal 'B' seal for RT-PCR plates	Bio-Rad
microtome	Thermo Scientific
Microwave	Privileg 9029GD
N2-tank	CHRONOS, MG Messer Griesheim
Overhead rotator (Intelli-mixer)	NeoLab
PCR strip tubes	Axygen, Corning
PCR tubes 0.65 ml	Carl Roth
Petri dishes	Greiner bio-one
pH-meter	Knick pH-Meter 766 Calimatic
Photometers	Amersham Biosciences Novaspec Plus
	PeqLab Nanodrop ND-1000
Plastic cuvettes	Sarstedt
Plate reader	BioTek
Polypropylene conical tubes 15 and 50 ml	BD Falcon, VWR
Polystyrene conical tubes 15 ml	BD Falcon
Polystyrene round-bottom tubes 5 ml	BD Falcon
Power supplies	Bio-Rad Power Pack 200 and 300
	Biometra Standard Power Pac P25
Prescision weight scale	Sartorius AZ3130, AC210P
RNase/DNase-free Microcentrifuge Tubes 1.5 ml	Sarstedt
RNAse-free Microcentrifuge Tubes 0.5 ml	Ambion
Roller-mixer	Stuart Scientific SRT9
Rotating wheel for tubes	Fröbel Labor Technik
RT-PCR plates (96 well)	Biozym
Safe-lock tubes 1.5 and 2 ml	Eppendorf, Sarstedt

SDS PAGE chambers	Bio-Rad Mini-PROTEAN II™ and Tetra-System
Semi-dry blotting apparatus	Bio-Rad Trans-Blot SD Semi Dry Transfer Cell
Shakers	IKA VXR basic Vibrax Unitwist 3-D, Uniequip
Syringe	Single-use, B Braun
Thermocycler	Biometra T Professional TRIO and T3000
Thermomixer	Eppendorf 5436; Eppendorf 5437
Tissue culture hoods	BDK
Transilluminator	Dark Reader, Clare Chemical Research
Vacuum-dryer	Savant DNA Speed-Vac
Vortexer	Heidolph
Water bath	Haake F3 Grant Sub Aqua Pro, Lab Amor Beads

3.2 Chemicals

Acrylamide/Bisacrylamide (30%)	Roth
Advance DMEM/F-12	Life Technologies
Advanced DMEM/F12	Life Technologies
Agar-agar, Kobe I	Roth
Agarose, Molecular Grade	Bioline
Ammonium peroxodisulfate (APS)	Roth
Ampicillin sodium sulfate (amp)	Sigma
Autoradiography films	Amersham Hyperfilm MP
B-27 Supplement	Life Technologies
Bacto agar	BD

Bacto tryptone	Roth
Bacto yeast extract	Serva
BafilomycinA1	Enzo Life science
Bovine serum albumin (BSA), Albumin Fraction V	PAA, Roth
Bradford Protein Assay Dye Reagent	Bio-Rad
Calcium chloride ($CaCl_2$)	Serva
Chemiluminescence films	Amersham Hyperfilm ECL
Chloroquine	Enzo Life science
Complete protease inhibitor tablets -EDTA	Roche
Cycloheximide	Enzo Life science
Deoxycholate	Sigma
Deoxynucleotide triphosphate (dNTPs)	Bioline
Dimethyl sulfoxide (DMSO)	Sigma
Disuccinimidylglutarate (DSG)	Santa Cruz
Dithiothreitol (DTT)	Sigma
DNA 1kb+ ladder	Thermo Fisher Scientific
DNAse	Sigma
Dulbecco's Modified Eagle Medium (DMEM)	Gibco
Dynabeads	Invitrogen
Earle’s Balanced Salts medium (EBSS)	Sigma
Enhanced chemiluminescence (ECL)	Immobilon, Millipore
Ethanol	Geyer
Ethidium bromide	Roth
Ethylene diamine tetraacetic acid (EDTA)	Amresco, Roth

Ethylene glycol tetraacetic acid (EGTA)	Sigma
Fetal calf serum (FCS)	Gibco
Ficoll	Sigma
Filter papers for transfer	Roth
Formaldehyde, (methanol free)	Sigma
GFP-Trap	ChromoTek
Glycerol	Roth
Glycine	Roth
Glycogen	Thermo Fisher Scientific
Heparin Sepharose	GE Healthcare Life Sciences
HEPES	Roth
HEPES	Roth
Hydrochloric acid (HCl)	Roth
Hydrogen peroxide (H_2O_2, 35%)	Roth
ImmuMount	Thermo Scientific
Isopropanol	Roth
Jagged-1	Gift from Christian Klotz
Kanamycin	Sigma
Leptomycin B	Cell signaling
Lipofectamine ™ RNAiMAX	Invitrogen
Lipofectamine2000	Invitrogen
Lipopolysaccharides	Sigma
Magnesium chloride ($MgCl_2$)	Roth
Matrigel	BD Bioscience
Methanol	Roth

MG132	Enzo Life science
N-2 Supplement	Life Technologies
N-acetylcysteine	Tocris
N-Ethylmaleimide	Sigma
Nonidet P-40 (NP-40) substitut (Igepal CA-630)	Sigma
OptiMEM I	Gibco
PageRuler prestained protein ladder	Thermo Fisher Scientific
Pefablock	Sigma
Penicillin/Streptomycin	Gibco
PhosStop Phosphatase Inhibitor	Roche
Poly d(I-C)	Roche
Polyethylenimine (PEI)	Polysciences Inc.
Potassium chloride (KCl)	Roth
Potassium dihydrogen phosphate (KH_2PO_4)	Roth
Protein-A-Sepharose	GE Healthcare
Protein-G-Sepharose	GE Healthcare
Puromycin	Sigma
PVDF membranes, pore size 0.45 µm	Roth, Millipore
Rapamycin	Selleck
recombinant EGF	Peprotech
recombinant Noggin	Peprotech
recombinant R-spondin	RD System
RNAse Zap	Ambion
RNase-free water	Promega
Roswell Park Memorial Institute (RPMI) 1640	Gibco

Skim milk powder	Serva
Sodium acetate (NaOAc)	Merck
Sodium bicarbonate ($NaHCO_3$)	Merck
Sodium chloride (NaCl)	Roth
Sodium dodecyl sulfate (SDS)	Serva
Sodium fluoride (NaF)	Sigma
Sodium hydrogen phosphate (Na_2HPO_4)	Roth
Sodium orthovanadate (Na_3VO_4)	Sigma
Sodium pyruvate	Gibco
tetramethylethylenediamine (TEMED)	Roth
TNFα	Enzo Life Science
TNFβ	Peprotech
Tris	Roth
Triton X-100	Sigma
Trypan Blue Stain	Gibco
Trypsin-EDTA	Merck
Tween-20	Sigma
X-ray developing solution	Sigma
X-ray fixation solution	Sigma
Xylene cyanol	BioRad
Y-27632	Gift from Christian Klotz
β-Glycerophosphate	Merck
β-Mercaptoethanol	Sigma

3.3 Kits and Enzymes

DAB Substrate Kit	Vector Laboratories
Dual-Luciferase® Reporter Assay System	Promega
Duolink PLA Kit	Sigma
FastDigest Restriction Enzymes and Buffer	Thermo Fisher Scientific
GoTaq qPCR Master Mix	Promega
Immobilon- horseradish peroxidase (HRP) Western Detection System	Millipore
iScript Select cDNA synthesis kit	Bio-Rad
NEBNext® High-Fidelity 2X PCR Master Mix	New England Biolabs
PeqGOLD Plasmid Miniprep Kit I	PeqLab
Proteinase K	Roche
Qiagen plasmid maxiprep kit	Qiagen
Qiaquick gel extraction kit	Qiagen
Qiaquick nucleotide removal kit	Qiagen
Qiaquick PCR purification kit	Qiagen
Restriction endonucleases and buffers	New England Biolabs
RNeasy Mini Kit	Qiagen
T4 Polynucleotide Kinase	New England Biolabs
T4-DNA ligase and buffer	New England Biolabs
TrueStart Taq Polymerase	Thermo Fisher Scientific

3.4 Bacterial Strains

E.coli DH5α, Gibco

Genotype: F-endA1 glnV44 thi-1 recA1 relA1 gyrA96 deoR nupG Φ80dlacZΔM15 Δ(lacZYA-argF) U169, hsdR17(rK-mK+),λ–

3.5 Eucaryotic Cell Lines

Cell Lines	Cell type	Company
U2OS	Human Bone Osteosarcoma Epithelial	DSMZ (ACC 785)
HEK-293	Human kidney epithelial	DSMZ (ACC 305)
HEK-293/T17	Human kidney epithelial	Gift from Michela Serresi
A549	Human adenocarcinomic alveolar basal epithelial	Gift from Michela Serresi
U2OS/GFP-LC3	Human Bone Osteosarcoma Epithelial	Gift from Ivan Dikic
THP1	Human monocytic (AML)	DSMZ (ACC 16)
HEK-293 WT	Human kidney epithelial	Gift from Anne Simonsen
HEK-293 ATG16L1 KO	Human kidney epithelial	Gift from Anne Simonsen
HEK-293 ATG16L1β	Human kidney epithelial	Gift from Anne Simonsen
RAW 264.7 WT	Murine monocyte/macrophage	Gift from Anne Simonsen
RAW 264.7 ATG16L1 KO	Murine monocyte/macrophage	Gift from Anne Simonsen
RAW 264.7 ATG16L1β	Murine monocyte/macrophage	Gift from Anne Simonsen
MEF	Mouse Embryonic Fibroblasts	ATCC (CF-1)
NF-κB/293/GFP-Luc	Human kidney epithelial	SBI System Biosciences

3.6 Antibodies for Western Blot, Immunohistochemistry and Immunofluorescence

Antibody	Clone	Company	Order no.	Conc. (WB)
IκBα	C-21	Santa Cruz	sc-371	1:1000
LDH-A	N-14	Santa Cruz	sc-27230	1:3000
NF-κB p65	F6	Santa Cruz	sc-8008	1:1000
Parp1	F2	Santa Cruz	sc-8007	1:1000
Parp1		Abcam	ab227244	1:1000
β-actin	13E5	Cell Signaling	4970	1:1000
LC3B		Cell Signaling	2775	1:1000
LC3B		Novus Biologicals	NB100-2220	1:1000
Phospho-NF-κB p65 (Ser536)	93H1	Cell signaling	3033	1:1000
Vinculin		Sigma	V9131	1:2000
NF-κB p50		Santa Cruz	sc-114P	1:1000
SQSTM1/p62	M01	Abnova	H00008878	1:1000
SQSTM1/p62		Cell signaling	5114	1:1000
SQSTM1/p62	BML	Enzolife	PW9860	1:1000
GFP		Abcam	ab6673	1:1000
c-myc	9E10	Sigma	M5546	1:1000
LAMP1		Abcam	ab24170	1:1000
(Active) β-Catenin (Ser33/37/Thr41)		Cell signaling	D13A1	1:500/1:1000
Cleaved Caspase-3 (Asp175)	5A1E	Cell signaling	9664	1:400/1:1000

E-Cadherin	36	BD-Biosciences	610181	1:500
Ki67		Abcam	ab15580	1:100
Lysozyme		DAKO	A 0099	1:1000
Mmp7		Santa Cruz	sc-515703	1:1000
Muc2		Santa Cruz	sc-15334	1:100
Olfm4	D6Y5A	Cell signaling	39141	1:400
Sox9		Millipore	AB5535	1:200

Seconday Antibody	Company	Order no.
HRP-conjugated anti-rabbit	JacksonImmunoResearch	711-035-152
HRP-conjugated anti-mouse	JacksonImmunoResearch	715-035-150
HRP-conjugated anti-goat	JacksonImmunoResearch	705-035-147
Alexa 488 donkey anti-goat	Invitrogen	A11055
Alexa 488 goat anti-rabbit	Invitrogen	A11008
Alexa 488 rabbit anti-mouse	Invitrogen	A11001
Alexa 546 goat anti-rabbit	Invitrogen	A11010
Alexa 546 goat anti-mouse	Invitrogen	A21123

3.7 Vectors and Oligonucleotides

3.7.1 Plasmids

Plasmid	Source
pcDNA3	Obtained from Invitrogen
pRenilla	Renilla
GFP-p62-WT	p62 full-length was subcloned into pEGFP-C2 (Wang et al.2016)

GFP-p62-ΔUBA	p62 fragment was subcloned into pEGFP-C2 (Wang et al.2016)
pcDNA3-human p65 FL	myc N-terminal (Hochrainer et al. Cell Mol Life Sci. 2012)
p65 aa 1-193	myc N-terminal and subcloning performed by Daniel Heinze
p65 aa 1-305	myc N-terminal and subcloning performed by Daniel Heinze
p65 aa 1-521	myc N-terminal and subcloning performed by Daniel Heinze
p65 aa 101-551	myc N-terminal and subcloning performed by Daniel Heinze
p65 aa 194-551	myc N-terminal and subcloning performed by Daniel Heinze
p65 aa 306-551	myc N-terminal and subcloning performed by Daniel Heinze
pGEX-4T1	GST only (87)
pGEX-4T1 LC3A dG	Gift from Ivan Dikic (87)
pGEX-4T1 LC3B dG	Gift from Ivan Dikic (87)
pGEX-4T1 LC3C dG	Gift from Ivan Dikic (87)
pGEX-4T1 GABARAP dG	Gift from Ivan Dikic (87)
pGEX-4T1 GABARAP-L1 dG	Gift from Ivan Dikic (87)
pGEX-4T1 GABARAP-L2 dG	Gift from Ivan Dikic (87)
pGEX-4T1 Ub	Gift from Ivan Dikic (87)
pGEX-4T1 4XUb	Gift from Ivan Dikic (87)
pGEX-4T1 dN LC3A dG	Gift from Ivan Dikic (169)
pGEX-4T1 dN LC3B dG	Gift from Ivan Dikic (169)
pGEX-4T1 dN GABARAP-L1 dG	Gift from Ivan Dikic (169)
pGEX-4T1 dN GABARAP-L2 dG	Gift from Ivan Dikic (169)
pGEX-4T1 LC3B F52A-V53A dG	Gift from Ivan Dikic (169)

3.7.2 RT-PCR Primers for expression analysis

Gene	Accession No.	Sequence (5' → 3')
hTNF	NM_000594.3	CTCTAATCAGCCCTCTGGCCC
		CAGCTTGAGGGTTTGCTACAACA
hNFKBIA	NM_020529.2	GAGGACGAGCTGCCCTATGA
		AGCCCCTTTGCGCTCATAAC
hSQSTM1/p62	NM_001142298.1	ATCCGAAGGGCCAAGCTCTC
		AGAGGGACTCAATCAGCCGC
hATG5	NM_001286106.2	TTT GCA TCA CCT CTG CTT TC
		TAG GCC AAA GGT TTC AGC TT
hATG16L1	NM_030803.7	CAGTTACGTG GCGGCAGGCT
		ACAACGTGCG AGCCAGAGGG
hCCL20	NM_004591.3	AGTTTGCTCCTGGCTGCTTTG
		TGCTTGCTGCTTCTGATTCG
hCXCL10	NM_001565.3	CCAGAATCGAAGGCCATCAAGA
		TCGATTTTGCTCCCCTCTGGT
hRELA/p65	NM_021975.3	CCTGTCCTTTCTCATCCCATC
		ACCTCAATGTCCTCTTTCTGC
hHPRT1	NM_000194.2	TGTAATGACCAGTCAACAGGG
		GGATTATACTGCCTGACCAAGG
hRPL13A	NM_012423.2	AAAGCCAAGATCCACTACCG
		GGAATTAACAGTCTTTATTGGGCTC
hTBP	NM_003194.4	GGGTTTTCCAGCTAAGTTCTTG
		CTGTAGATTAAACCAGGAAATAACTCTG
mLysozyme	(Heuberger et al. 2014) (170)	GCAGCCATACAATGTGCAAAGAGG
		TTTGCCCTGTTTCTGCTGAAGTCC
mCryptdin-1	(Tsai et al. 2014) (171)	AGG AGC AGC CAG GAG AAG
		ATG TTC AGC GAC AGC AGA G
mMath1	(Heuberger et al. 2014)	GTTGCGCTCACTCACAAATAAGGG
		TGGCAGTTGAGTTTCTTCAAGGCG

mDll4	(Heuberger et al. 2014)	TTA CTG CAG CAA GCC AGA TG
		CAT TCT TGC ACG GAG AGT GG
mAscl2	(Heuberger et al. 2014)	AAAGCTTGGTCCGGTTCTTCATCC
		GCAGATGCTTAGCTTATTGCGTCC
mLgr5	(Heuberger et al. 2014)	CCTACTCGAAGACTTACCCAGT
		GCATTGGGGTGAATGATAGCA
mOlfm4	(Heuberger et al. 2014)	CAAGCCTGGCTCGACGGCC
		CGCGAACATCTTCAGGTTCT
mSpedf1	(Heuberger et al. 2014)	AACATGTATCCCGACGATAGCAGC
		TCAATATCTTTCAGGACCTCGCCC
mGob5	(Heuberger et al. 2014)	TGAAATTGTGCTGCTGACCGATGG
		TGCTGCGAAAGCATCAACAAGACC
mKlf4	(Al Alam et al. 2015) (172)	GAGTTCCTCACGCCAACG
		CGGGAAGGGAGAAGACACT
mMuc2	(Heuberger et al. 2014)	TGTGATGCCAATGACAAGGTGTCC
		ACCACAATGTTGATGCCAGACTCG
mAxin2	NM_015732.4	ACTGACCGACGATTCCATGT
		CTGCGATGCATCTCTCTCTG
mSST	(Mustata et al. 2011)	ACCGGGAAACAGGAACTGG
		TTGCTGGTTCGAGTTGGC
mChromoA	(Mustata et al. 2011)	TCCCCACTGCAGCATCCAGTTC
		CCTTCAGACGGCAGAGCTTCGG
mDll1	(Zhang et al. 2019) (173)	CCGATGACCTCGCAACAGAA
		CCAGGGTCGCACATCTTCTC
mHes1	(Zhang et al. 2019)	GGAGAAGAGGCGAAGGGCAAGA
		CGT GGACAGGAAGCGGGTCA
mGfi1	(Zhang et al. 2019)	TCCACACTGTCCACACACCT
		CTGGCACTTGTGAGGCTTCT
mWnt3a	(Farin et al. 2012)(174)	TGGAACTGTACCACCATAGATGAC
		ACACCAGCCGAGAGCGATG
mWnt10a	NM_009518	GAGAGCCTCACAGAGACATCCAT

		TACTGTGCGGAACTCAGGCGT
mSox9	NM_011448	GACTCCCCACATTCCTC
		CCTCTCGCTTCAGATCAAC
mIcam1	NM_010493	CTGCGTTTTGGAGCTAGCGG
		TTGGCTCCCTTCCGAGACCT
mTnf	NM_013693	TCCCAAATGGCCTCCCTCTCC
		CCACTTGGTGGTTTGCTACGA
mIL6	NM_031168	ACAAAGCCAGAGTCCTTCAGAGA
		AGCCACTCCTTCTGTGACTCC
mIl1α	NM_010554.4	GGAGAGCCGGGTGACAGTATC
		TCTGGGTTGGATGGTCTCTTC
mGapdh	NM_008084	AGCAAGGACACTGAGCAAGAG
		GCAGCGAACTTTATTGATGGT
mHprt	NM_013556	GGATATGCCCTTGACTATAATGAG
		GGCAACATCAACAGGACTC
mNfkbia	NM_010907	AGGAGTACGAGCAAATGG
		CAGGCAAGATGTAGAGGG
mCxcl12	NM_021704.3	TCTTCGAGAGCCACATCGCC
		AGCCGTGCAACAATCTGAAGG
mLcn2	NM_008491.1	ACTTCCGGAGCGATCAGTTC
		TTTTTCTGGACCGCATTGCC
mNos2	NM_001313921.1	TTTCACCCGCTTTGCCAAGT
		GTCTCTGCGCATCCCAGTCA
mNox1	NM_172203.2	CTCCAGCCTATCTCATCCTGAG
		AGTGGCAATCACTCCAGTAAGGC
mTnfip3	NM_001166402.1	GTCAGGAAGCTCGTGGCTCT
		TTAAGGGTGCTGCAGAGGGC
mLbp	NM_008489.2	TGCTGTTTGCTGCAGACAAC
		TGGGTCCAACCAAAACCTTC
mSmoc2	NM_022315.2	AGCTGGGGCAATTCTTTCAG
		AATGAGCAAAGGCCTTCTGC
mLgr1	(Heuberger et al. 2014)	ATTTGATGGTCTGTCGCGGT
		GTGCAGCACGTGCATCTTAG

mTert	NM_009354.2	AGAAACGTGCTGGCTTTTGG
		AACAGTGTTGGGCAAGTAGC
mHopx	NM_001159900.1	AGTTCCTTCCCTTACAGCTGTG
		ACTTGCTTTTCTGCCCCTTG
mCcdn1	NM_001379248.1	AGTTCATTTCCAACCCACCC
		AGACCAGCCTCTTCCTCCAC
mEdn1	NM_010104.4	ACTACGAAGGTTGGAGGCCA
		CAATGTGCTCGGTTGTGCGT
mProm1	NM_001163577.1	CTGAAGATTGCCCTCTATGA
		AGTTTCTGGGTCCCTTTGAT
mEphb3	NM_010143.1	GACCTTGCTGCCCGAAACAT
		CCCACATGACAATCCCATAGCT
mMsi1	NM_001376960.1	AAAACCACCAACAGGCACAG
		TGGGCTTTCTTGCATTCCAC
mTnfrsf19	NM_001164155.1	TGAAAGTGGCGGTGAATGTG
		AACATTCACAGCCAGGCTTC
mIl1β	NM_008361.4	TGAAGCAGCTATGGCAACTG
		GGGTCCGTCAACTTCAAAGA
mCxcl15 (Il8)	NM_011339.2	ATGCTCCATGGGTGAAGGCT
		AGAAGCTTCATTGCCGGTGG

3.7.3 siRNAs sequences

Gene	Sequences
SQSTM1 (S)_1	5’-GGACCCAUCUGUCUUCAAA UU
SQSTM1 (AS)_1	3’-UU CCUGGGUAGACAGAAGUUU
SQSTM1 (S)_2	5’-GCCAUCCUGUUAAAUUUGU UU
SQSTM1 (AS)_2	3’-UU CGGUAGGACAAUUUAAACA
ATG5_Sigma	EHU085781
Non-targeting	5’-UUCUCCGAACGUGUCACGU

Non-targeting	5'-ACGTGACACGTTCGGAGAA

3.8 Buffers and Solution

3.8.1 Bacterial Growth Media

Super Optimal Broth (SOB) medium

Bacto tryptone	20 mg/ml
Bacto yeast extract	10 mg/ml
NaCl	10 mM
KCl	2.5 mM
$MgCl_2$	10 mM
$MgSO_4$	10 mM
pH 6.7-7	

Luria-Bertani (LB) medium

Bacto tryptone	10 g/l
Bacto yeast extract	5 g/l
NaCl	10 g/l

LB-Agar plates

LB medium + Bacto agar	(15 g/l)
Amp (1000x)	100 mg/ml

3.8.2 Agarose gel electrophoresis

Tris borate EDTA (TBE)

Tris	50 mM
Borate	50 mM
EDTA	1 mM

Agarose gel (1%)

TBE	**50 ml**
Agarose	0.5 g

6x DNA sample buffer

Bromphenol blue	1% (w/v)
Xylene cyanole	1% (w/v)
Glycerol	40% (v/v)

3.8.3 Cell extracts

RIPA buffer complete (whole cell extracts)

Tris-HCl pH 7.4	50 mM
NaCl	150 mM
Na-deoxycholate	0,5 %
SDS	0,1 %
EDTA	2 mM
NaF	50 mM
NP-40	1%
Complete Protease inhibitor cocktail - EDTA	1 tablet/50 ml
PhosStop Phosphatase inhibitor	1 tablet/10 ml

Buffer A (cytoplasmic extracts)

Hepes pH 8	10 mM
MgCl2	1.5 mM
KCl	10 mM
PhosStop Phosphatase inhibitor	1 tablet/10 ml
Complete Protease inhibitor cocktail –EDTA	1 tablet/50 ml

Buffer B (nuclear extracts)

Hepes	20 mM
Glycerol	25% (v/v)
NaCl	0.46 M

MgCl2	1.5 mM
EDTA	0.2 mM
PhosStop Phosphatase inhibitor	1 tablet/10 ml
Complete Protease inhibitor cocktail -EDTA	1 tablet/50 ml

Protein IP Buffer (whole cell extracts for IP)

NaCl	150 mM
Tris pH 7.5	50 mM
NP-40	1%
Glycerol	5%
Deoxycholate	0.5%
Sodium dodecyl sulfate	0.1%
Complete Protease inhibitor cocktail -EDTA	1 tablet/50 ml
PhosStop Phosphatase inhibitor	1 tablet/10 ml

IP wash buffer

NaCl	150 mM
Tris pH 7.5	50 mM
Glycerol	5%

3.8.4 Sodium Dodecyl Sulfate-Polyacrylamide Gel Electrophoresis (SDS-PAGE)

Stacking gel buffer

H2O	6.8 ml
Acrylamid mix (30%)	1.7 ml
Tris-HCl pH 6.8, 1 M	1.25 ml
10 % SDS	0.1 ml
10 % APS	0.1 ml
TEMED	0.01 ml

Separating gel buffer (10%)

H2O	4 ml
Acrylamid mix (30%)	3.3 ml
Tris-HCl pH 6.8, 1.5 M	2.5 ml
10 % SDS	0.1 ml
10 % APS	0.1 ml
TEMED	0.004 ml

6x Laemmli sample buffer

Tris-HCl pH 6.8	300 mM
EDTA	12 mM
Glycerol	40% (v/v)
SDS	12% (w/v)
DTT	10% (w/v)
Bromphenol blue	Trace amount

SDS-running buffer

Tris-HCl pH 7.3	25 mM
SDS	0.1% (w/v)
Glycine	192 mM

3.8.5 Western Blot

Transfer buffer

Tris-HCl pH 8.3	48 mM
Glycine	39 mM
Methanol	20% (v/v)
SDS	0.037% (w/v)

Phosphate buffered saline (PBS)

NaCl	137 mM
KCl	2.7 mM
Na_2HPO_4	10 mM
KH_2PO_4	1.7 mM

Tris buffered saline (TBS)

Tris	400 mM
NaCl	2.7 M
pH 7.6	

TBS-Tween (TBST)

20 ml Tween-20 was to 1 l of TBS to obtain a final concentration of, 0.02% (v/v).

3.9 Software and Internet Sources

- Bio-Rad CFX Manager
- FlowJo
- Ensembl Genome Browser http://www.ensembl.org/
- Primer3 http://frodo.wi.mit.edu
- Primer Blast: https://www.ncbi.nlm.nih.gov/tools/primer-blast/
- Creative Suite CS5 Adobe
- GraphPad Prism 8
- Zotero
- Biorender.com

4. METHODS

4.1 Cell culture techniques

4.1.1 Cell culture maintenance

HEK293, all U2OS, A549, RAW 264.7 and MEF cells were grown in Dulbecco's Modified Eagle Medium (DMEM, Gibco) and were supplemented with 10 % heat-inactivated fetal calf serum (FCS, Gibco), 2 mM L-glutamine, 100 unit/ml penicillin and 100 µg/ml streptomycin and grown in a humidified incubator containing 5 % CO_2 at 37 °C. THP1 cell lines were grown in RPMI medium 1640 (Gibco) and were supplemented and grown as described above. Subculture were performed every two or three days as described by the DSMZ.

4.1.2 Freezing and Thawing of Cell Lines

Cell lines were frozen in culture medium with 20% FCS and 10% DMSO at $5x10^6$ cells per ampoule. For freezing, cells were resuspended in 1 ml of freezing medium and transferred to a cryovial, which was then frozen in a cyrobox filled with isopropanol. This allowed the cells to slowly cool down and freeze at -80°C. The vials were then transferred to the liquid nitrogen tank for long-term storage.

To thaw cells the cryovials were warmed in warm water until medium was thawed. Cells were then resuspended in warm culture medium and centrifuged at 1050 rpm for 5 min to remove the DMSO. According to the optimal cell density given by the DSMZ cells were seeded in culture plates.

4.1.3 Treatment of Cells

A final concentration of 10 ng/ml or 10µg/ml was used to treat cells with **TNFα** or **LPS**, respectively. Cells were stimulated for a specific time as indicated for each experiment to analyze the NF-κB activation of the canonical signaling pathway.

Proteasomal inhibition was performed with 10 µM **MG-132** for 6h. As a control, DMSO was added in the same volume to the cells.

Genotoxic stress (20 Gy) was applied by ionizing irradiation of cells with a Cs137 source (OB29 Irradiator, STS Braunschweig).

To inhibit the late phase of autophagy (fusion between autophagosome and lysosome), cells were pre-treated with 200 nM of **Bafilomycin A1** or with 60 µM of **Chloroquine** (or DMSO, as mock treatment) for 2 or 5h, respectively if not indicated differently in the result's figure legends.

To induce autophagy degradation, cells were treated with 1 µM of **Rapamycin** for 4 or 5h (or DMSO, as mock). Cells were starved using **Earle's Balanced Salts medium (EBSS)** (Sigma) for 4h after washing cells with 1x PBS.

Protein nuclear export was inhibited using 40nM **Leptomycin B** for 4h before cotreatment with LPS.

4.1.4 Cycloheximide-chase assay

In order to study the protein turnover of p65/NF-κB, Hek293 cells were stimulated with 10ng TNFα for 15 min, washed once with 1x PBS and finally treated with 10µg/ml of cycloheximide for a total of 6h.

4.1.5 Transient Plasmid Transfection

For transient transfection, 0.5 $x10^6$ cells were seeded into each well of a 6-well plate 24 h prior transfection. 1 µg DNA and 3 µl PEI were each diluted in 150 µl OptiMEM to obtain a ratio of 1:3 DNA to PEI. The DNA mixture was added to PEI and the reaction mixture was incubated for additional 20 min at RT. The cell culture medium was exchanged with DMEM without antibiotic and the reaction mixture was added drop wise to the cells while slowly rocking the plate followed the incubation at 37°C and 5% CO_2. Cells were harvested 24 - 48 h after transfection.

Transfection using Lipofectamin 2000 was performed according to manufacturer's protocol. In brief, $5x10^5$ cells were seeded into each well of a 6-well plate 24 h prior transfection. Medium was replaced with DMEM without antibiotic shortly before transfection. 1 µg DNA and 9 µl Lipofectamin were each diluted in 250 µl OptiMEM and incubated for 5 min. The mixtures were combined and incubated for 20 min at RT. The DNA-Lipofectamin complex was added to the cells while rocking the plate. Cells were harvested 24 - 48 h following transfection.

4.1.6 Transient knock-down by siRNAs

$2x10^5$ cells were seeded into each well of a 6-well plate one day before the transfection. 10µM of working solutions for each siRNA was prepared. 3 µl of siRNA working solution was added to 150 µl of OPTIMEM. 9 µl of RNAimax was also added into 150 µl OPTIMEM medium in a separate tube. The mixtures were combined and incubated at RT for 15 minutes before adding to the cells in a dropwise manner. Subsequent experiments were done 72 hours post-transfection.

4.1.7 Luciferase Reporter Assay

The activity of NF-κB luciferase reporter cell line was measured according to manufacturer's protocol (ONE-Glo™ Promega) into 96-well plates with white walls and bottom to reduce the cross-contamination of the signal between wells. Briefly, the NF-κB luciferase activity was measured after 8 hours of TNF or irradiation treatment as

described in section 2.1.3. Cells were then detached from the seeding dishes and washed once with 1xPBS. A volume of 50 µl of cells diluted in 1 ml PBS was added into each well of a white 96-well plates (each sample in triplicates) together with additional 50 µl of FireFly (luciferase substrate) solution in a 1:1 ratio. Three separated wells were filled with an equal volume of only PBS with FireFly solution and used as background signal. The plate was mixed and incubated at 37°C for 10 minutes. The Luciferase signal was measured using a plate reader. Subsequently, 50 µl of 1xStop&Glo reagent was added to each well and the plate was incubated at room temperature for other 10 minutes. Renilla Luciferase signal was also measured by the plate reader. Background signal of dilution buffers was subtracted from the luciferase signals and each Luciferase signal was then divided by the respective Renilla signal obtained from the same well to obtain the average NF-κB luciferase activity.

4.1.8 Organoid cultures

Mouse intestine organoid culture in Matrigel was performed as described previously (175). Briefly, duodenal (PSI) crypts were isolated by dissecting the whole small intestine. The intestine was transferred to cold 1x PBS, carefully flushed with 1x PBS for three times using a 21G syringe and opened sagittal. The opened intestine was washed three times with cold 1x PBS prior of removal of villi by scraping the intestine with a cover slip, then separate in 0.5 cm pieces and transferred into a 50 ml tubes with 30 ml 1x PBS on ice. The intestinal pieces were washed up to ten times, with cold 1x PBS by carefully vortexing, followed by incubation in 8mM EDTA/1xPBS buffer for 5 min on ice and rotating in 2mM EDTA/1x PBS at 4°C for 20 min. After this treatment crypts can be separated from tissue by intensive shaking in 50 ml tubes refilled with 10 ml PBS. A total of 7 fractions were created and supernatants (20 µl) were microscopically controlled. The supernatants containing the highest numbers of isolated crypts were pooled and centrifuged at 4°C (300 g / 5 min). The pellet was then resuspended in adv.DMEM (Pen/Strep) and filtered through a 70 µm cell strainer (BD Falcon) into a new 15 ml tube. The filtrate was centrifuged for additional 3 min at 300 g to remove single cells. The pellet was resuspended in 1 ml adv.DMEM (Pen/Strep) and the total number of crypts was calculated. ~500 crypts were embedded in 50 µl Matrigel and cultured in Advanced DMEM/F12 medium, supplemented with N2 and B27, mNoggin (100 ng/ml), R-spondin (500ng/ml), mEGF (mouse epidermal growth factor, 50 ng/ml), and N-acetylcysteine (500 µM). For single cell sorting experiments, isolated crypts were incubated in culture

medium for 45 min at 37 °C followed by trituration with a glass pipette. Dissociated cells were passed through a cell strainer with a pore size of 40 µm. EGFP+ cells were sorted by flow cytometry (BD FACS ARIA™ II). Single viable epithelial cells were gated by forward scatter, side scatter and pulse-width parameter, and by negative staining for propidium iodide. Sorted cells were collected in culture medium and embedded in Matrigel containing Jagged-1 peptide (1 µM) at 100 cells/well (in 48-well plates,10 µl Matrigel). After sorting the culture medium (250 µl for 48-well plates) was supplemented with Y-27632 (10 µM) for 24 hrs. Thereafter, Y-27632-free medium was used and changed every day. For passage, organoids were removed from Matrigel and mechanically dissociated into single-crypt domains, and then transferred to new Matrigel.

4.2 Histological techniques

4.2.1 Mouse strains

The following genetically modified lines were used for our study:

Mouse strain	abbreviation	origin
129;129P2-ctnnb1$^{tm(NFKBIA\Delta N)1RSU}$	ΔN	Schmidt-Ullrich et al. 2001
129;129P2-ctnnb1$^{tm(NFKBIA\Delta Nfl/fl)RSU}$	loxPΔN	Schmidt-Ullrich et al. 2001
B6-Tg(κ-EGFP)3Pt/Rsu	κ-EGFP	Tomann et al. 2016
B6.129P2-Lgr5$^{tm1(cre/ERT2)Cle}$	Lgr5-EGFP	Barker et al. 2007
B6.129P2-Lgr5$^{tm1(cre/ERT2)Cle}$; 129.129P2-ctnnb1$^{tm(NFKBIA\Delta N)1Rsu}$	Lgr5-EGFP x delta N	Schmidt-Ullrich
Spdef $^{tm1.1Cle}$	Spdef-/-	Gregorieff et al. 2009
Spdef $^{tm1.1Cle}$; B6-Tg(κ-EGFP)3Pt/Rsu	Spdef-/- x Igk-EGFP-3/Ola	Brischetto et al. 2021
Tg(Vil-cre)20Syr;B6;129P2-Nfkbia^{tm1Kbp};	villinCRE x iKB alpha fl/fl x Igk-EGFP-3/Ola	Mikuda et al. 2020

For each experiment n = 3 – 7 mice/group (line) were used. Mice were sacrificed at 8 – 12 weeks of age, or postnatal day 9 and 15 as indicated.

4.2.2 Tissue preparation of small intestine

To isolate the entire small intestine of 8–10-week-old mice the abdomen was opened, and the proximal end of the small intestine was separated from the stomach. The separated end was then carefully pulled out to isolate the entire small intestine. The distal end of the small intestine was then separated close to the Caecum. Connective tissue of the entire small intestine was completely removed using scissors. The isolated intestine was transferred into cold 1x PBS and divided into six equal pieces. Each piece was flushed three times with cold 1x PBS and then opened sagittal using a scissor. The opened intestinal pieces were washed three times in cold 1x PBS and formed to a “swiss role (176)” prior to overnight fixation. For in situ hybridization or immunohistochemical analysis one piece of each the proximal, medium and distal region was fixed in 4% PFA/PBS for 24 h prior to overnight fixation in 70% EtOH. Afterwards, tissue was dehydrated by performing the following alcohol series: it was incubated for 30 min 80% in EtOH, 30 min 90% in EtOH, 1h 96% in EtOH and 30 min 96% in EtOH, followed by 1h 100% EtOH, 30 min 100% EtOH, 15 min 100% EtOH/Toluol (1:1) and terminally incubated for 1h in Toluol and for 30 min in fresh Toluol prior to fixation in paraffin (Paraplast, Leica) at 61°C overnight. For paraffin embedding, tissue was transferred to embedding mould, arranged planar to the bottom and hardened on ice for 20 min. Tissue was stored at 4°C. A microtome (Thermo Scientific, HM 355S) was used to achieve 5 µm thick sections of the paraffin blocks. Sections were transferred to microscope slide (SuperFrost) and dried at 37°C for at least 1h.

4.2.3 Immunofluorescence staining and immunohistochemistry of Paraffin-Embedded Tissue

For immunofluorescence, 5 µm thick sections were rehydrated by serial immersion two times each for 10 min in Xylol, followed by two times 5 min in 100% EtOH and 5 min each in 96% EtOH, 90% EtOH, 80% EtOH, 70% EtOH and terminally 5 min in distilled water. Antigen retrieval was performed by boiling sections for 15 min in citrate buffer (10mM, pH 6). Sections were cooled down for 20 min on ice and for 5 min in distilled water before incubating for 5 min in 1x $TBST_{0.1\%}$ (50 mM Tris, pH 7,5, 150mM NaCl, 0.1% Tween 20). Sections were blocked with blocking solution (5% donkey or goat serum, respectively in PBS) for 1 hour at room temperature to avoid unspecific antibody binding,

followed by primary antibody incubation at 4°C overnight. Slides were then rinsed three times in PBS and fluorescent secondary antibody diluted in blocking solution/PBS was added for 90 min at room temperature. Slides were again washed three times for 10 min in PBS, nuclei were labeled with 4´,6´-diamidino-2-phenylindole (DAPI, 1:5000) diluted in PBS, for 5 min, briefly washed in distilled water. Finally, slides were mounted with ImmuMount (Thermo Scientific). Images were acquired using a confocal microscope (Zeiss LSM800).

For immunohistochemistry slides were dehydrated as describe above. Endogenous peroxidases were inactivated by incubating slides for 10 min at room temperature in hydrogen peroxide solution (5% H2O2 in distilled water). Antigen retrieval and blocking of slides were performed as described above. Primary antibodies were added and incubated in a humid chamber at 4°C overnight. Slides were washed in PBS three times each for 10 min and secondary HRP-conjugated antibody incubation was carried out for 1 hour at room temperature in humid chamber. Slides were washed again three times for 10 min in PBS and stain reaction was performed at room temperature for 3 to 5 min using the DAB kit (Invitrogen). Alcian-Blue or nuclear fast red staining, were carried out according to standard protocols.

4.3 Protein Analysis Methods

4.3.1 Whole-Cell Extracts

Whole-cell extracts were obtained with RIPA Buffer complete. To this end cells were washed once with cold PBS. Adherent cells were scratched from the culture plates in lysis buffer while suspension cells were first centrifuged for 5 min at 1200 rpm and 4°C and next the pellet was resuspended in three volumes RIPA Buffer complete. Samples were incubated for 30 min at 4°C on a shaker. Following incubation, samples were centrifuged for 30 min at 14000 rpm to remove cell debris. The supernatant was then transferred to a new tube and stored at -80°C.

Freshly isolated small intestine was shock frozen in liquid nitrogen and pulverized using a

mortar. The pulverized sample was incubated in 500 µl RIPA lysis buffer for 4 h on a rotating table before centrifugation as previously described.

4.3.2 Cytoplasmic and Nuclear Extracts

For cytoplasmic and nuclear extracts, cells were washed once with PBS. Differently from suspension cells, which were directly incubated on ice with complete Buffer A, adherent cells were detached from the cell culture plates with Trypsin and incubated for 5 min at 37°C. Trypsin was then inactivated by adding normal growth medium to the plate and cells were transferred to 15 ml tubes followed by centrifugation. Additional wash with PBS was removed after centrifugation and the samples were incubated for 30 min on ice in three volumes Buffer A supplemented with 0.1% NP-40 and 1mM DTT. Samples were then centrifuged at 14000 rpm for 30 min. The obtained supernatant containing cytoplasmic extracts was transferred to a new tube. Samples were washed in complete Buffer A, centrifuged for additional 30 min at 14000 rpm and 4°C and resuspended in two volumes Buffer C supplemented with 0.5% NP-40. Following 30 min incubation at 4°C, lysates were centrifuged for 20 min at 14000 rpm to remove cell debris. The supernatant was transferred to a new tube to obtain nuclear extracts. Samples were stored at -20°C and at -80°C for long-term storage.

4.3.3 Protein Quantification

The protein concentration was measured using Bradford reagent according to the manufacturer's protocol. In total 1 ml 1x Bradford reagent and 1 µl cell lysate were added in a cuvette. As a blank, pure buffer without protein was added instead of the cell lysate. The absorption was measured at 595 nm using a photometer. The photometer was standardized with a BSA serial dilution to obtain a concentration-absorption curve.

4.3.4 SDS-PAGE

Size-separation of proteins was performed using SDS-PAGE. To this end, gels were prepared containing acrylamide. Polymerization was induced by adding APS and TEMED. Pore size was altered by adding varying amounts of acrylamide – the higher the amount the smaller the pore sizes. The final concentration varied between 6 and 15%. Samples were boiled with 6x Laemmli sample buffer for 5 min at 95°C to reduce and denature the protein, allowing the separation according to size, not charge or conformation.

For SDS-PAGE, 15-20 µg of whole-cell extract, cytoplasmic or nuclear extract sample were loaded onto the gel. Samples were run discontinuously through a 4% acrylamide-containing stacking gel (pH 6.8) followed by a separating gel with varying percentages

of acrylamide to separate proteins according to size. SDS running buffer was used to perform electrophoresis. Gels were run with 100 V. A prestained protein ladder was run in parallel to the samples for size-estimations of the proteins of interest.

4.3.5 Western blot

Following SDS-PAGE, protein samples were transferred onto a PVDF membrane. The membrane was first activated with a short incubation in methanol. The membrane was then washed and equilibrated with transfer buffer to allow efficient uptake of proteins. Transfer was performed using a wet tank blotting apparatus at 200 mA for 1.5 h.

Following transfer, the membranes were blocked with 5% BSA or milk in TBST for 1 h at RT to avoid unspecific antibody binding to the membrane. The membrane was then incubated with the specific primary antibody dilution overnight at 4°C on a shaker. On the next day, membranes were washed three times with TBST for 10 min each. The HRP-conjugated secondary antibodies were diluted in TBST (1:10,000) and incubated with the membranes for 45 min at RT. Washing was performed three times with TBST and one time with PBS for 10 min each.

Blots were analyzed by chemiluminescence, using a commercially available ECL solution (Millipore) following manufacturer's protocol. The membranes were covered with ECL solution and incubated for 30-60s. Blots were developed using ECL films or the Fusion machine. Developing times varied according to intensity of signals derived from the protein of interested. Protein bands were detected by the luminol-based substrate that emits light due to the HRP-mediated oxidation.

4.3.6 Co-IP

Magnetic Dynabeads protein G were washed three times with 800 µl IP Washing Buffer. After the final wash a 50% slurry was prepared with IP Buffer. Cells were harvested with IP Buffer. 20 µg protein samples were prepared as Input samples and 2-4 mg proteins were used for co-IP. For pre-clearing, 15 µl of the 50% slurry of Dynabeads were added to the samples and incubated for 30 min at 4°C, while rotating. DynaMag ™ magnet was used for removing the supernatant that was transferred to a new tube with additional 15 µl of Dynabeads together with 3 µg of primary antibody and rotated overnight at 4°C. The day after, the supernatant was discarded using the magnet. Beads were washed three times with IP washing buffer to remove contamination, diluted in 2x Laemmli buffer and

boiled for 5 min at 95°C. In parallel, input samples were boiled. Input and co-IP samples were further analyzed by SDS-PAGE and Western blot.

Co-IP using the GFP beads was performed according to manufactore's protocol ChromoTek GFP-Trap.

4.3.7 GST pull-down

GST fusion LC3s, GABARAPs and Ub proteins were kindly provided by Ivan Dikic and the expression was induced as previously described (169). Briefly, fusion proteins were expressed in Escherichia coli BL21 (DE3) cells in LB medium after addition of 0.5 mM IPTG and incubation at 37°C for 5 hr. Harvested cells were lysed using sonication in a lysis buffer (20 mM Tris-HCl pH 7.5, 10 mM EDTA, 5 mM EGTA, 150 mM NaCl) and GST fused proteins were immuno-precipitated using Glutathione Sepharose 4B beads (GE Healthcare). Fusion protein-bound beads were used directly in GST pull down assays. HEK293 cells were used for endogenous pull down of p65. Lysates were cleared by centrifugation at 14000 g for 30 min, and incubated with GST fusion protein-loaded beads over-night at 4°C. Beads were then washed three times in lysis buffer, resuspended in 2x Laemmli buffer and boiled. Supernatants were loaded on SDS-PAGE.

4.4 DNA and RNA Methods

4.4.1 RNA isolation

RNA extraction was performed according to manufacturer's protocol using QiaShredder and the RNeasy kit (Qiagen). The total RNA concentration was determined by the NanoDrop. The ratios of the wavelength 260/280 and 260/230 were used to determine purity of the RNA.

4.4.2 Determining of Nucleic Acid Concentration

The DNA and RNA concentration was assessed at optical density (OD)260 by a NanoDrop. The ratios of the wavelength 260/280 and 260/230 were measured to determine contamination with protein or buffer residues. Values around 2 showed purity of the samples.

4.4.3 cDNA synthesis

In total 1µg RNA was used for cDNA synthesis. cDNA was reverse transcribed using iScript cDNA synthesis kit according to manufacturer's protocol.

4.4.4 Quantitative RT-PCR (qRT-PCR)

All primers for qRT-PCR analysis were designed according to the Minimum Information for Publication of qRT-PCR Experiments (MIQE)-guidelines. The primer design was performed and specificity was evaluated with NCBI Primer Blast. The primers were designed to amplify an amplicon size of 75-100 bp, with an optimal size of 85 bp and with a melting temperature of 60-63°C, with an optimal temperature of 62°C.

The primer efficiency was determined using a serial dilution of cDNA. To this end, cDNA was diluted 1:5 and was further used to create a serial dilution of 1:3. In total, 2 µl/well of the cDNA dilution was used to analyze efficiency.

The qRT-PCR was carried out using the CFX96 Real Time System (Bio-Rad) and GoTaq® qPCR Master Mix (Promega). Two references were used for normalization and the fold induction of mRNA of the target of interest was calculated compared to the control sample using the ΔΔCq method. All samples were analyzed in triplicates.

The following qRT-PCR master mix was used for analysis of mRNA:

GoTaq qPCR master mix	**5 µl**
Primers forward/reverse mix (3 µM)	1 µl
cDNA (1 ng/µl)	2 µl
ddH2O	2 µl

All qRT-PCR results were analyzed in triplicates and are shown as mean, with the error bar representing the SEM.

4.5 Imaging-based assays

4.5.1 Proximity Ligation Assay (PLA)

Cells were grown in coverslips and fixed with 4% PFA for 10 minutes at room temperature. PFA was then removed and cells were washed three times with PBS and permeabilized in 0,1% Triton in PBS solution for 10 minutes at room temperature. After

additional three times washing with PBS, one drop ~40 µl of Duolink Blocking solution was added to each coverslip and incubated in a heated humidity chamber for 1 hour at 37°C. Primary antibodies dilution was done in Duolink® Antibody Diluent and one drop of this mixture was added to each coverslip and incubated overnight at 4°C. For a 40 µl reaction, 8 µl of PLA MINUS stock and 8 µl of PLA PLUS stock were added to 24 µl of antibody diluent. Coverslips were washed with Wash Buffer A two times for 5 minutes. Washing buffer was removed, and coverslips were incubated with the diluted PLUS and MINUS probes in a pre-heated humidity chamber for 1 hour at 37°C. Coverslips were then washed two additional times for 5 minutes with Wash Buffer A at room temperature. Duolink Ligation buffer was diluted in high purity water at a 1:5 ratio and ligase was added to the diluted buffer at 1:40 ratio. Coverslips were incubated with the ligation solution in a pre-heated humidity chamber for 30 minutes at 37°C and then washed two times with Wash Buffer A at room temperature. DNA polymerase was diluted in the Duolink amplification buffer at a 1:80 ratio. One drop of amplification solution was added to the coverslips and incubated in a pre-heated humidity chamber for 100 minutes at 37°C. All the downstream steps were carried out in light-sensitive conditions. Coverslips were washed twice with Wash Buffer B for 10 minutes and finally with 0.01 x Wash Buffer B for 1 minute and incubated with a minimal volume of Duolink DAPI Mounting Medium for 15 minutes. Images were obtained using confocal microscopy (Zeiss) with a 20X or 40X objectives.

4.5.2 Indirect Immunofluorescence

Cells were grown in coverslips and fixed with 4% PFA for 10 minutes at room temperature, following three times PBS washing. Cells were then incubated with a quenching buffer (0.12% glycine, 0.2% saponin in PBS) for 10 minutes at room temperature and incubated with a permeabilization buffer (0.2% saponin in PBS) for additional 10 minutes at room temperature. After three times washing with PBS (5 minutes each), cells were incubated with a blocking buffer (10% FBS, 0.2% saponin in PBS) for 1 hour at room temperature. The respective antibody was diluted in the blocking solution according to the manufacturer`s dilution range recommendations. Coverslips were embedded in the prediluted primary antibody solution and incubated at 4 C° overnight. Coverslips were collected and washed three times with the permeabilization buffer (10 minutes each). A FITC conjugated secondary antibody recognizing the host species of the respective primary antibody was diluted in the blocking buffer according to the manufacturer`s dilution range recommendations and add to the samples for 1 hour

at room temperature following three times washing with the permeabilization buffer (10 minutes each) and mounted in DAPI media. Images were obtain using LSM800 Zeiss confocal.

4.6 Statistical analysis

Statistics was performed using GraphPad Prism 8. Significance was estimated using either unpaired Student's t-test with Welch´s correction or Multiple t-test with Bonferroni correction for the *in vivo* project and 2-way ANOVA to analyzes the effect of two independent variables on two continuous dependent variables. p-values below 0.05 ($p<0.05$) were defined as significant. Mean and SEM are reported in the figure legends. FACS data were analyzed using FlowJo_v10, and ImageJ was used for protein and QuPath for cell quantifications.

5. RESULTS

Part I:

Functional interplay between autophagy and NF-κB signaling in the regulation of inflammation.

5.1 The NF-κB pathway and the autophagy process are induced under the same stress conditions.

Autophagy was previously associated with the NF-κB pathway, depending on the stimulus and cell type (125). For this reason, different cell lines were used to study the cellular context-dependence of tumor necrosis factor-alpha (TNFα)-, lipopolysaccharide (LPS)- and genotoxic stress-triggered autophagy, which are well-known NF-κB inducers (Fig. 5-1). Western blotting analysis were performed to evaluate the autophagy level after and during NF-κB activation. Microtubule-associated protein light chain 3 (LC3) is an essential protein for the maturation of the autophagosome and also the most used marker for monitoring the autophagosome formation through the biochemical detection of its membrane-associated form (LC3-II) (177). My results showed an increased amount of LC3-II, suggesting that autophagy is induced not only 30 minutes after TNFα treatment but also rapidly after irradiation or LPS treatment in THP1 and MEF cells. (Fig.5-1A and B). The level of p65 phosphorylation and IκBα degradation was used to measure the activation of NF-κB at the same time points. Another widely used method to assess autophagosome maturation is through subcellular localization of the green fluorescent protein (GFP)-fused LC3 (177). Human osteosarcoma U2OS cells stably expressing GFP-LC3 were used for this purpose. The appearance of multiple LC3-positive punctate structures suggested an increase of autophagosome formation in U2OS cells at 1-hour post-irradiation (IR) or post TNFα treatment compared to the untreated control and the *bona fide* induction of autophagy by nutrient starvation (EBSS), confirming TNFα- and DNA damage-induced autophagy (Fig.5-1C). However, these methods are not fully sufficient for the estimation of autophagic activity, which is a dynamic process. Thus, these results were confirmed by LC3 Turnover Assay in the presence or not of Bafilomycin A1, an inhibitor of the late phase of autophagy, which is based on the observation that LC3-II is degraded in autolysosomes (Fig.5-1D; See also Materials and Methods paragraph 4.1.3).

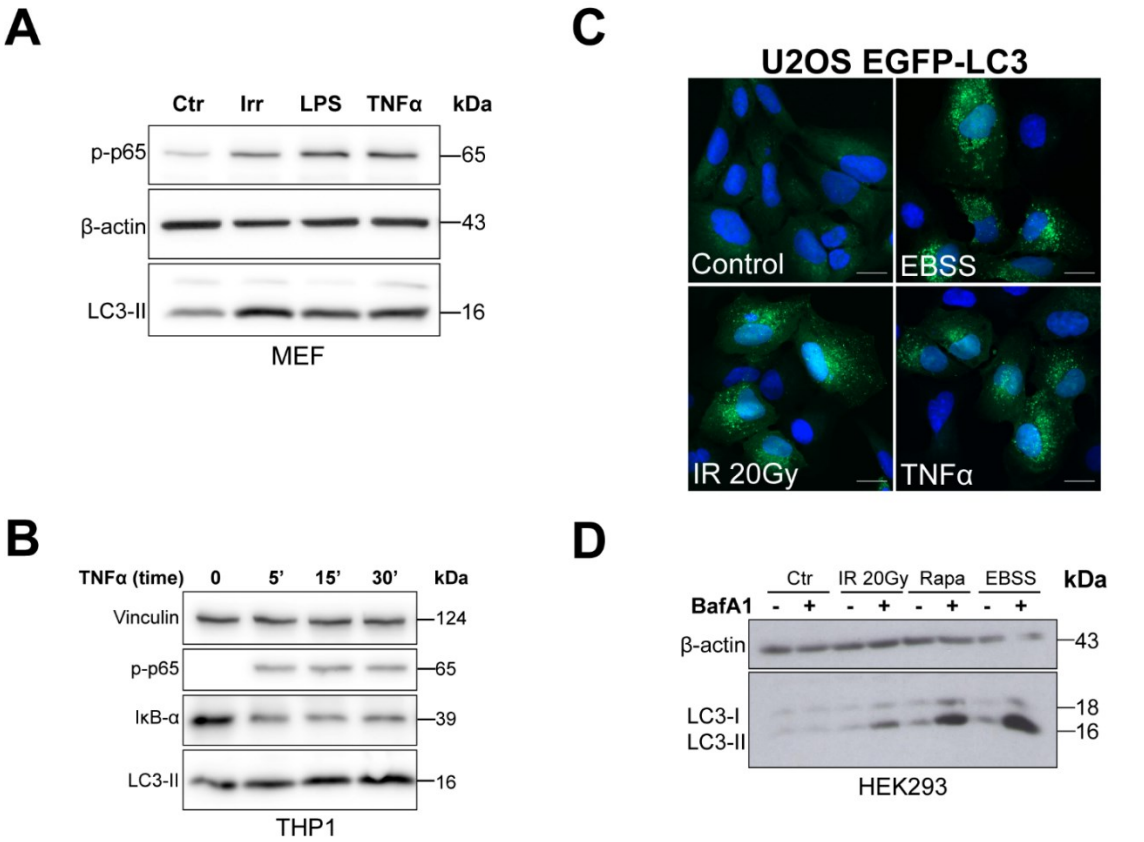

Figure 5-1: Autophagy induction after NF-κB activation in different cell lines. (A, B) Western blot (WB) analysis for the autophagy protein marker LC3, phosphorylated NF-κB subunit p65 and IκBα proteins after 90 min irradiation (80 Gy), 1-hour LPS (10µg) or TNFα (10ng) treatment in embryonic fibroblasts (MEF) (A) or after TNFα (10ng) treatment in monocytic leukemia cells (THP1) (B) at different time points as indicated. **(C)** U2OS osteosarcoma cells stably expressing GFP-LC3 were used in a GFP-LC3 puncta formation assay and analyzed 1 hour after irradiation (20 Gy) or TNFα treatment. Earle's Balanced Salt Solution (EBSS) for starvation treatment was used as autophagy positive control. Images are representative fluorescence confocal microscopic photographs (scale bars 20 µm). **(D)** HEK293T cells were pre-treated with Bafilomycin A1 (200 nM) or DMSO (negative control) for 2-hours and analyzed by WB 1-hour after irradiation (IR 20 Gy). Rapamycin and starvation treatments were used as positive controls for autophagy induction. All data are representative of n=3 independent experiments.

5.2 p65 binds to LC3s/GABARAPs in the nucleus after NF-κB activation.

A recent study showed that a number of LC3B (MAP1LC3B) interacting proteins are present in the nucleus where they control various activities. Interestingly, NF-κB pathway components including IKK subunits, IκBα or RelA/p65 were also found among the nuclear interacting proteins in the same analysis (178,179) suggesting that nuclear

autophagy could be involved in the regulation of NF-κB. For this reason, A549 cells were used to visualize a possible co-localization of NF-κB/p65 subunit and the autophagy protein LC3. Data showed co-localization of p65 with LC3 at 90 minutes post-irradiation and 60 minutes after TNFα treatment in the nuclear compartment compared to the control (untreated), suggesting a strong interaction after NF-κB activation (Fig. 5-2A). A method to detect protein interactions with high specificity and sensitivity is the Proximity Ligation Assay (*in situ* PLA) which was previously used to study the dynamics of NF-κB regulation (180). This technology was performed to investigate a co-localization of LC3 with p65. Results showed that the endogenous proteins, LC3 and p65, bound mainly in the cytoplasm in untreated cells and that their interaction increased in the nucleus after stimulation with TNFα or irradiation (Fig. 5-2B).

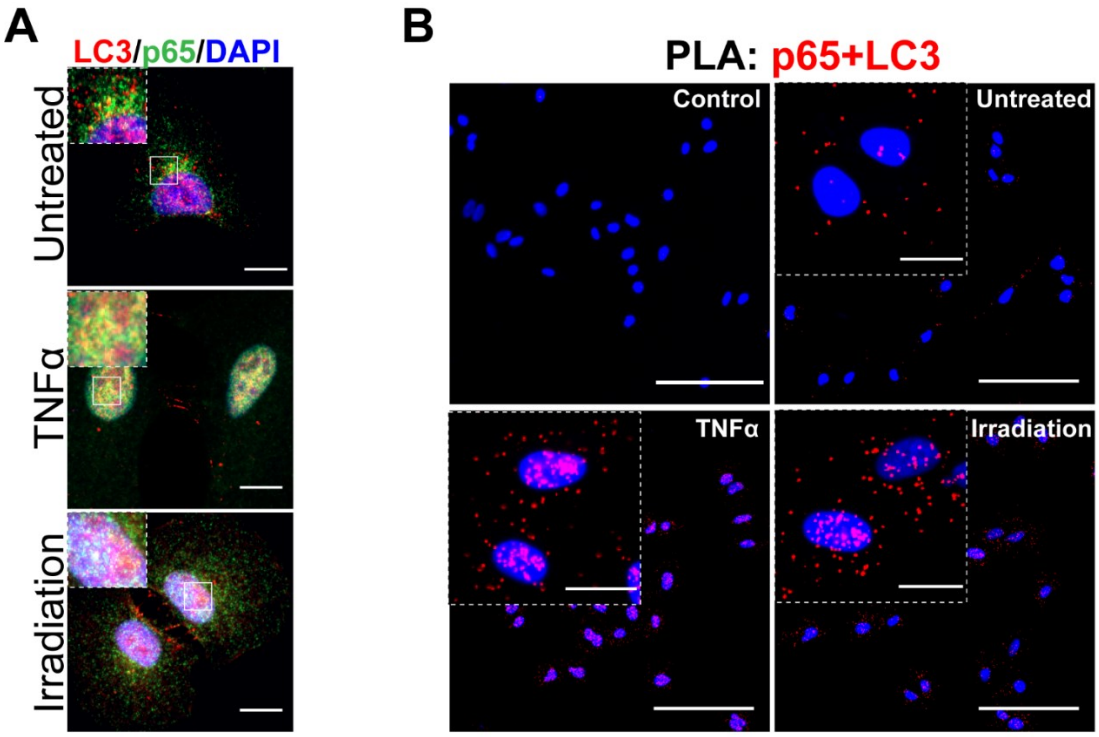

Figure 5-2: LC3 and p65 binding increased in the nucleus after NF-κB activation. (A) Immunofluorescence staining for LC3 (red) and p65 (green) using A549 cells in untreated, TNFα and irradiation conditions. Nuclei were stained with DAPI. The images shown are representative fluorescence confocal microscopic photographs (scale bars 10 µm). **(B)** Proximity Ligation Assay (PLA) was used to demonstrate the direct binding between LC3 and p65 after TNFα (10 ng) or irradiation (20 Gy) treatments using A549 adenocarcinoma cells. Cells stained only with p65 antibody were used as negative technical control. Each red spot represents a single interaction. Nuclei were stained with DAPI. Scale bars: 50 µm and 20 µm (insets).

To study the interaction between LC3-related proteins and p65, I performed *in vitro* pull-down experiments using GST-tagged ATG8 protein family members as affinity baits. Endogenous p65 but also overexpressed Myc-tagged p65 were captured from cell lysates by all four LC3-like modifiers, but not by mono- or tetra-ubiquitin (negative controls) indicating that p65 does not possess ubiquitin-binding abilities (Fig. 5-3A and D). To further define the interaction between p65 and LC3s/GABARAPs, I analyzed LC3 mutants. Endogenous p65 did not bind when the pull-down was performed with LC3 protein family members lacking the unique amino-terminal region or with LC3B mutated in the LIR-binding pocket which is important for recognition and interaction mechanisms (Fig. 5-3B and C). The same results were obtained with overexpressed Myc-tagged p65 (Fig. 5-3E and F). This indicated that p65 interacts with LC3 through a classical LIR motif (LC3 Interacting Region) or through ubiquitin cargo receptors (85,181).

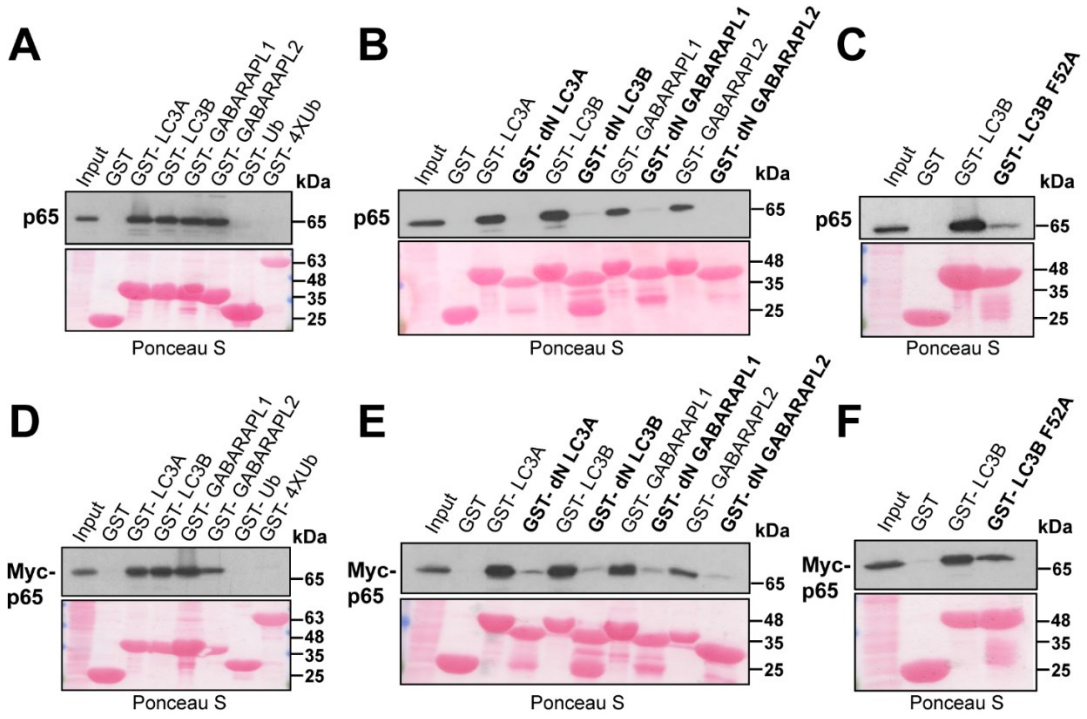

Figure 5-3: GST-tagged LC3s/GABARAPs pull down. (A-C) HEK293T cell lysates were added to beads with immobilized GST fusion LC3-like modifiers (GST, GST-LC3A, GST-LC3B, GST-LC3C, GST-GABARAP, GST-GABARAP-L1, GST-GABARAPL2, GST-Ub, GST-4XUb (A) or the LC3 like modifiers lacking the unique N-terminus (dN) (B) and GST-LC3BF52A-V53A (C)), followed by WB using an antibody against endogenous p65. **(D-E)** HEK293T cells were transfected with the Myc tagged p65. Cell lysates were added to beads with the followed immobilized GST-fusion LC3-like modifiers, followed by WB using an antibody against Myc tag**.** All data are representative of n≥3 independent experiments.

5.3 LC3s/GABARAPs interact with the Rel Homology Domain of NF-κB/p65 subunit through an ubiquitin cargo receptor.

To characterize the binding site of p65 that interacts with ATG8 protein family members, C-terminal and N-terminal deletion mutants of p65 were generated. Pull-down experiments showed that LC3 interacts with the RHD domain of p65 between amino acids 193 to 306 (Fig. 5-4A and B). Bioinformatics analysis of the p65 protein sequence revealed the presence of eight putative LIR motifs (https://ilir.warwick.ac.uk, (182)). It has been shown that the substitution of the two hydrophobic amino acids within the LIR motif is sufficient to ablate the interaction with ATG8 protein family members (183). For this reason, sequential mutagenesis and *in vitro* pull-down of each of the p65 LIR mutants was performed. None of the single LIR mutants completely lost the interaction with LC3s/GABARAPs (data not shown). Degradation of selective material (cargo) can be mediated also by specific cargo receptors that are able to recognize damaged organelles, pathogens, or over-abundant proteins and aggregates. A high number of cargo receptors have been reported (184). Many of the receptors present a UBA domain through which they bind to the ubiquitinated cargo and an LIR domain to bind the autophagosome membrane for the following degradation. Adding N-ethylmaleimide (NEM), an inhibitor of deubiquitinases, to the protein lysates made it possible to evaluate if the binding between p65 and LC3 is ubiquitin-mediated. As shown in figures 5-4C and D, GST-LC3 is able to bind to p65 and the NF-κB binding complex proteins (p50 and IκBα) only in the presence of NEM, suggesting that their interaction depends on ubiquitin-conjugation (Fig. 5-4C and D).

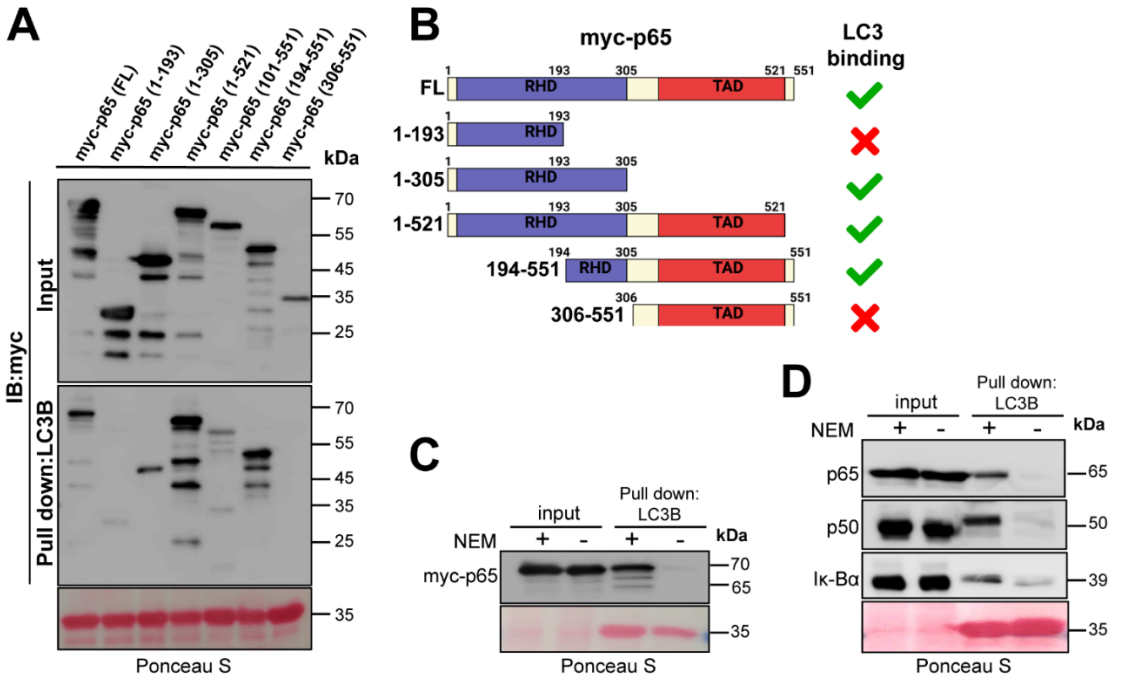

Figure 5-4: Autophagy proteins interact with the RHD of p65 through ubiquitin. (**A**) Full-length Myc-p65 and truncation mutants have been transfected into HEK293T cells. Cell extracts were added to beads with immobilized GST-LC3B and immunoblotted for Myc. LC3B was able to bind only the truncation mutants including residues 193 to 306. (**B**) Schematic representation of Myc-p65 full length (FL) and truncation mutants highlighting which of them bind LC3. (**C, D**) HEK293T cell lysates were added to GST-LC3B in presence or absence of NEM (N-ethylmaleimide). Both, overexpressed Myc-p65 (C) and endogenous p65, including p65-associating p50 and IκBα (D), bind to LC3B only in the presence of NEM. All data are representative of n=3 independent experiments.

5.4 Autophagy influences stress-induced NF-κB activation.

In order to understand if autophagy can influence the NF-κB transcriptional activity, I used the NF-κB reporter (luc)-HEK293 cell line. This cell line was designed for the specific monitoring of the NF-κB signal transduction pathway *in vitro* by the detection of luciferase (see Materials and Methods chapter 4.1.7). The NF-κB reporter (luc)-HEK293 cell line was treated with TNFα or irradiation in the presence (or absence) of chloroquine, an inhibitor of autophagy flux by decreasing autophagosome-lysosome fusion and degradation (Fig. 5-5A, right panel). Cells were transfected with Renilla luciferase reporter vector 24 hours before treatment as internal control for data normalization. Results showed a significant increase in NF-κB luciferase activity after TNFα or irradiation treatment in presence of chloroquine compared to its absence (Fig. 5-5A, left panel), suggesting that autophagy degradation impairment can modulate the NF-κB

response. To assess this hypothesis, the NF-κB reporter cell line was treated using the same stress conditions (TNFα or irradiation), but this time in the presence (or not) of rapamycin, the most common inhibitor of mTOR, which is able to consequently hyperactivate autophagy (Fig. 5-5A, right panel). As expected, rapamycin significantly reduced NF-κB luciferase activity (Fig. 5-5A, left panel). Recent mechanistic insights into the autophagic machinery revealed the importance of ATG16L1 protein as an essential autophagy component required for efficient LC3 lipidation and autophagosome maturation (185,186). Thus, expression of various NF-κB target genes was examined after TNFα treatment using HEK293 cells depleted for both, α and β isoforms of ATG16L1 (*16L1* knock-out (KO)) (Fig. 5-5B) (187). mRNA expression of pro-inflammatory chemokines (*CCL20, TNFα*) was significantly upregulated in presence of TNFα in *16L1* KO cells when compared to wild-type cells (WT) (Result Fig. 5-5B, left panel). Interestingly, HEK293 *16L1* KO cells stably expressing only the *ATG16L1β* isoform (*16L1* KO + *16L1β*), which is known to be sufficient to rescue the autophagic flux (187) significantly decreased *CCL20* and *TNFα* gene expressions (Fig. 5-5B, left). Together, my results indicate that the activation of NF-κB is altered when autophagy degradation is impaired.

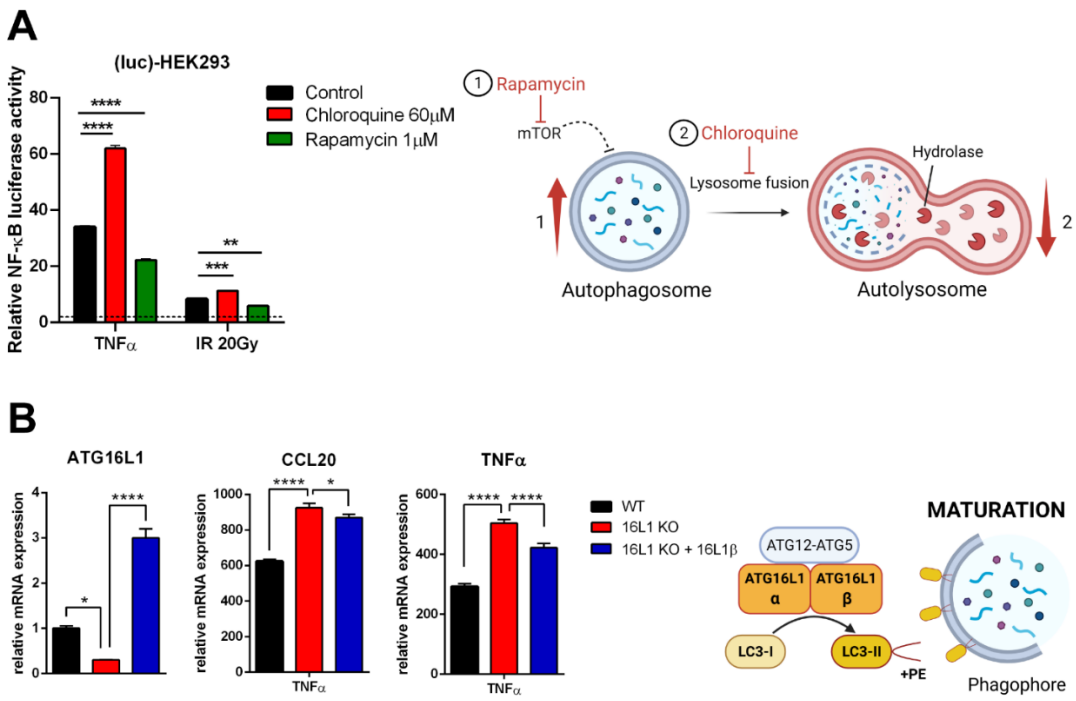

Figure 5-5: Autophagy degradation significantly influences NF-κB activation. (**A, left**) The NF-κB reporter (luc)-HEK293 cell line was treated with TNFα (10 ng) or irradiation (20 Gy) in the presence or absence of chloroquine (60 μM) or rapamacyn (1 μM). Cells were harvested 5 h after treatment and were subjected to luciferase activity analysis. Renilla luciferase reporter vector was used as internal control. (**A,**

right) Schematic representation of rapamycin (1) and chloroquine (2) inhibitory functions. (**B, left**) mRNA expression of *ATG16L1, CCL20*, and *TNFα* genes was detected by real-time RT-qPCR in WT and *ATG16L1* KO HEK293 cells rescued or not with *ATG16L1β* and treated with TNFα (10 ng). Results are normalized to their controls, respectively. Data are means ± SEM of three or more independent experiments. Statistical analyses were performed by Two-way Anova followed by Bonferoni's multiple comparison test (*p < 0.05, **p<0.01, ***p<0.001) using GraphPad Prism 8. (**B, right**) Schematic representation of the ATG16L1 complex function essential for the phagophore maturation. Illustrations were created with BioRender.com.

5.5 LC3s/GABARAPs bind p65 through the cargo receptor SQSTM1/p62.

The SQSTM1 protein (p62) has been reported as the major cargo receptor able to deliver proteins for degradation to the autophagosome (188,189). Interestingly, previous studies proposed a role of p62 also as a protein adapter able to regulate signal transduction in NF-κB pathways through the interaction with TRAF6 and RIP1 (190,191). However, its potential role in binding and targeting polyubiquitinated NF-κB subunits to the autophagosome during stress conditions needs to be investigated. Thus, I decided to study whether LC3 binds to p65 through the cargo receptor p62. First, I performed immunoprecipitations after transient overexpression of p62-GFP wild-type (WT) or of a p62 mutant that lacks the UBA domain involved in binding to ubiquinated substrates (ΔUBA; (192)). Endogenous p65 is indeed able to bind to full-length p62-GFP (WT), but only in a greatly reduced manner to the ΔUBA mutant, confirming that their interaction is promoted by ubiquitin conjugation (Fig. 5-6A). Next, PLA analysis using U2OS cells stably expressing GFP-LC3 was performed to evaluate the possible binding between p62 and p65 at the level of the autophagosome membrane. My results suggested a co-localization of p62 and p65 with LC3-positive punctiform structures, which seems to increase in the proximity of the nucleus under stress conditions (see yellow arrowheads Fig.5-6B). Immunofluorescence analysis still revealed that p62 and p65 proteins co-localized in the cytoplasm in untreated cells, and localisations increased in the proximity of the nucleus after TNFα or irradiation treatment (Fig. 5-6C). To finally prove my previous results, immunoprecipitation of endogenous p65 followed by immunoblot for anti-p62 was performed, confirming again that their interaction increased after TNFα induced NF-κB activation, as suggested by the decreased IκBα protein level (Fig. 5-6D). Collectively, these findings are a further indication that autophagy could control the protein level of p65 in the nucleus after activation through p62 binding.

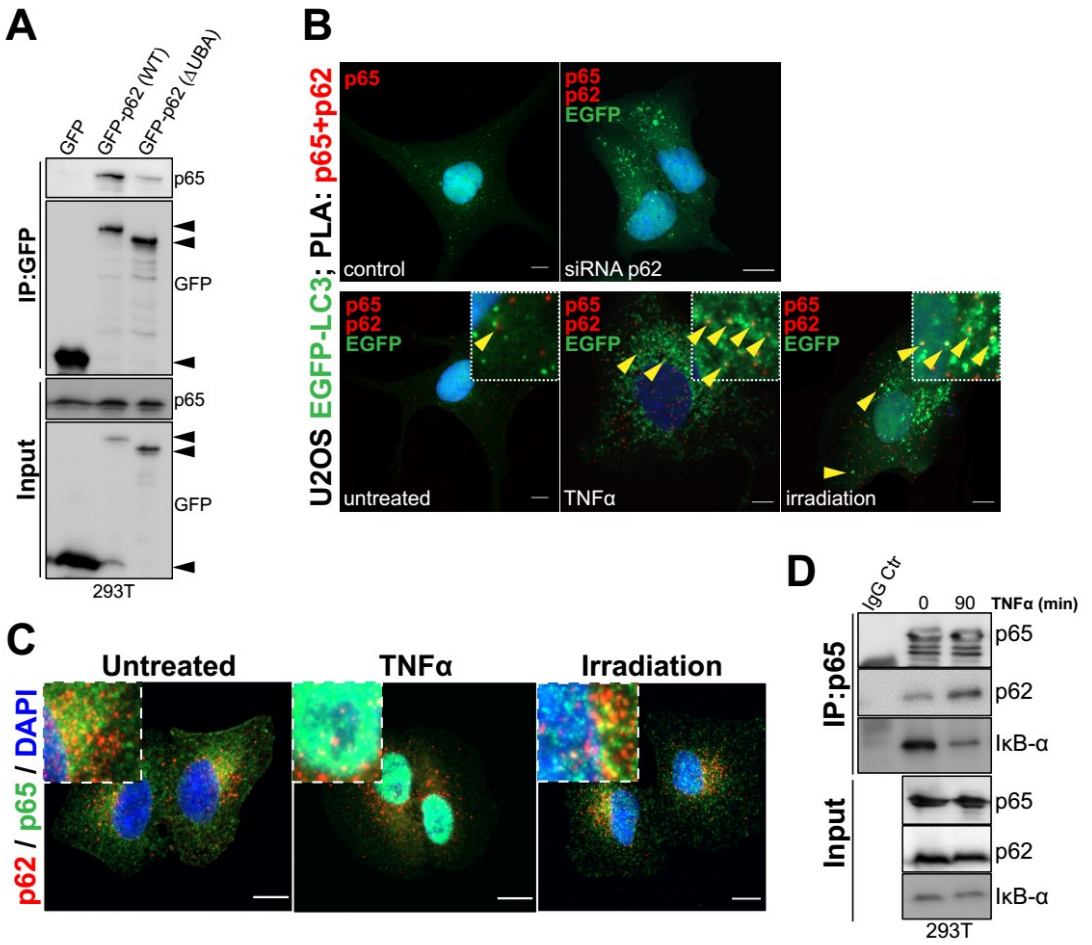

Figure 5-6: LC3 binds p65 through p62. (**A**) HEK293T cells were transfected with empty GFP vector (control), WT, or ΔUBA deleted mutant of GFP-tagged p62. After 24 hours, cell lysates were immunoprecipitated with GFP-Trap beads and immunoblotted for GFP fusion proteins and p65. (**B**) PLA between p65 and p62 (red spots) was performed in U2OS cells stably expressing GFP-LC3 (green spots). Top panels are representative images of cells stained only with p65 antibody (top left panel) or cells prior transfected with p62 siRNA (top right panel) which were used as negative technical controls. Bottom panels are representative images of PLA performed in untreated, TNFα (10 ng) or irradiation (20 Gy) conditions. Each red spot represents a single interaction of p62 and p65 proteins. Yellow arrowheads point to p62-p65 interacting proteins (PLA red signals) that co-localize with LC3 puncta structures (autophagosome in green). Nuclei were stained with DAPI. Scale bars 10 µm. (**C**) Immunofluorescence staining for p62 (red) and p65 (green) using A549 cells in untreated, TNFα and irradiation conditions. Nuclei were stained with DAPI. Images are representative fluorescence confocal microscopic photographs (scale bars 10µm). (**D**) HEK293T cell extracts were harvested at 0 or 90 minutes after TNFα treatment followed by immunoprecipitation (IP) with anti-p65 antibody and WB analysis with the antibodies indicated. IgG was used as IP control.

5.6 SQSTM1/p62 depletion increases early stress-induced NF-κB activation.

As briefly mentioned above, it has been reported that p62 overexpression or activating Paget's disease of the bone (PDB) mutations in vitro and in vivo leads to SQSTM1/p62 protein accumulation which can activate NF-κB via its TRAF6 binding motif downstream of cell stimulation by interleukin 1 (IL-1), RANK ligand (RANKL), or nerve growth factor (NGF) (191,193–195). Additionally, persistent impairment of autophagic degradation was also shown to trigger the activation of NF-κB as a result of p62 accumulation (196). My results showed that after 5 hours, while stress induced-autophagic degradation was active (Fig. 5-1), *p62* mRNA expression was not induced by TNFα and irradiation (Fig. 5-7).

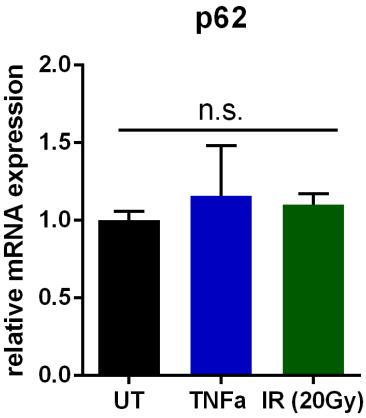

Figure 5-7: mRNA expression of SQSTM1/p62 does not change after TNFα or irradiation-induced NF-κB activation. RT-qPCR analysis of *p62/SQSTM1* expression in HEK293 cells after 5 hours of treatment with TNFα (10 ng) or irradiation (20 Gy). Results are normalized to the unstimulated (UT) control. Data are means ± SEM of three or more independent experiments. Statistical analyses were performed by one-way ANOVA followed by Bonferroni's multiple comparison test (n.s.= not significant) using GraphPad Prism 8.

Thus, the choice to study NF-κB activation at early time points excludes any effect that the accumulation of p62 protein could exert. In addition, using different inducers, like TNFα or genotoxic stress, which stimulate different NF-κB activation pathways, would help to exclude additional factors that can influence the experimental read-out. In order to further explore whether autophagy influences NF-κB activity through selective binding of p62 to p65, NF-κB luciferase reporter assays were performed after knocking down p62. The NF-κB reporter (luc)-HEK293 cell line was transfected with two different siRNAs against p62 48 hours before treatment with TNFα or irradiation and luciferase activity was measured as previously described. Data showed a significant increase in NF-κB luciferase activity after TNFα or irradiation treatment when p62 was downregulated (Fig.

5-8A) which was also reflected by the increased expression of NF-κB pro-inflammatory target genes (Fig. 5-8D). The p62 siRNA knockdown efficiency was confirmed by western blotting and RT-qPCR (Fig. 5-8B and C).

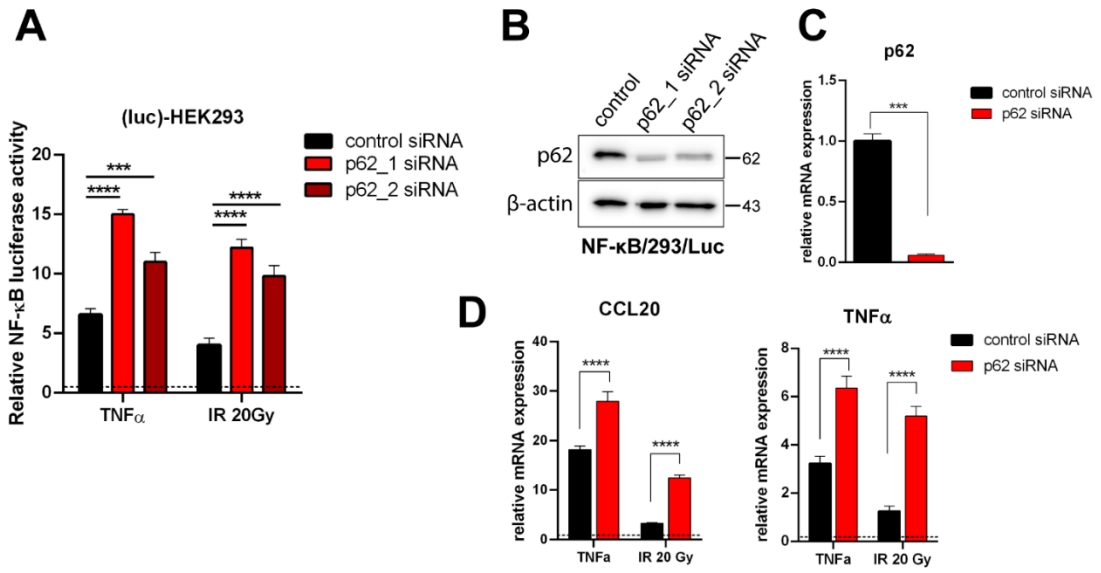

Figure 5-8: SQSTM1/p62 restricts NF-κB activation. (**A**) The NF-κB reporter (luc)-HEK293 cell line was treated with TNFα (10 ng) or irradiation (20 Gy) 48 hours after siRNA transfection. Cells were harvested 5 hours after treatment and were subjected to luciferase activity analysis. Renilla luciferase reporter vector was used as internal control. (**B**) Western blot analysis of p62 confirming the siRNA knockdown efficiency. β-actin is used as loading control. (**C**) p62 mRNA expression in HEK293 cells 48 hours after transfection with siRNA control or a mixture of two siRNA targeting p62; (**D**) *CCL20* and *TNFα* mRNA expression was detected by real-time RT-qPCR in HEK293 cells expressing control or p62-specific siRNAs and analyzed 5-hours after TNFα (10 ng) treatment or irradiation (IR 20 Gy). Results in A, C, and D are normalized to the unstimulated controls, respectively. Data are means ± SEM of three or more independent experiments. Statistical analyses were performed by Two-way Anova followed by Bonferroni's multiple comparison test (***p<0.001, ****p<0.0001) using GraphPad Prism 8.

5.7 SQSTM1/p62 attenuates NF-κB activity through its autophagic activity.

Previously, it has been proposed that autophagy could trigger p65 degradation (197–199), but the mechanism of action is still debated. To further prove that autophagy can inhibit NF-κB activation through selective degradation of p65, confocal imaging analysis was performed to visualize co-staining of p65 and lysosome-associated membrane glycoprotein (LAMP1), a well-known lysosomal marker (Fig. 5-9A) (200). Autophagolysosomal degradation is a very dynamic process. Therefore, to assess the

autophagy-/lysosome-dependent clearance of p65, bafilomycin A1, a potent V-ATPase inhibitor (as described above in Results 5.1) was used. U2OS cells were pre-treated or not with bafilomycin A1 and immune stained 5 hours after TNFα treatment. Results showed increase co-localization between p65 and LAMP1, as well as between p65 and LC3 after TNFα stimulation compared to control, when bafilomycin A1 was added (Fig. 5-9A). These data suggested that p65 is delivered to the lysosome mainly after activation, probably to attenuate prolonged inflammation-driven NF-κB expression and to promote transcriptional termination, as previous results suggested (see Fig. 5-5B and 5-8D). Cycloheximide (CHX)-chase experiments were performed to determine the turnover rates of p65 protein after activation (Fig. 5-9B and C). Since different protein production rates influence the measurements of protein turnover (201), cells were transiently transfected with Myc-p65 24 hours before treatment to avoid the influence of p65 expressed asynchronously. Subsequently, cells were stimulated for 15 min with TNFα and chased for four-time points (0-6 h) by cycloheximide addition in a fresh medium. The abundance of the Myc-p65 protein was analyzed at specific time points by western blot analysis, revealing a significant protein reduction at 6 hours and a half-life between 3 and 6 hours. Moreover, immunoprecipitation of overexpressed GFP-LC3 showed initial binding with endogenous p65 at 1 hour which increased at 3 hours and is lost at 6 hours after TNFα treatment (Fig. 5-9D). Saccani et al. (2004) proposed that p65 sequestered to its specific DNA binding sites is degraded by the proteasomal pathway (49). In order to clarify if autophagy plays also a role in regulating the protein level of p65 after TNFα treatment, I performed the cycloheximide-chase assay with co-treatment or not of a proteasomal (MG132), or an autophagy-lysosome (chloroquine, CQ) inhibitor. Surprisingly, Myc-p65 protein degradation was only partially blocked by proteasome inhibition (Fig. 5-9E, upper panel), contrary to chloroquine which was able to completely rescue its protein level (Fig. 5-9E, bottom panel), suggesting autophagy as an alternative mechanism responsible for p65 degradation after NF-κB activation.

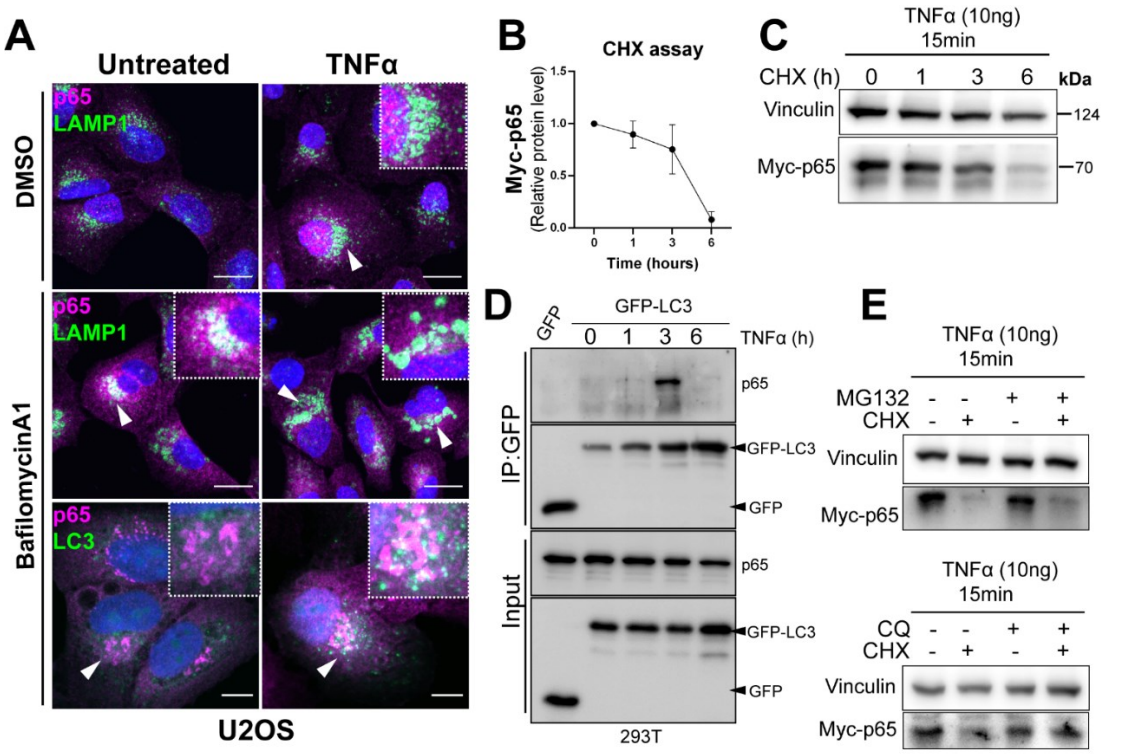

Figure 5-9: Lysosomal degradation of NF-κB/p65. (**A**) Immunofluorescence staining for p65 (magenta) and LAMP1 or LC3 (green) using U2OS cells pre-treated 30 minutes with bafilomycin A1 (200 nM) or DMSO (control) in untreated and TNFα (10 ng) stimulated conditions. DAPI was used for the staining of nuclei. Z-stack images shown are representative fluorescence confocal microscopic photographs (scale bars 20 µm). (**B, C**) Cycloheximide-chase assay performed in HEK293 transfected with Myc-p65 plasmid 24 hours before treatment. Cells were washed once after 15 minutes of TNFα stimulation and cycloheximide was added. The time course was performed for a total of 6 hours as shown in the graph and analyzed by western blot at the times indicated using an antibody against Myc (B). Vinculin is used as loading control and quantification of the protein abundance was done using ImageJ (C). (**D**) HEK293T cells were transfected with GFP empty vector (control) or GFP-LC3. After 24 hours, cells were treated with TNFα (10 ng) and cell lysates were collected at the time points indicated. Immunoprecipitation was performed with GFP-Trap beads and samples immunoblotted for GFP fusion protein and p65. (**E**) HEK293 were transfected with Myc-p65 plasmid 24 hours before the 15 minutes TNFα treatment. Cells were washed once and cycloheximide was added for 6 hours with or without MG132 (10 µM) or chloroquine (CQ, 60 µM). Western blot analysis was performed using antibodies against Myc and Vinculin. All data are representative of n=3 independent experiments.

5.8 Autophagy modulates inflammation-driven NF-κB expression in macrophages affecting nuclear p65 protein abundance.

Macrophages are heterogeneous immune cells and can be generally classified into two phenotypes with distinct functions: classically activated M1 (immune active) and

alternatively activated M2 (immunosuppressive) cells (202). Autophagy plays an important role in innate immunity by degrading intracellular pathogens but also participating in the regulation of inflammatory cell response during macrophage polarization. In addition, the NF-κB family of transcription factors is a well-known key regulator of macrophage polarization through the expression of numerous inflammatory genes by both toll-like receptors (TLRs) and intracellular pathogens (112,203). However, the complex interplay between NF-κB and autophagy in macrophage polarization and their specific role in modulation the inflammatory response remains to be fully investigated. Interestingly, Chang et al. (2013) showed for the first time that hepatoma-derived TLR2 signals can drive macrophage polarization towards the M2 phenotype through selective autophagic degradation of p65/NF-κB (204). This recent evidence prompted me to further validate the previous results using murine macrophage RAW264.7 cells and human monocytic THP1 cells as functional models for the current study. Lipopolysaccharide (LPS) is a potent pro-inflammatory pathogen-associated molecular pattern that is able to induce both NF-κB and autophagy signaling pathways via Toll-like receptor 4 (TLR4) in macrophages (Fig.5-1A) (113,205,206) and, for this reason, was used as a treatment condition for the following analysis. RAW264.7 cells depleted (knock-out, KO) or not (wild-type, WT) of the autophagy gene *ATG16L1* were used to study the expression of NF-κB inflammatory target genes (*TNFα, IL8, IL6* and *IL1 α* and *β*) in response to LPS (Fig. 5-10A) (187). Data showed significant overexpression of NF-κB induced-cytokines after LPS treatment in absence of autophagy (*ATG16L1* KO) compared to wild-type (WT). Interestingly, autophagy rescued cells (KO + *ATG16L1β*) were sufficient to reduce significantly the cytokine expressions at the level of WT macrophages (Fig. 5-10A). It has been shown that p62 undergoes fast nucleo-cytoplasmic shuttling through two nuclear localization signals and one nuclear export signal, but little is known about its possible nuclear roles (188). Co-localization of p62 and p65 was also observed in the proximity of the nuclei after stress-induced NF-κB activation (Fig. 5-6B and C). In order to determine if p62 controls a fraction of nuclear p65 in response to LPS treatment, immunoprecipitation of endogenous p65 was performed in cytoplasmic and nuclear fractions from THP1 cells. Although p62 co-immunoprecipitated with p65 mainly in the cytoplasm, a small quantity of their binding was also found in the nucleus after LPS-induced NF-κB activation (Fig. 5-10B). Nucleo-cytoplasmic shuttling of p62 before (UT) and after LPS treatment was further confirmed using Leptomycin B (LMB) which is a potent and specific nuclear export inhibitor (Fig. 5-10C) (207) suggesting that p62 could potentially bind p65 in the nucleus and translocate it to the cytoplasm where they are accumulated together with LC3 for autophagic

degradation. To finally determine the impact of autophagy on the oscillatory dynamics of NF-κB/p65 after activation, nuclear translocation of p65 subunit in response to LPS treatment was quantified in a time-dependent manner by western blotting. My results indicated significantly increased and prolonged permanence of p65 in the nucleus at 3 and 6 hours after LPS stimulus in autophagy knock-out macrophages (*16L1* KO) compared to wild-type control (WT) (Fig. 5-10D and E). Collectively my data revealed a potentially novel role for the cargo receptor p62 in trafficking nuclear ubiquitinated p65 subunit to autophagosomes for degradation in a time-dependent manner in response to stress to control inflammation-driven NF-κB hyperactivation.

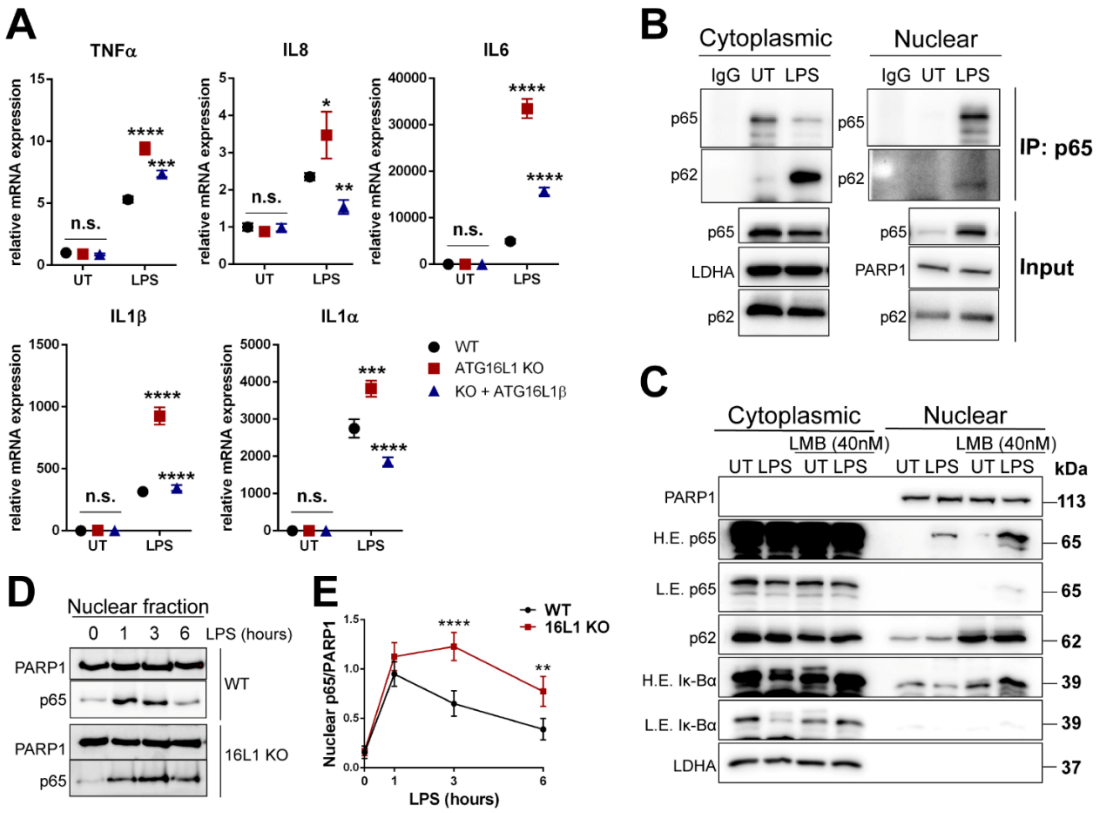

Figure 5-10: Autophagy impairment affects inflammation and p65 nuclear retention. (**A**) mRNA expression of *TNFα*, *IL8, IL6, IL1α* and *IL1β* genes was detected by real-time RT-qPCR in WT and *ATG16L1* KO RAW 264.7 cells rescued or not with *ATG16L1β* (KO + *ATG16L1β*) and treated with LPS (10 μg). Results are normalized to untreated WT cells (UT) as controls. Data are means ± SEM of three independent experiments. Statistical analyses were performed by Two-way Anova followed by Bonferroni's multiple comparison test (*p < 0.05, **p<0.01, ***p<0.001, ****p<0.0001) using GraphPad Prism 8. (**B**) Cytoplasmic and nuclear fractions from THP1 cells were extracted at 0 or 90 min after LPS (10 μg) treatment for immunoprecipitation (IP) with anti-p65 antibody, followed by WB analysis with anti-p65 or anti-p62 antibodies. LDHA and PARP1 antibodies were used as loading controls for cytoplasmic and nuclear fractions, respectively. IgG was used for IP control. (**C**) Western blotting of cytoplasmic and nuclear extracts from THP1 cells pre-treated with leptomycin B (LMB 40 nM) for 4-hours followed by 90 min LPS (10 μg)

treatment. Antibodies against IκBα and p65 (H.E. high exposition and L.E. low exposition) were used as NF-κB activation and LMB treatment controls. LDHA and PARP1 antibodies were used as loading controls for cytoplasmic and nuclear fractions respectively. (**D, E**) Nuclear extracts from WT and ATG16L1 KO RAW 264.7 cells were collected at the time points indicated after LPS (10µg) treatment and analysed by WB (D) for p65. PARP1 is used as nuclear loading control. Quantifications of the protein abundance (E) was measured using ImageJ and statistical analysis was performed by Two-way Anova followed by Bonferroni's multiple comparison test (**p<0.01, ****p<0.0001) using GraphPad Prism 8.

Part II:

NF-κB in cell fate decisions and stem cell maintenance in the small intestinal epithelium.

5.9 NF-κB activity in the crypts of the small intestine.

The function of canonical NF-κB activity in context of colon carcinoma and inflammatory bowel disease (IBD) is well defined (146,208,209). Either constitutive NF-κB activation or intestinal epithelial cell (IEC)-specific deletion of components of the NF-κB signalling pathway was shown to lead to inflammation through infiltration of immune cells which resulted in increased IEC death and tissue damage (139). However, the role of NF-κB signaling in the homeostasis of the small intestinal (SI) epithelium remains unknown. In order to study NF-κB activity in the intestinal epithelium under physiological conditions, I used an NF-κB reporter mouse line which expresses the green fluorescent protein EGFP under control of the NF-κB consensus binding site in the Igκ light chain enhancer (*κ-EGFP*; (210)). Furthermore, I used a mouse model with ubiquitously suppressed NF-κB activity (here referred to as *ΔN*), in which NF-κB activation is prevented by ubiquitous expression of the NF-κB super-repressor *IκBαΔN* under control of the endogenous β-catenin (*ctnnb1*) promoter which however does not impair expression and activity of the β-catenin protein (136,211). High EGFP expression is shown in the crypts of the SI in *κ-EGFP* mice when compared to offspring resulting from cross-breeding *κ-EGFP and ΔN* mice (*κ-EGFP;ΔN*) (Fig. 5-11A, B).

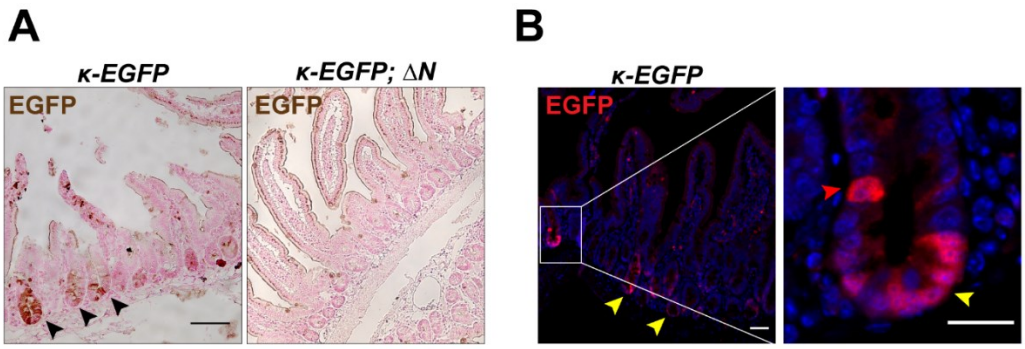

Figure 5-11: Analysis of NF-κB activity in the SI epithelium using *κ-EGFP* reporter mice. (A) Representative images of EGFP immunohistochemistry (IHC; DAB (brown) performed on SI tissue sections of *κ-EGFP* reporter mice. SI tissue from *κ-EGFP; ΔN* mice was used as a negative control for staining specificity. Black arrowheads indicate NF-κB activity at the bottom of the SI crypts. Scale bar: 100 µm. **(B)** Indirect immunofluorescence of EGFP in *κ-EGFP* reporter mice. Inset shows higher magnification of a single

SI crypt with EGFP expression/NF-κB activity. Scale bar: 20 µm. Yellow arrowheads indicate EGFP staining at the bottom of the crypts and red arrowhead points to +4/TA positions.

The SI crypt base consists of highly proliferative intestinal stem cells (ISC) interposed between Paneth cells (see introduction chapter 1.10 and Fig. 5-12A). To understand which cell types displayed NF-κB activity, co-staining of EGFP with Alcian blue (Fig. 5-12B, left panel) or intestinal stem cell (ISC) marker Olfm4 (Olfactomedin 4; (212)) (Fig. 5-12B, right panel) was performed. The results revealed NF-κB activity mainly in Paneth cells, which are characterized by the production of electro-dense vesicles filled with lysozyme (Fig. 5-12B). However, NF-kB activity was also observed in +4/TA (transit-amplifying) cell positions in which potential early secretory progenitors are located, as well as in occasional CBCs (Fig. 5-12B; (158,166)).

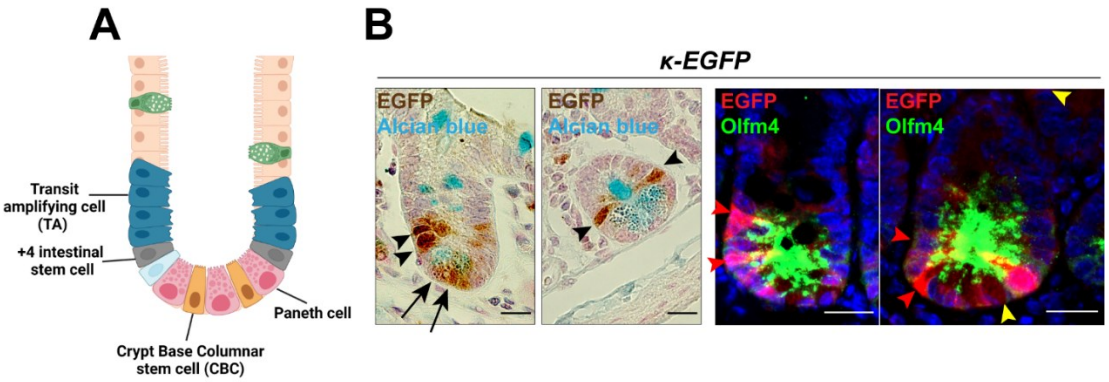

Figure 5-12: Cell type-specific NF-κB activity in SI crypts. (A) Schematic representation of a SI crypt and its cell types. Illustrations were created with BioRender.com. **(B)** EGFP immunohistochemistry (IHC; DAB (brown) plus Alcian Blue staining (left panels) and IF co-staining of EGFP with Olfm4 antibodies (right panels) on SI sections of *κ-EGFP* mice (n=3). Black arrows or yellow arrowheads point to Paneth cells; black or red arrowheads indicate EGFP expression/NF-κB activity in ISCs, mainly in +4 and TA position. Scale bars: 20 µm.

5.10 Analysis of IEC proliferation rate and cell death in *ΔN* mice.

5.10.1 NF-κB activity does not influence the overall proliferation rate of the intestinal epithelium in vivo.

NF-κB is an important regulator of cell fate decisions (213). Ki67 staining was performed to investigate the proliferative status of IEC in *ΔN* mice lacking NF-κB activity. Ki67 is a

cell proliferation marker that is detectable in actively dividing cells. Quantitative analysis of Ki67-positive cells in SI sections showed no significant change between control and *ΔN* (Fig. 5-13). Nevertheless, a different distribution of proliferating cells in the bottom of the SI crypts was observed in *ΔN* mice in which ISCs occupied the entire crypt base space compared to controls where instead we observed Ki67-positive CBCs adjacent to post-mitotic Paneth cells. This result was supported by previous 5-Bromo-2'-deoxyuridine (BrdU)-pulse/chase method performed in our laboratory (K. Krieger, data not shown; see reference (211)). Similar to Ki67, anti-BrdU staining revealed that, even if the absence of NF-κB activity does not influence the overall proliferative rate of the intestinal epithelium, it appears to lead to altered crypt cell composition.

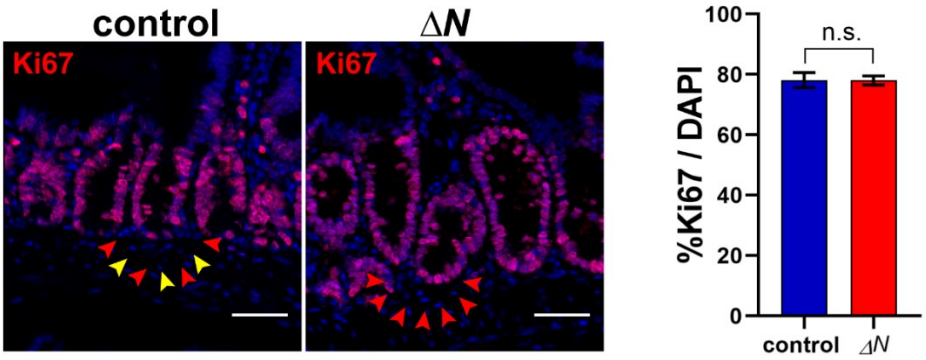

Figure 5-13: Unaltered IEC proliferation rate in *ΔN* mice. (Left panels) Immunofluorescence staining using an anti-Ki67 antibody on small intestine (SI) sections of control and *ΔN* mice (n=3 animals/group). Yellow arrowheads point to Paneth cells; Red arrowheads indicate ISCs. DAPI was used for nuclei staining. The images shown are representative fluorescence confocal microscopic photographs (scale bars 50 µm). **(Right panel)** Quantification analysis of Ki67 positive cells in the SI crypts of control and *ΔN* mice expressed in percentage of total cell numbers (DAPI). n=3/group, n>20 crypts/mouse; Statistical analysis was performed by Unpaired t-test with Welch's correction (n.s.= not significant) using GraphPad Prism 8.

5.10.2 Cell death remains unaltered in the absence of NF-κB activity.

It was shown that intestinal epithelium-specific knock-out of IKKγ (NEMO), a subunit of the IKK complex (see above, Introduction chapter 1.2.2), or of NF-κB subunit p65 induced apoptosis of Paneth cells due to massive intestinal inflammation caused by IEC-specific inhibition of NF-κB signaling (214). In order to examine IEC death in mice with ubiquitous suppression of NF-κB activity (i.e. *ΔN* mice), cleaved caspase-3 (Asp175) was used as a marker for apoptosis. Activated caspase-3 is easily detectable through the formation of two protein fragments (19 and 17 kDa) which are recognized by a

specific antibody against the aspartic residue (Asp175) exposed only after cleavage-induced caspase-3 activation (17 kDa). Western blotting analysis of entire SI tissue and freshly isolated crypts showed no difference between control and *ΔN* mice, as both only revealed the 19 kDa inactive caspase-3 band (Fig. 5-14A). In contrast, SI tissue samples from γ-irradiated mice that were used as positive control for activated caspase-3, inactive (19 kDa) and activated, cleaved caspase-3 (17 kDa) was observed (Fig. 5-14A). This result was further confirmed by cleaved caspase-3 immunohistochemistry of SI sections, which showed absence of apoptotic cells in *ΔN* and control mice but highly increased cell death in γ-irradiated mice (Fig. 5-14B). Note that *ΔN* mice have ubiquitous suppression of NF-κB activity, which blocks NF-κB-driven inflammation (136). In fact, analysis of the most common inflammatory cytokines by RT-qPCR affirmed no increase in inflammation in SIs of *ΔN* mice (Fig. 5-14C).

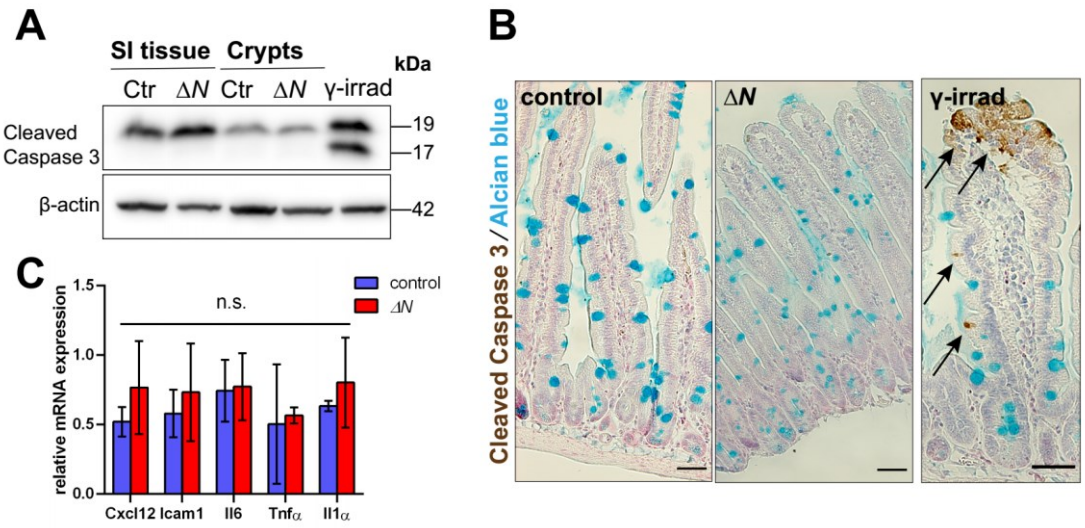

Figure 5-14: Ubiquitous absence of NF-κB activity does not lead to cell death or inflammation. (A) Western blot analysis was performed using antibodies against cleaved caspase-3 and β-actin (loading control) to analyze apoptosis in the SI epithelium or in isolated crypts of control and *ΔN* mice. Tissue sample extract from γ-irradiated mice was used as positive control for cleaved caspase-3. n=3 mice/group. **(B)** Cleaved caspase-3 immunohistochemistry (IHC; DAB (brown)) and Alcian Blue staining performed on paraffin sections of SI from control and *ΔN* mice. Paraffin sections of SI from γ-irradiated mice were used as positive control for cleaved caspase-3 staining. Black arrows show apoptotic cells (n=3/group). Scale bars: 200 µm. **(C)** Relative mRNA expression of *Cxcl12, Icam1, Il6, Tnfα,* and *Il1α* was analyzed by real-time RT-qPCR in control and *ΔN* mice. Data are means ± SEM of three independent experiments. Statistical analyses were performed by Multiple t-tests with Bonferroni's correction (n.s.= no significant) using GraphPad Prism 8.

5.11 NF-κB activity is required for the correct differentiation of goblet and Paneth cells.

NF-κB activity was observed in SI crypts where Paneth cells, CBCs and secretory precursor cells are located (See Fig. 5-11B, 5-12B) (159). My previous results suggested an altered crypt cell composition in *ΔN* mice. To evaluate the role of NF-κB in intestinal epithelial cell (IEC)-fate determination, analysis of different secretory cell types was performed.

5.11.1 Loss of NF-κB activity increased the number of goblet cells in SI crypts.

Alcian blue is a polyvalent basic dye reacting with acid mucosubstances and used as a common staining method to identify secretory goblet cells which produce acidic mucopolysaccharides (215). Histological sections of the proximal small intestine (PSI) from *ΔN* mice were analyzed either using alcian blue or immunofluorescence technique against Muc2 (mucin-2), intestinal-type secretory mucin, that is expressed in goblet cells (Fig. 5-15A). Interestingly, both methods showed an increase of goblet cells in the bottom of crypts in *ΔN* mice when compared to controls. Previous Alcian blue stainings conducted in our laboratory using mice with intestinal epithelium-specific suppression of NF-κB activity (*Villin-ΔN*) also suggested a dramatic increase of goblet cells located in crypts where normally only Paneth cells and ISCs reside (data not shown; (211)). Quantitative analysis of Alcian blue-positive cells per crypt confirmed this finding (Fig. 5-15B). Given the increased amount of goblet cells in absence of NF-κB activity, the expression of goblet cell-specific markers was examined and quantified by RT-qPCR. In accordance with my previous results, the data showed a significant increase of *Gob5* (also called Chloride channel accessory 1, *Clca1*) and *Muc2* mRNA expression in *ΔN* mice when compared with controls. Surprisingly, no differential expression rates were detected for *Klf4* (Krüppel-like factor 4) when comparing *ΔN* and controls (Fig. 5-15C). However, it was previously described that *Klf4* is dispensable for final goblet cell differentiation while *Muc2* and *Gob5* are considered mature goblet cell markers (216,217). Collectively, these data suggest that NF-κB may act downstream of *Klf4* as a regulator of secretory cell fate decisions.

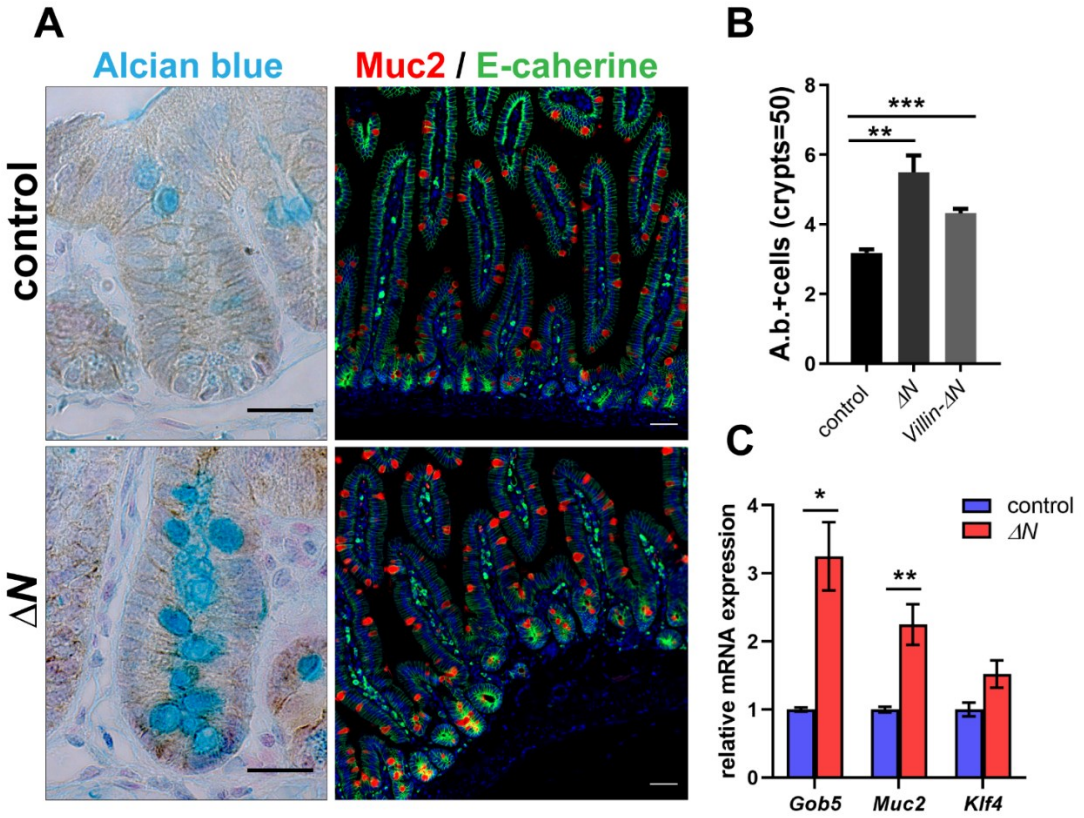

Figure 5-15: Increased number of goblet cells in SI crypts of *ΔN* mice. (A, left panels) Alcian blue staining of goblet cells on paraffin-embedded SI sections from control and *ΔN* mice. Nuclear Fast Red was used for nuclear staining. Scale bar 20 µm. **(A, right panels)** Immunofluorescence staining of goblet cell-marker Muc2 (red) and cell membrane marker E-cadherin (green). DAPI was used for nuclear staining. The images shown are representative photographs using a confocal microscope (scale bars 50 µm). **(B)** Quantification of Alcian blue positive cells/crypt in control, *ΔN,* and *Villin-ΔN* mice. A total of 50 crypts were analyzed per genotype (n=3/group). Counting was performed by Karsten Krieger (see Brischetto et al., 2021 (211)). Statistical analysis was performed by Unpaired t-test with Welch's correction (**p<0.01; ***p<0.001) using GraphPad Prism 8. **(C)** Relative mRNA expression of *Gob5, Muc2,* and *Kl4* by RT-qPCR in control and *ΔN* mice. Data are means ± SEM of three independent experiments. Statistical analyses were performed by Multiple t-tests with Bonferroni's correction (*p<0.05; ** p<0.01) using GraphPad Prism 8.

5.11.2 Strongly reduced Paneth cells in *ΔN* mice.

Paneth cells are specialized secretory epithelial cells containing dense granules of antimicrobial enzymes including α-Lysozyme (218). In order to understand if Paneth cells were also affected by the loss of NF-κB, immunohistochemical analysis (IHC) of α-Lysozyme expression was performed in mice with ubiquitous suppression of NF-κB activity (*ΔN*). The results revealed a dramatic reduction of cells positive for anti-lysozyme antibody in SI sections of *ΔN* mice with 0 to maximally 2 Paneth cell/crypt when

compared to the typical 3 or 4 Paneth cells seen in controls (Fig. 5-16A and C). Quantification of Paneth cells per crypt in the SI of *Villin-ΔN* mice confirmed the significant decrease in *ΔN* mice (Fig. 5-16C;(211)). Accordingly, in situ hybridization (ISH) using a labelled mRNA probe against Paneth cell-specific defensin Cryptdin-1 on histologic sections of SIs was also strongly reduced in absence of NF-κB activity (Fig. 5-16B). mRNA expression of *Lysozyme* and *Cryptdin-1*, both major markers of mature Paneth cells, by RT-qPCR using RNA extracts from the SIs of control and *ΔN* mice further confirmed this finding (Fig. 5-16D). Interestingly, an increased number of goblet cells were observed exactly in those *ΔN* crypts with reduced or even missing Paneth cells. In addition, those Paneth cells that were still detectable in absence of NF-κB activity did not show a normal lysozyme positive-granule structure, but they mostly appeared like either defective or immature cells. Therefore, additional experiments were performed to address if NF-κB plays a role in the cell fate determination between goblet and Paneth cells during cell maturation processes as shown in the following paragraph (see 5.12).

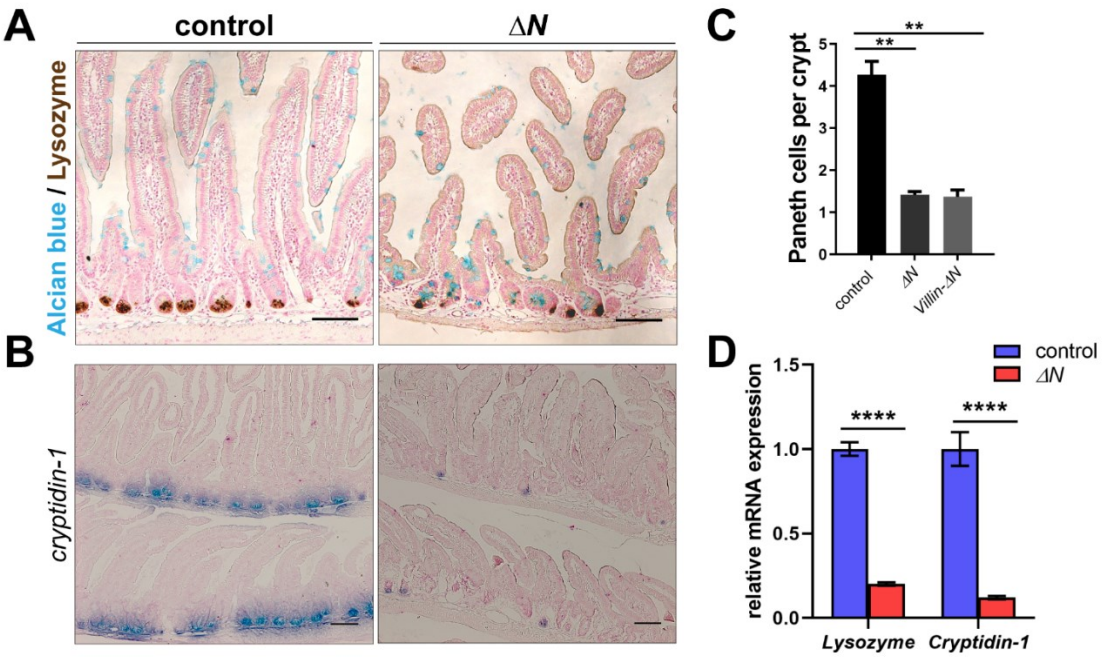

Figure 5-16: Reduced numbers of or missing Paneth cells in SI crypts of *ΔN* mice. (A) Immunohistochemistry for Lysozyme (IHC; DAB (brown signal)) on paraffin-embedded SI sections from control and *ΔN* mice. Alcian blue was used to stain goblet cells and Nuclear Fast Red for nuclei. Scale bars: 100 µm. **(B)** In situ hybridization (ISH) using a riboprobe against cryptdin-1 (blue signal) on SI sections from control and *ΔN* mice was kindly performed by Inge Krahn. Counterstaining was performed using Nuclear Fast Red. Scale bars: 100 µm. Insets show higher magnification of a single SI crypt with cryptidin-1 expression. **(C)** Quantification of Lysozyme-positive Paneth cells/crypt in control (4.1 ± 0.3), *ΔN* (1.5 ± 0.1) and *Villin-ΔN* (1.4 ± 0.3) mice. n≥150 crypts/sample were analysed (n=3/group). Counting was performed by Karsten Krieger (see Brischetto et al., 2021 (211)). Statistical analysis was performed by Unpaired t-test

with Welch's correction (**p<0.01) using GraphPad Prism 8. **(D)** Relative mRNA expression of *Lysozyme* and *Cryptdin-1* by RT-qPCR in control and *ΔN* mice. Data are means ± SEM of three independent experiments. Statistical analyses were performed by Multiple t-tests with Bonferroni's correction (**** p<0.0001) using GraphPad Prism 8.

5.11.3 Enteroendocrine cells (EECs) are not affected by the absence of NF-κB activity.

Apart from Paneth and goblet cells, the hormone secreting enteroendocrine cells (EECs) represent yet another secretory cell type in the SI. To evaluate the status of EEC, RT-qPCR analysis was made for two EEC-specific markers, Chromogranin A (*ChromoA*) and Somatostatin (*SST*). mRNA expression data showed no significant change between control and *ΔN* for both EEC markers (Fig. 5-17), in line with previous histological analyses performed in our laboratory, which showed Chromogranin A-positive cells present in equal numbers in control and *ΔN* mice (data not shown; see (211)).

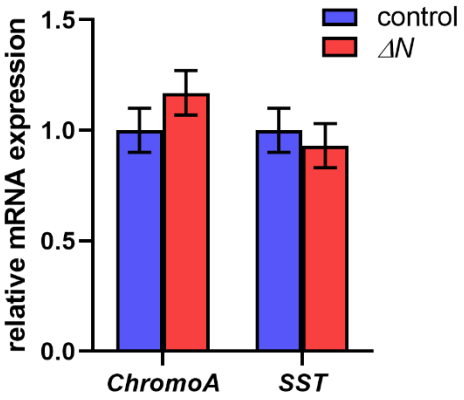

Figure 5-17: NF-κB activity does not affect EEC formation. Relative mRNA expressions of *ChromoA* and *SST* by RT-qPCR in control and *ΔN* mice. Data are means ± SEM of three independent experiments. Statistical analyses were performed by Multiple t-tests with Bonferroni's correction using GraphPad Prism 8.

5.12 NF-κB activity is required for complete Paneth cell maturation.

Paneth and goblet cells arise from a common secretory progenitor found in a subpopulation of transit-amplifying cells, which is located above the stem cell/Paneth cell zone (see Fig. 5-12A) (219). To elucidate if the differentiation of specialized secretory progenitors involved in goblet/Paneth cell fate decisions is affected by NF-κB activity, mRNA expression of different secretory progenitor markers was examined. Basic helix-loop-helix (bHLH) transcription factor Math1 (also Atoh1, atonal homolog 1) and Gfi1

(Growth factor independent-1) were shown to act in early secretory progenitors to define Paneth/goblet versus enteroendocrine cell fate decisions (220). RT-qPCR data showed that the rate of *Gfi1* and *Math1* transcription is similar in control and *ΔN* mice (Fig. 5-18A). Given that the loss of NF-κB activity does not affect the number of enteroendocrine cells (see above paragraph 5.11.3), this result suggests that early secretory precursor cells are still generated in the absence of NF-κB activity.

Two Notch-ligands, Delta-like 1 and 4 (Dll1 and 4), and bona fide Notch target Hes1 (hairy and enhancer-of-split 1) also control secretory commitment in the small intestine (221). Interestingly, *Dll1* and *Hes1* expression was significantly reduced in *ΔN* mice when compared to controls, while *Dll4* remained unchanged (Fig. 5-18A). Note that decreased levels of *Dll1* expression reduce Notch signaling and *Hes1* mRNA expression. Moreover, previous studies showed that intestinal epithelium-specific loss of Dll1 increased goblet cell numbers without affecting the proliferative compartment which would fit at least in part with our results (see above 5.11.1; (216,222)).

Spdef (Sam-Pointed Domain Ets Transcription Factor) is another important transcription factor for intestinal secretory cell specification. It was reported to regulate terminal differentiation of Paneth and goblet cells (219,223). Surprisingly, mRNA expression of *Spdef* was not altered in the intestinal epithelium of *ΔN* mice (Fig. 5-18A) indicating that both transcription factors might work independently. To validate our hypothesis, we bred *Spdef* knock-out mice with *κ-EGFP* reporter mice to monitor NF-κB activity in the absence of *Spdef* expression (Fig. 5-18B). Immunohistochemical analysis of EGFP expression in SI sections from either NF-κB reporter mice lacking Spdef1 (*Spdef -/-; κ-EGFP*) or controls (*Spdef +/+; κ-EGFP*) showed no difference in NF-κB activity, supporting the previous transcription data (Fig.5-18A and B).

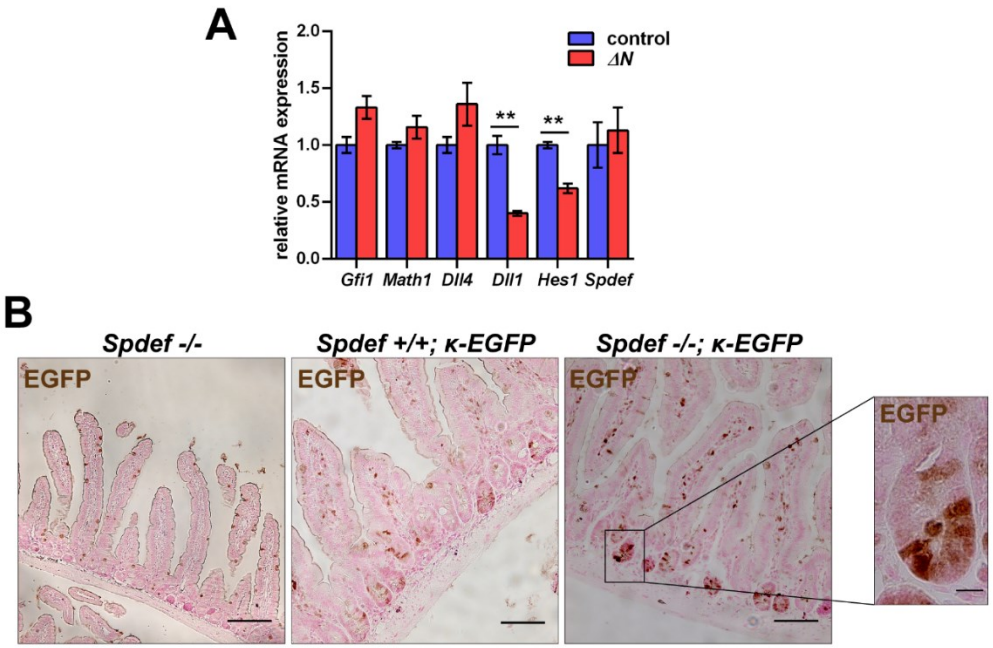

Figure 5-18: Expression of secretory progenitor markers is partly affected in *ΔN* mice. (A) Relative mRNA expressions of *Gfi1, Math1, Dll4, Dll1, Hes1,* and *Spdef* by RT-qPCR in control and *ΔN* mice. Data are means ± SEM of three independent experiments. Statistical analyses were performed by Multiple t-tests with Bonferroni's correction (**p<0.001) using GraphPad Prism 8. **(B) NF-κB activity is independent of Spdef.** Immunohistochemistry for EGFP (IHC; DAB (brown signal)) on paraffin-embedded SI sections from *Spdef -/-* (Spdef KO used for staining control), *Spdef1+/+; κ-EGFP* and *Spdef1 -/-; κ-EGFP* mice (n=3/group). Nuclear Fast Red was used for nuclear staining. Inset shows high magnification of a single crypt from Spdef1 -/-; *κ-EGFP* mice. Scale bars are 75 µm for the main panels and 10 µm for the inset.

In order to investigate a potential role for NF-κB in early Paneth cell formation, comparative studies of *ΔN* and control mice were performed at postnatal days 9 (P9) and 15 (P15) and at 8 weeks of age (adulthood). These time points were chosen in accordance with previously published data that showed first differentiated, Lysozyme-expressing Paneth cells at 7 - 10 days after birth, but maturation is not completed until 15 - 17 days after birth (224). Immunofluorescence co-staining of EGFP and Lysozyme conducted in SIs of *κ-EGFP* reporter mice affirmed that NF-κB was already active at P9, together with the appearance of the first Paneth cells as shown by Lysozyme staining (Fig. 5-19).

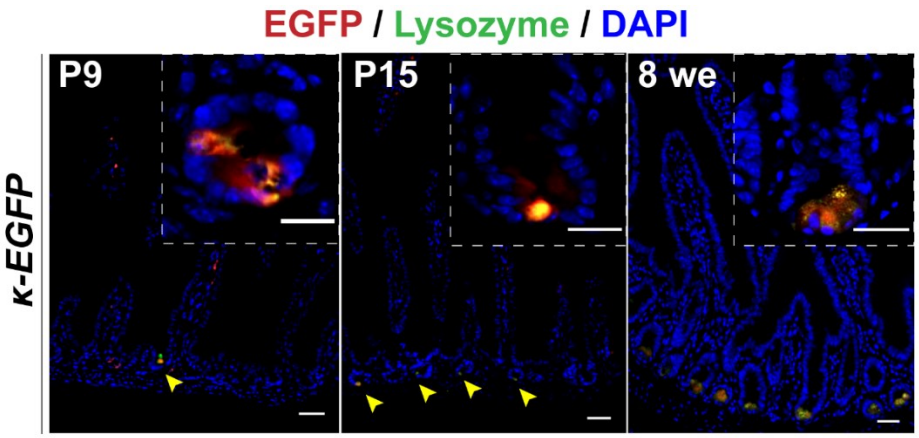

Figure 5-19: NF-κB is active from the beginning of Paneth cells formation. Immunofluorescence staining of EGFP (red) and Lysozyme (green) on sections of *κ-EGFP* SIs at P9, P15 and 8 weeks after birth (n=3/group). DAPI was used for nuclear staining. Yellow arrowheads indicate NF-κB activity in early Paneth cell precursors at postnatal days 9 and 15. The images shown are representative photographs using fluorescence confocal microscopy. Scale bars main panels are 50 µm and insets (showing single crypt) are 20 µm.

In contrast to α-Lysozyme expression, which first appears about 7-9 days after birth, Cryptdin-1 expression starts as early as postnatal day 1 (P1) (224). Thus, in situ hybridization using a riboprobe for Cryptdin-1 followed by quantification was used to find out if the absence of NF-κB activity affects early differentiation/maturation of Paneth cells. *ΔN* mice already displayed a 50% reduction of Cryptdin-positive crypts at P9, thus before final differentiation occurs (Fig. 5-20A and B). By P15, in *ΔN* mice the number of Cryptdin-positive crypts remained strongly reduced until adulthood (8 weeks), while in controls Cryptdin-1 expression constantly increased during the chosen time frame (Fig. 5-20A and B). In line with this finding, immunohistochemistry for Lysozyme at P15 and 8 weeks of age further indicated a strong reduction of mature Paneth cells in crypts of *ΔN* mice (Fig. 5-20C). Collectively, my data support the hypothesis that the strong reduction of Paneth cells in absence of NF-κB activity is not due to apoptotic events but most certainly a consequence of the impairment of final Paneth cell differentiation in favor of goblet cells.

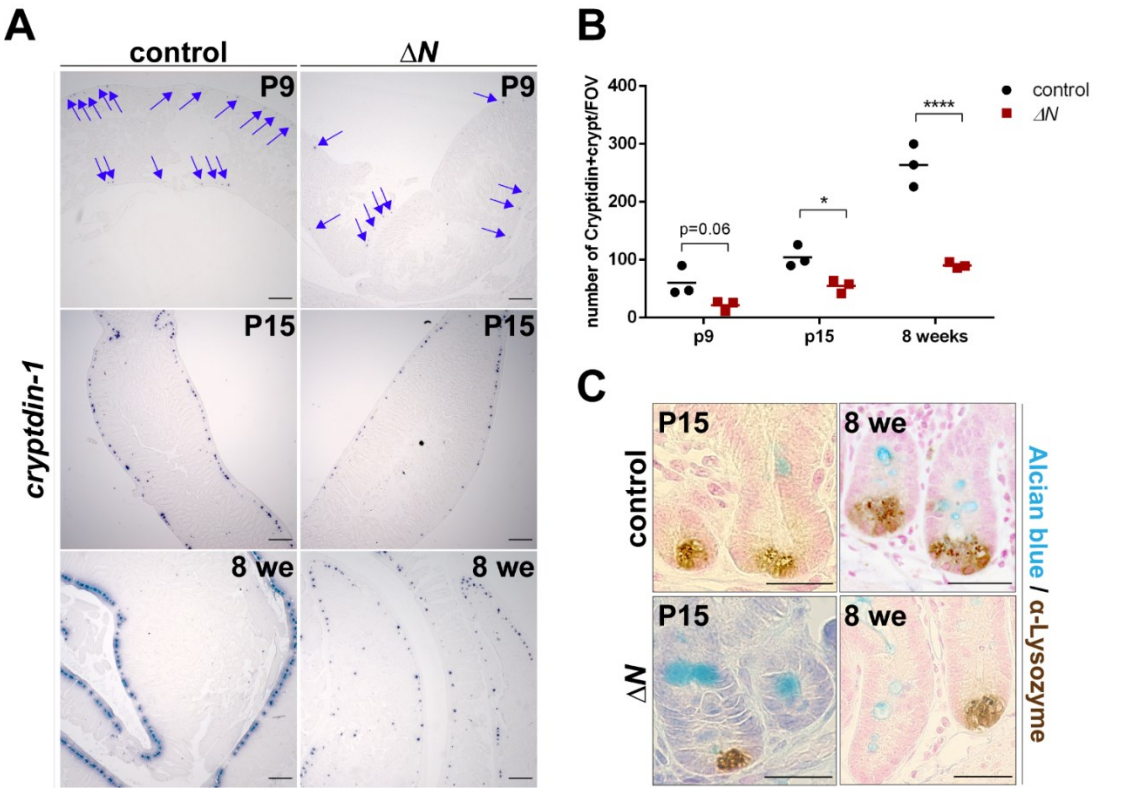

Figure 5-20: Postnatal Paneth cell differentiation requires NF-κB. (A) In situ hybridization (ISH) using a riboprobe for Cryptdin-1 on SI sections of control and *ΔN* mice (n=3/group) at P9, P15, and 8 weeks of age was kindly performed by Inge Krahn (Brischetto et al., 2021). Blue arrows in the P9 panels point to Cryptdin-1 positive cells. Scale bars = 200 µm. **(B)** Quantification of Cryptdin-positive crypts in controls and *ΔN* mice at indicated time points (n=3/group). Statistical analysis was performed by two-way ANOVA using GraphPad Prism 8, *: p<0.05; ****: p<0.0001**;** error bars = SEM; FOV = field of view. **(C)** Immunohistochemistry for α-Lysozyme (IHC; DAB (brown signal)) and Alcian blue staining on paraffin-embedded SI sections from control and *ΔN* mice at P15 and 8 weeks of age (n=3/group). Nuclear Fast Red stains for nuclei. Scale bars: 50 µm.

5.12.1 Accumulation of intermediate cells in crypts of ΔN mice.

Secretory cell lineages can also be classified based on their cell and secretory granule morphologies (225). Therefore, we decided to further characterize the crypt-based secretory cell types in *ΔN* mice by transmission electron microscopy (TEM) and compare them with controls (Fig. 5-21A). As expected, TEM images confirmed a massive reduction of mature Paneth cells in *ΔN* crypts, which are typically distinguished by their electron-dense apical secretory granules (see yellow arrowheads in control crypt Fig. 5-21A, and 5-21B for quantification). However, cells with altered granule morphology (reduced size) and reduced electron density were observed in *ΔN* mice (Fig. 5-21A). Interestingly, these cells perfectly resembled immature intermediate cells with granules

that also contained small amounts of mucin. Garabedian et al. (1997) previously described intermediate cells as precursors of both Paneth and goblet cells (225).

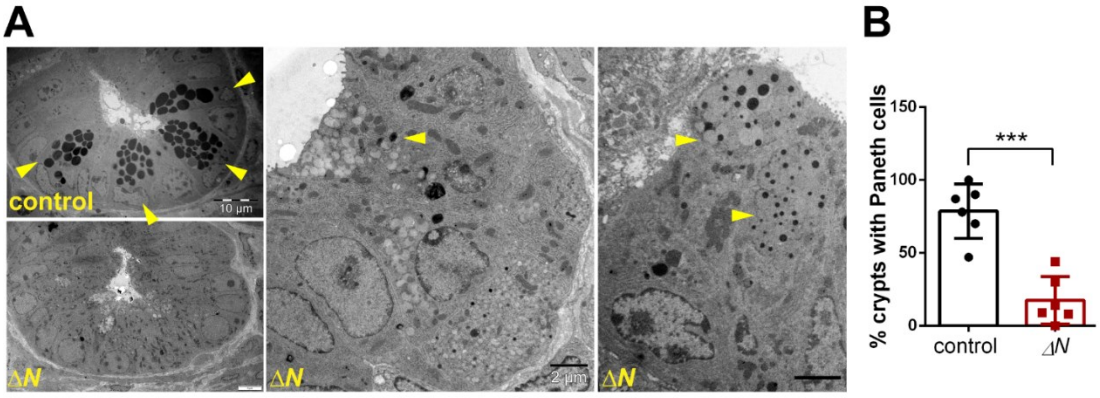

Figure 5-21: Paneth cells are replaced by intermediate cells in *ΔN* mice. (A) Transmission electron microscopy analysis of SI crypts of *ΔN* and control mice (n=4/group). Yellow arrowheads indicate mature Paneth cells in control and immature intermediate cells in *ΔN* mice. Scale bar in left panels = 10 µm (control), 5 µm (*ΔN*), in middle panel (*ΔN*) = 2 µm. Images were produced by Séverine Kunz from the EM facility at the MDC. **(B)** Quantification of crypts with Paneth cells expressed in percentage comparing control and *ΔN* mice (n=4/group). Statistical analysis was performed by Unpaired t-test with Welch's correction (*** p<0.001) using GraphPad Prism 8. Error bars= SEM.

To confirm the presence of intermediate cells observed in crypts of *ΔN* mice, a combinatorial staining method using phloxine/tartrazine solutions and Alcian Blue (PTAB) was performed on SI sections. Phloxine/tartrazine (red-yellow) stains highly granulated cells like mature Paneth cells (PT+AB-), while Alcian blue stains mucin-positive goblet cells (PT-AB+). Intermediate cells instead showed both, granule- and mucin-positive staining (PT+AB+) which allowed us to distinguish these cells from mature Paneth or goblet cells (Fig. 5-22A). Quantification of PTAB staining confirmed accumulation of intermediate cells (blue arrowheads, Fig.5-22A) in crypts of *ΔN* mice (Fig. 5-22B). My data reveal that NF-κB is important for cell fate determination of intestinal Paneth/goblet cells.

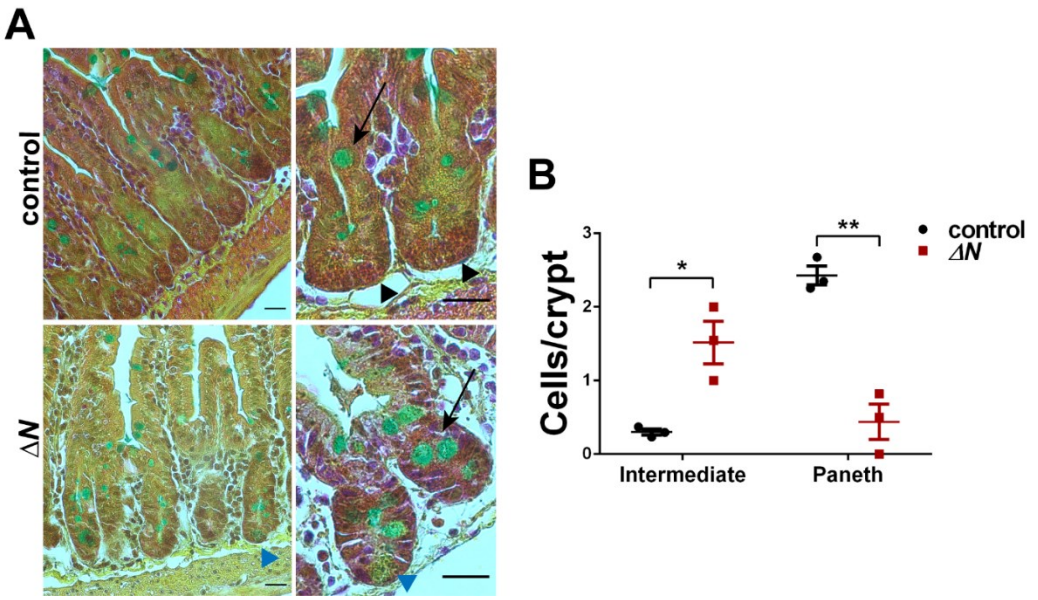

Figure 5-22: Absence of NF-κB induces accumulation of intermediate cells in SI crypts. (A) PTAB (Phloxine-Tartrazine/Alcian Blue) staining on SI sections of *ΔN* and control mice (n=3/group). Black arrowheads point to mature Lysozyme-containing Paneth cells (red-yellow granules) in controls, blue arrowheads to intermediate cells (blue-yellow granules), and black arrows to mature goblet cells (blue). **(B)** Quantification of immature intermediate cells versus mature Paneth cells in *ΔN* and control mice (n=3/group). Statistical analysis was performed by Multiple t-tests with Bonferroni's correction (* $p<0.05$, ** $p<0.01$) using GraphPad Prism 8.

5.13 Loss of Lgr5+ intestinal stem cells (ISC) and altered Wnt-dependent CBC markers in *ΔN mouse SIs.*

Based on previous results (Fig. 5-12B and Fig. 5-23A), NF-κB was also found active in a subset of CBC. Thus, expression of different ISC markers was analysed by RT-qPCR in SI tissue from *ΔN* and control mice. Olfactomedin-4 (*Olfm4*), or SPARC Related Modular Calcium Binding 2 (*Smoc2*), Leucine-rich repeat-containing G protein-coupled receptor 1 (*Lgr1*), Telomerase Reverse Transcriptase (*Tert*) and homeobox protein *Hopx*, all of which are typically classified as a subset of ISCs markers independent of Wnt signaling (226), showed no changes in mRNA expression (Fig. 5-23B). However, most of the genes directly regulated by Wnt/β-catenin, like Cyclin D1 (*Ccnd1*), Endothelin-1 (*Edn1*), TNF Receptor Superfamily Member 19 (*Tnfrsf19*), Achaete-scute family bHLH transcription factor 2 (*Ascl2*) and Leucine-Rich Repeat Containing G Protein-Coupled Receptor 5 (*Lgr5*) were found significantly downregulated in SIs of *ΔN* mice when compared to controls. Three further Wnt-dependent factors, Ephrin type B Receptor 3 (*Ephb3*), Musashi RNA Binding Protein 1 (*Msi1*), and Prominin 1 (*Prom1*)

remained unaltered (Fig. 5-23C). These 3 factors are also expressed in secretory precursors (227). Immunofluorescence staining of SIs of Lgr5-GFP knock-in reporter mice also revealed a diminished number of Lg5-positive CBCs in absence of NF-κB activity (*Lgr5-EGFP; ΔN*), which was confirmed by quantification of fluorescent Lgr5-EGFP-positive cells using flow cytometry (Fig. 5-23D and E). Moreover, although the overall proliferation rate was not affected in SI crypts of *ΔN* mice (see paragraph 5.10.1), the Ki67+/Lgr5+ cell ratio was significantly higher in *ΔN* compared to controls, which is further evidence of altered ISCs composition in *ΔN* crypts (Fig. 5-23F). Accordingly, a recent study using SI crypt organoids from mice with constitutively activated NF-κB signaling in IEC showed a significant increase in Wnt activity, which led to an expansion of Lgr5-positive ISCs (146). Together, these results suggest that NF-κB activity regulates Lgr5+ CBC maintenance by controlling Wnt signaling.

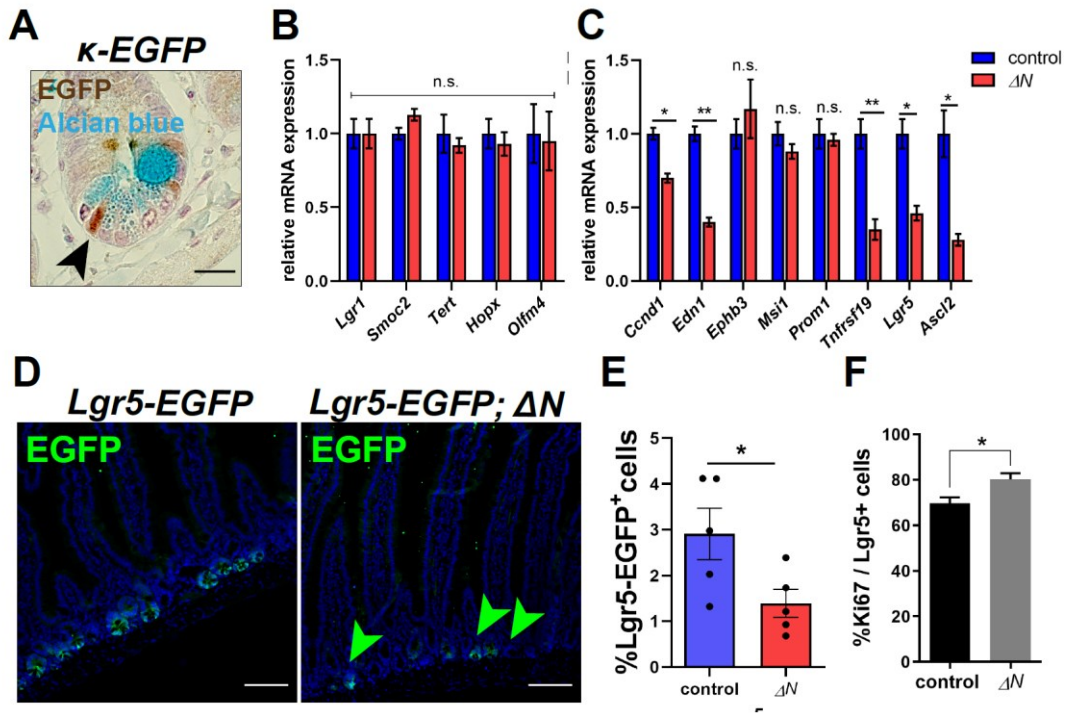

Figure 5-23: Altered ISCs composition in SI crypts of *ΔN* mice. (A) EGFP immunohistochemistry (IHC; DAB (brown) plus Alcian Blue staining on SI sections of κ-EGFP mice (n=3**).** Black arrowhead indicates a CBC with active NF-κB. Scale bar: 20 µm. **(B, C)** RT–qPCR for Wnt-independent (**B**) and -dependent (**C**) ISC markers in control and *ΔN* mice. Data are means ± SEM of three independent experiments. Statistical analyses were performed by Multiple t-tests with Bonferroni's correction (n.s= not significant; *p<0.05; **p<0.01) using GraphPad Prism 8. **(D)** Immunofluorescence staining of EGFP in SIs of *Lgr5-EGFP* (control) and *Lgr5-EGFP; ΔN* (*ΔN*) mice (n=3/group). DAPI was used for nuclear staining. Green arrowheads indicate reduced numbers of Lgr5-positive cells in crypts of *ΔN* mice. The images shown are representative photographs using fluorescence confocal microscopy. Scale bars are 100 µm. **(E)** Quantification (in %) of

FACS-isolated Lgr5-EGFP-positive cells in *ΔN* and control mice (n=5/group) using GraphPad Prism 8. Error bars= SEM. **(F)** Quantification (in %) of Ki67- versus Lgr5-positive cells in SI of *Lgr5-EGFP* and *Lgr5-EGFP; ΔN mice* (n=3/group). Statistical analysis (E and F) was performed by Unpaired t-test with Welch's correction (* $p<0.05$).

5.14 Intrinsic functions of NF-κB in IECs using 3D organoids derived from small intestinal crypts.

The high turnover of the intestinal epithelium results from intrinsic- and extrinsic-epithelium niche factors, such as Wnt and Notch ligands, that regulate the capacity of self-renewal of Lgr5-expressing ISCs. Two different cell types appear to provide these factors *in vivo*. Paneth cells interspaced between ISCs maintain the essential local niche in SI crypts, while subepithelial telocytes support the entire epithelium by secreting Wnt proteins (165,228,229). However, isolated single Lgr5+ ISC can also independently generate crypt-like structures, called organoids (or mini-guts), in a Matrigel-based culture system in the absence of the underlying mesenchymal cells (i.e., telocytes) if the culture medium contains all signals required (230). Thus, a culture of self-organising organoids generated from SI crypts or single Lgr5+ ISC (see Materials and Methods 4.1.8) was established to evaluate the IEC-intrinsic role of NF-κB in Lgr5+ ISC maintenance and further Paneth/goblet cell fate decisions *ex-vivo*.

5.14.1 Wnt3 rescues *ex-vivo* growth of *ΔN* organoids.

Previous results showed that the proliferative capacity of ISC and their progenitors are not affected by suppression of NF-κB activity in *ΔN* mice (Fig.5-13). As further validation, SI crypt organoid growth was also examined. In contrast to *in vivo* analyses, quantitative viability assays, including Ki67 expression and light microscopy visualization, revealed a strongly reduced formation (% of crypt organoids per well; Fig. 5-24A, C) and growth (% of Ki67/DAPI; Fig. 5-24B) of *ΔN* crypt organoids when compared to controls after 4, 5 or 8 days of culture in standard medium (ERN). Interestingly, addition of Wnt3A-conditioned medium to ENR medium (WENR medium) was sufficient to restore *ΔN* organoid growth to the level of controls after 5 to 8 days of culture (Fig. 5-24A, B and C). Note that the organoid growth of controls was not affected by the supplement of Wnt3a. Single EGFP-positive Lgr5-expressing ISC obtained from *Lgr5-EGFP; ΔN* (*ΔN*) and control mice (*Lgr5-EGFP*; (153)) by FACS were also used to study the ability of stem cells to generate self-organizing organoids in the absence of NF-κB activity (Fig. 5-24D and E). After FACS sorting, WENR medium was used to culture single Lgr5-EGFP+ ISC in Matrigel for the

first 3 days (Fig. 5-24D). This allowed single Lgr5-positive cells to proliferate independently from the suppression of NF-κB activity and to overcome the physical and/or biological stress of the isolation procedure (230). After 3 days, the organoid medium is exchanged and replaced with either ENR or WENR medium. *ΔN* and control organoids were followed every other day and inspected by inverted microscopy until day 6. My results confirmed that *ΔN* organoids are unable to survive in absence of Wnt3 in culture medium (Fig. 5-24E). In 2011, Sato and colleagues provided the first evidence of Paneth cells as the main local source of Wnt3 and Notch ligands for Lgr5+ ISC support and maintenance in culture. Accordingly, single Lgr5-positive cells were able to form fully differentiated organoids only in presence of Paneth cells (165). Therefore, the inability of *ΔN* organoids to grow in standard ENR culture medium could be a consequence of the lack of Paneth cells, which might be overcome by the addition of Wnt3A to support ISC function. However, supplementation of wild-type murine SI organoid (control) cultures with exogenous Wnt3a induces the formation of cyst-like structures called “spheroids” (see Fig. 5-24E). This is mediated by Wnt pathway activation (231). Yet, *ΔN* organoids never assume any cystic morphology in WENR medium. Instead, they display budding (crypt-like) structures (Fig. 5-24C, E), probably due to lower Wnt signaling in the absence of NF-κB activity.

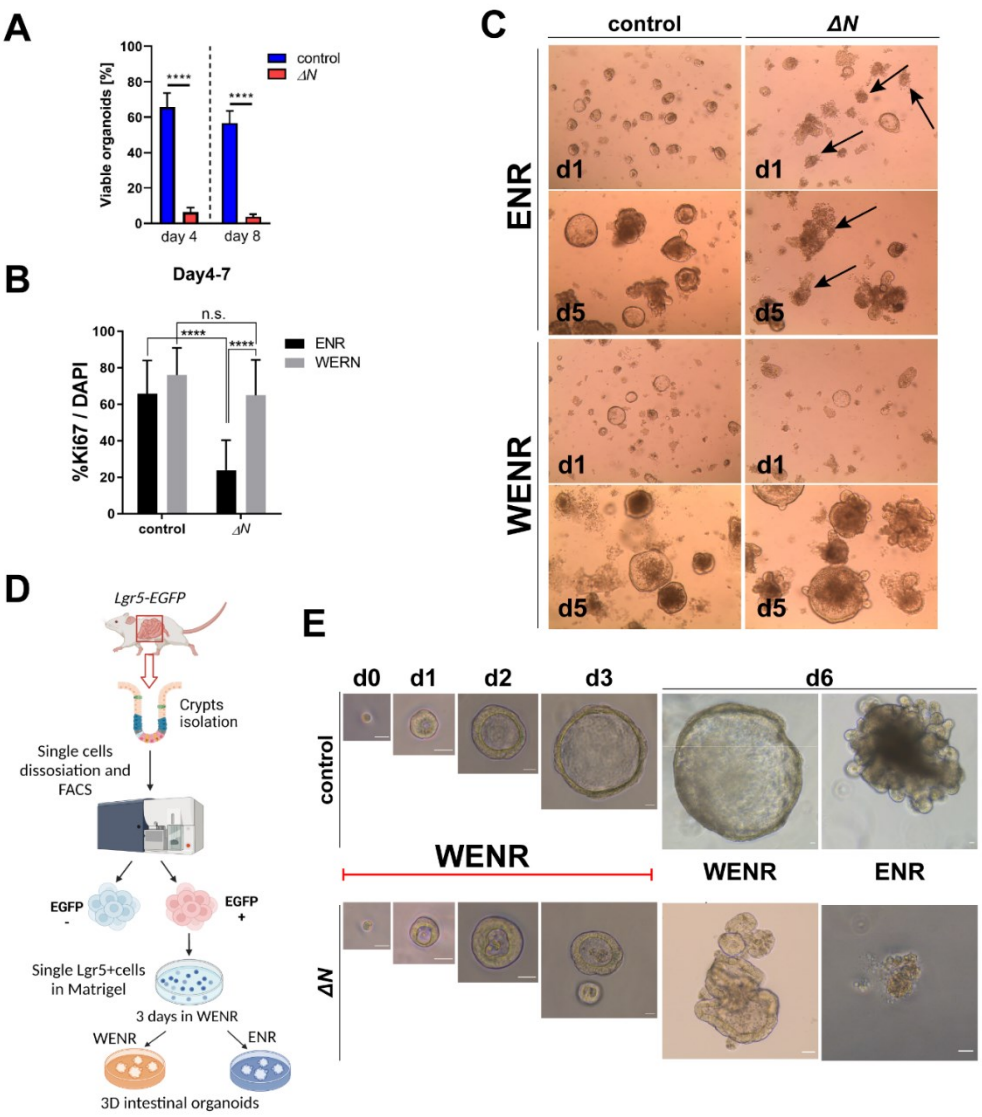

Figure 5-24: Exogenous Wnt restores *ΔN* organoid growth. (A) Quantification of organoid growth in ENR (without Wnt) or WENR (plus Wnt) medium at days 4 and 8 after isolation of SI crypts from control or *ΔN* mice (n=3/group). Unpaired t-test: *p<0.05, n.s. = not significant, error bars = SD. These experiments (A, B) were performed in collaboration with Christian Klotz at the RKI (211). **(B)** Quantification (in %) of Ki67-positive cells of bulk control and *ΔN* organoids grown for 7 days either in ENR or WENR medium. Two-way ANOVA with Bonferroni´s multiple comparison test, ****p<0.0001, n.s. = not significant; error bars = SEM. **(C)** Upper panels: Representative images of crypt organoids cultured in ENR medium at day 1 (d1) and day 5 (d5) past isolation of SI crypts from control and *ΔN* mice (n=4/group). Black arrows indicate apoptotic organoids. Lower panels: Representative images of crypt organoids cultured in WENR medium at day 1 (d1) and day 5 (d5) post isolation of SI crypts from control and *ΔN* mice (n=3/group). All images are 200x original magnification. **(D)** Schematic representation of the experimental design shown in (**E**). Illustration created with BioRender.com. **(E)** Single EGFP-positive cells isolated from *Lgr5-EGFP* (control) or *Lgr5-EGFP; ΔN* mice (*ΔN*) by FACS and cultured in the presence (WENR) or absence of Wnt (ENR). n=3 independent experiments; d0 – d6 = days of culture.

Comparative mRNA expression analysis of CBC markers *Lgr5* and *Ascl2* in control and *ΔN* organoids grown in either ENR or WENR medium was performed by RT-qPCR (Fig. 5-25). Similar to the *in vivo* situation, *ex vivo ΔN* organoids showed reduced *Lgr5* and *Ascl2* mRNA expression in standard ENR medium, which however was significantly increased in WERN medium when compared to controls (Fig. 5-25A). The Ki67/Lgr5+ cell ratio in *ΔN* and control organoids grown in the absence (ENR) or presence of Wnt3 (WENR) also showed that Lgr5 expression is re-established when adding exogenous Wnt to the culture medium (Fig. 5-25B). Collectively, my data support the hypothesis that rescued growth of *ΔN* organoids in the presence of Wnt might be due to the re-establishment of a functioning stem cell niche.

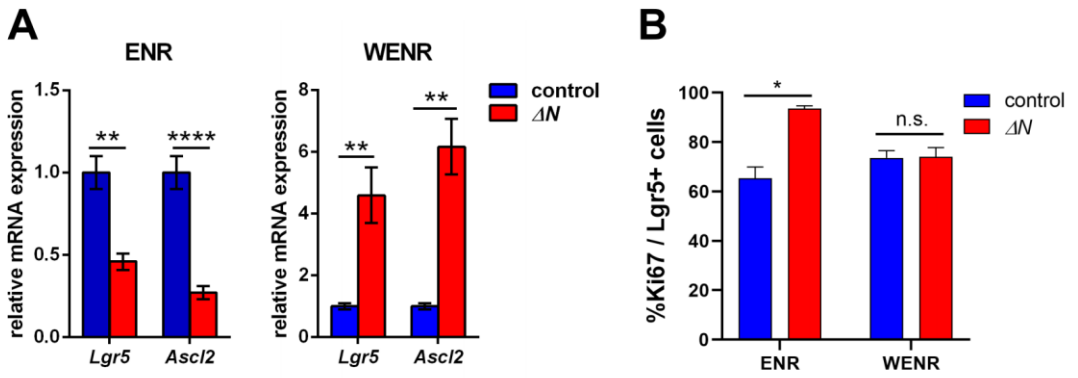

Figure 5-25: Exogenous Wnt restores mRNA expression of *Lgr5* and *Ascl2* in *ΔN* organoids. (A) RT–qPCR for stem cell markers *Lgr5* and *Ascl2* using RNA isolated from bulk organoids from control and *ΔN* mice grown in either ENR or WENR medium. Data are means ± SEM of three independent experiments. Statistical analyses were performed by Multiple t-tet-testsh Bonferroni's correction (**: p<0.01, ****: p<0.0001) using GraphPad Prism 8. **(B)** Quantification (in %) of Ki67 versus Lgr5 expression on crypt organoids grown in the absence (ENR) or presence of Wnt3 ligand (WENR) for 14 days (3rd passage) and stained with antibodies against Ki67 and Lgr5. Two-way Analysis of variance (ANOVA) with Bonferroni´s multiple comparison test, *: p<0.05, n.s.= not significant, error bars = SEM.

5.14.2 Wnt3 is not sufficient to determine Paneth versus goblet cell fate decision in *ΔN* organoids.

In order to explore the importance of NF-κB in Paneth versus goblet cell fate decisions, cell-specific NF-κB activity, as well as the cell composition of *ΔN* and control SI organoids were examined. First, crypt organoids derived from *κ-EGFP* reporter mice were generated and EGFP immunofluorescence co-staining with Paneth cell marker Lysozyme showed that NF-κB was mostly active in Paneth cells confirming our previous

in vivo data (yellow arrows; Fig. 5-26A). Next, SI *ΔN* and control organoids were left grown in standard ENR medium for 7 days after extraction, and Paneth and goblet cells were monitored during crypt-villus axis formation *in vitro*. In control organoids, 2 days after extraction it was already possible to visualize an increase of secretory Paneth cells located in initial crypt structure (bud) formation areas (green signals; Lysozyme Fig. 5-26B). Conversely, the few *ΔN* organoids that survived in ENR medium already showed a strong reduction of Lysozyme-positive cells at an early time point (day 2; d2). This trend is maintained until day 7 (d7) when control organoids exhibited multiple differentiated crypt-villus structures with high numbers of Paneth cells while *ΔN* organoids displayed impaired differentiation and strongly reduced numbers of Paneth cells (Fig. 5-26B). Similar to SI crypts, immunofluorescence staining of goblet cell marker Muc2 also revealed an increased number of goblet cells in *ΔN* organoids when compared to controls (Fig. 5-26B).

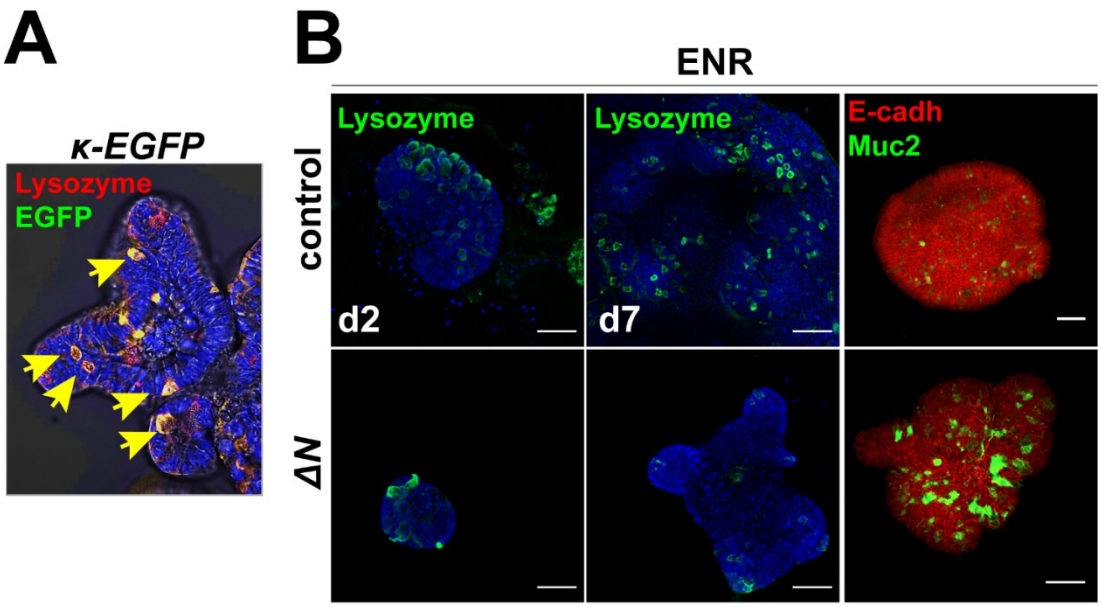

Figure 5-26: Altered numbers of Paneth and goblet cells were observed in *ΔN* organoids. (A) immunofluorescence co-staining of lysozyme and EGFP using crypt organoids derived from *κ-EGFP* reporter mice. Yellow arrows point to Paneth cells displaying NF-κB activity. Experiment kindly provided by Christian Klotz from the RKI (see Brischetto et al., 2021). Scale bar 20 µm. **(B)** Representative images of immunofluorescence using anti-lysozyme antibody with nuclear DAPI staining (blue; left panels) or anti-Muc2 and -E-cadherin antibodies (right panels) on control and *ΔN* organoids in ENR medium at indicated days. Scale bars: 50 µm.

The addition of Wnt3A to the standard organoid culture medium (WENR) was sufficient to rescue *ΔN* organoid growth. To evaluate if this is also valid for reestablishing normal

Paneth and goblet cell numbers in *ΔN* organoids, mature Paneth and goblet cell markers were examined in presence of Wnt3A (WENR). The results showed that although growth was indeed restored in *ΔN* organoids (EdU incorporation and staining, Fig. 5-27), the number of Lysozyme-positive Paneth and Muc2-positive goblet cells remained altered when compared to controls (Fig. 5-27).

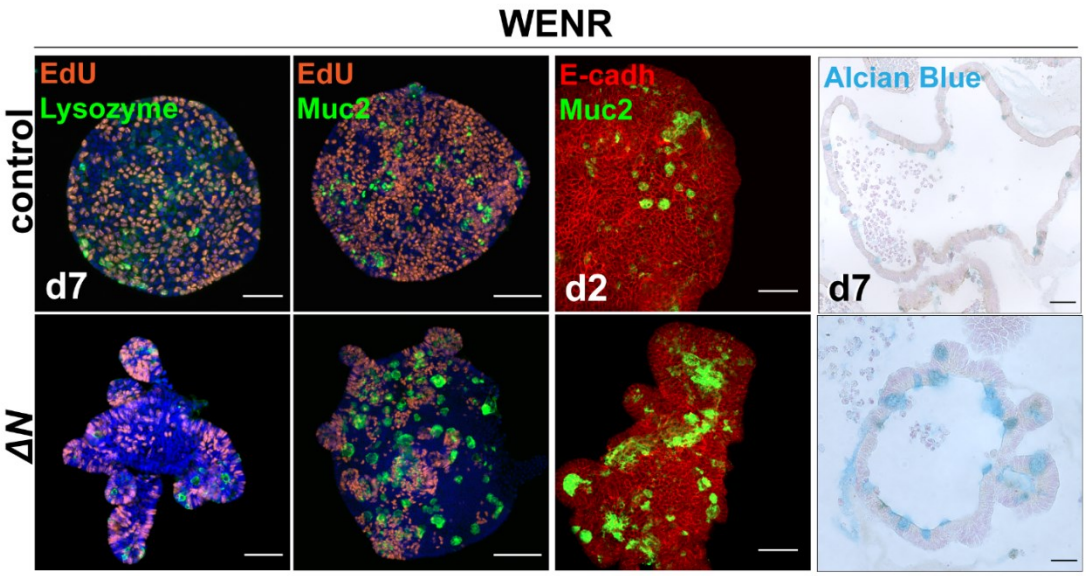

Figure 5-27: Exogenous Wnt does not restore Paneth and goblet cell numbers in *ΔN* organoids. From the left, panels are showing representative images of immunofluorescence staining of EdU (orange), and Lysozyme and Muc2 (green) performed on day 7 control and *ΔN* organoids grown in WENR medium. DAPI was used for nuclear staining. Immunofluorescence staining of Muc2 (green) and E-cadherin (red) was performed on day 2 control and *ΔN* organoids grown in WENR medium. Alcian blue staining for visualizing goblet cells in control and *ΔN* organoids in WENR medium at day 7. All scale bars are 50 µm.

Expression of Paneth cell marker Lysozyme and goblet cell marker Muc2 in *ΔN* and control organoids was further verified by qRT-PCR (Fig. 5-28). The data confirmed reduced *Lysozyme* and increased *Muc2* expression in *ΔN* organoids independent of Wnt3A in organoid culture medium, indicating that Wnt3A alone is not sufficient to re-establish Paneth cell formation and reduce the numbers of goblet cells.

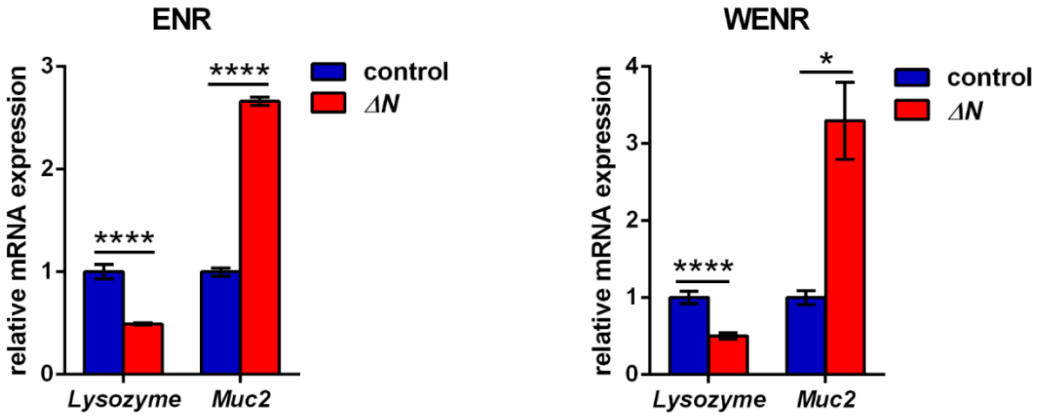

Figure 5-28: Exogenous Wnt does not restore Paneth and goblet cell numbers in *ΔN* organoids. RT–qPCR for Paneth cell *Lysozyme* and goblet cell *Muc2* using RNA isolated from bulk organoids from control and *ΔN* mice grown either in ENR or WENR medium. Data are means ± SEM of three independent experiments. Statistical analyses were performed by Multiple t-tests with Bonferroni's correction (*: p<0.05, ****: p<0.0001) using GraphPad Prism 8.

5.15 Analysis of potential molecular mechanisms behind impaired Paneth cell differentiation in SIs of *ΔN* mice.

Precise tuning of the Wnt/β-catenin signaling pathway was shown to be the key for homeostasis of the intestinal epithelium by maintaining correct stem cell proliferation and controlling secretory lineage differentiation (161). Moreover, crosstalk between Wnt and NF-κB pathways was also previously proposed in regulating stem cell expansions and dedifferentiation in SI crypts during inflammation or tumorigenesis (146,232,233). My previous results showed an altered ISC composition in the SI crypts of *ΔN* mice which was re-established by exogenous Wnt in *ex-vivo* intestinal organoids (See paragraph 5.14.1). Based on these observations, Wnt activity and expression of Wnt pathway components have been examined. Analysis of bona fide Wnt/β-catenin target *Axin2* mRNA expression showed no significant change between control and *ΔN* mice suggesting that the overall Wnt activity was maintained (Fig. 5-29A and C). This was further supported by previous analyses performed in our laboratory using WNT-reporter mice with suppressed NF-κB activity (*cond-lacZ*; *ΔN*) which showed unaltered Wnt activity in IEC (data not shown; see Brischetto et al., 2021 (211)). However, mRNA expression of *Wnt3* was found significantly down-regulated in isolated SI crypts and organoids derived from *ΔN* mice grown in either ENR or WENR medium (Fig. 5-29B and C) when compared to controls. As mentioned above (see chapter 5.14.), Paneth cells

are the main IEC-producer of Wnt3 and Notch-ligand Delta-like 1. Therefore, the lack of Paneth cells in the absence of NF-κB activity is most likely the reason for the diminished expression of these two important factors for controlling stem cell niche functions. Interestingly, we detected mRNA expression of yet another Wnt ligand, *Wnt10a*, specifically in crypts of control mice, while its expression was strongly reduced in *ΔN* mice (Fig. 5-29C and D). To validate these results, two additional controls were used: 1) as expected, a sense riboprobe for *Wnt10a* (negative control) did not give any signal on SI tissue of controls (Fig. 5-29D). 2) Anti-sense *Wnt10a* riboprobe on sections of anagen hair follicles known to express Wnt10a (positive control) gave a clear signal (Fig. 5-29D) (137). A recent publication suggested Paneth cells as a potential source of Wnt10a and previously it was identified as a downstream target of NF-κB, which strongly supports our findings (137,234,235).

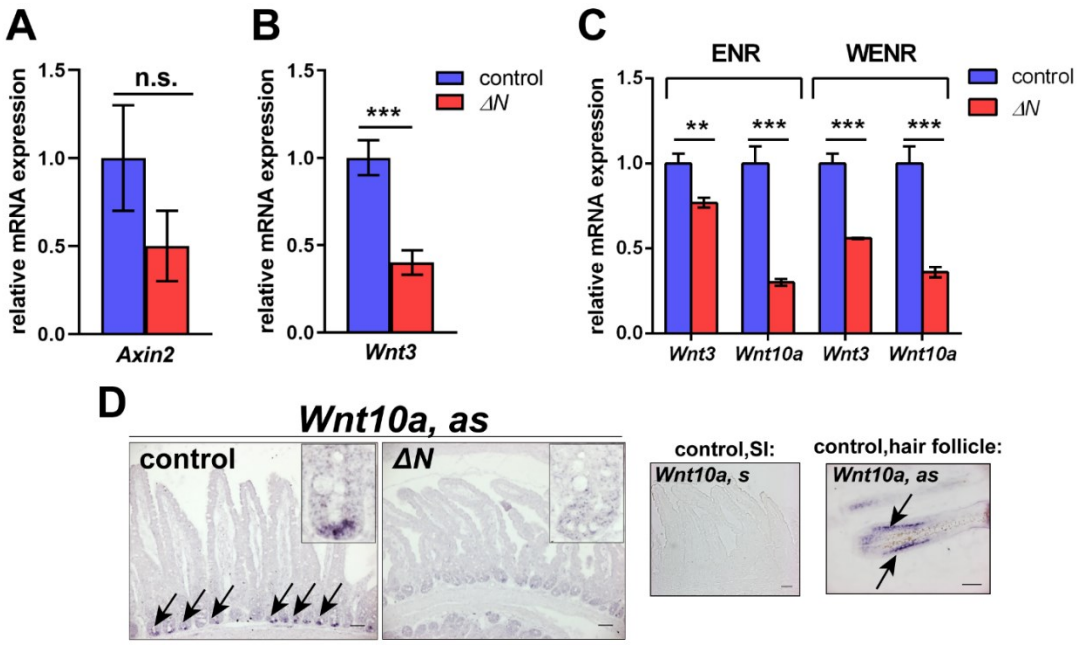

Figure 5-29: Expression of *Wnt3* and *Wnt10a* ligands is significantly reduced in SI crypts of *ΔN* mice. **(A, B)** RT–qPCR for Wnt target *Axin2* **(A)** and Wnt ligand *Wnt3* **(B)** using RNA isolated from SI crypts of control and *ΔN* mice. Data are means ± SEM of three independent experiments. Statistical analyses were performed by Multiple t-tests with Bonferroni's correction (n.s.=not significant; ***: p<0.001) using GraphPad Prism 8. **(C)** RT–qPCR for *Wnt3, Wnt10a* using RNA isolated from bulk organoids from control and *ΔN* mice grown in either ENR or WENR medium. Data are means ± SEM of three independent experiments. Statistical analyses were performed by Multiple t-tests with Bonferroni's correction (**: p<0.01, ***: p<0.001) using GraphPad Prism 8. **(D)** In situ hybridization **(**ISH) using an antisense riboprobe for *Wnt10a* on SI sections of control and *ΔN* mice (n=3/group). Black arrows indicate mRNA expression in crypts of controls. Right small panels: sense riboprobe for Wnt10a on SI sections of controls (negative control), and Wnt10a antisense riboprobe on sagittal skin sections showing Wnt10a mRNA expression in the inner root sheath of an anagen

hair follicle (black arrows; positive control). Results were provided by Inge Krahn and Karsten Krieger (see Brischetto et al., 2021 (211)).

Prior NF-κB-dependent transcriptomes and Chromatin-IP studies revealed transcription factor *Sox9* (SRY-box containing gene 9) as an NF-κB and Wnt target gene in epithelial cells (210,236). Moreover, Sox9 is expressed in TA cells, but also in Paneth cells where it is required for final differentiation (237). Thus, Sox9 represents an optimal candidate to clarify the possible molecular mechanism involved in defective Paneth cell differentiation in *ΔN* mice. The presence of Sox9 protein was analyzed by Western blot and IHC staining revealing a strong reduction in SI crypts of *ΔN* mice when compared to controls (Fig. 5-30A and B). In addition, diminished *Sox9* mRNA expression was also found in absence of NF-κB activity (*ΔN*), while it was significantly up-regulated in mice with constitutively activated NF-κB signaling in IECs ($I\kappa Ba^{IEC\text{-}KO}$) (Fig. 5-30C). Finally, nuclear localization of Sox9 was shown in Paneth and progenitor cells displaying NF-κB activity (EGFP expression) in SI crypts of *κ-EGFP* reporter mice (yellow arrows; Fig. 5-30D). Altogether, my data support the hypothesis that defective Paneth cell differentiation in *ΔN* mice is most likely a consequence of down-regulated Sox9 expression.

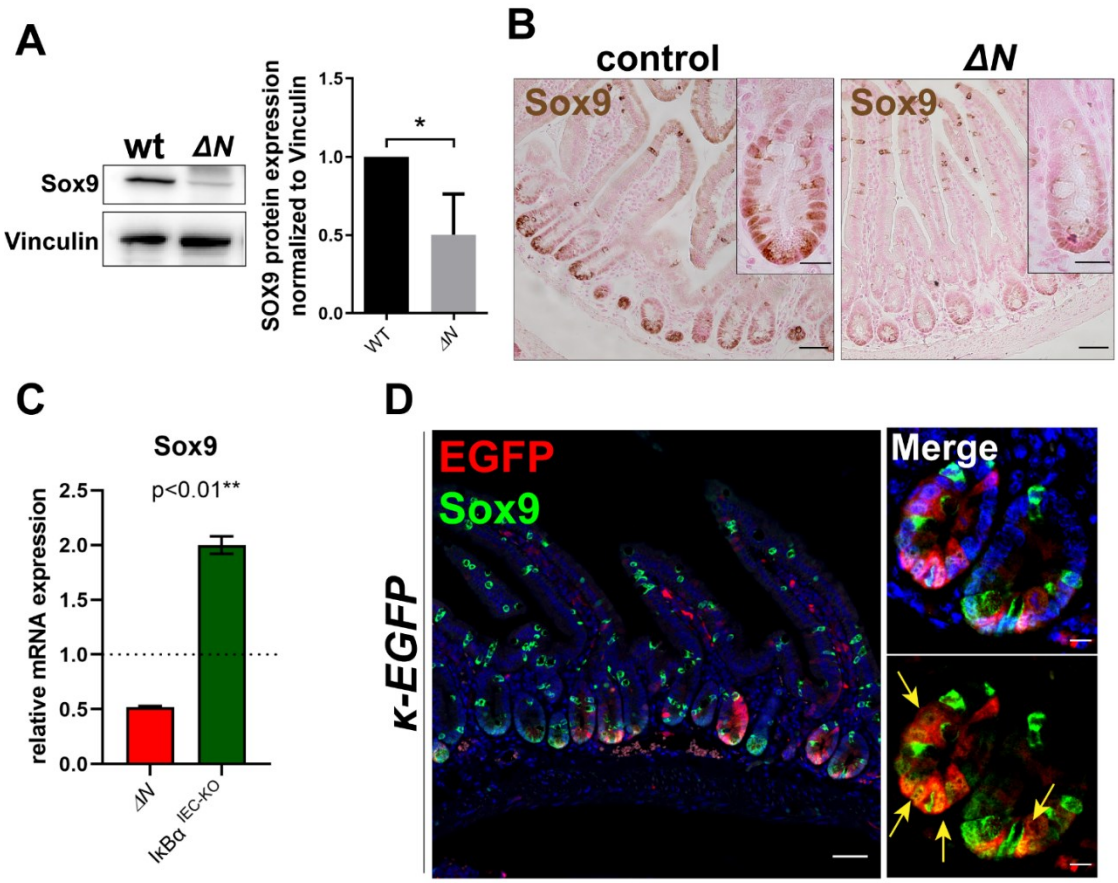

Figure 5-30: Down-regulation of Sox9 expression in intestinal crypts of *ΔN* mice. (A) Left panel: Western blotting (WB) analysis of Sox9 using protein extracts from isolated intestinal crypts of control and *ΔN* mice (n=3/group). Right panel: Quantification of Sox9 protein expression normalized to vinculin. Statistical analysis was performed by Unpaired t-test with Welch's correction (*p<0.05, error bars =SEM). (**B)** IHC using a Sox9 antibody on SI sections of control and *ΔN* mice (n=3/group) shows strongly reduced Sox9 expression in intestinal crypts of *ΔN* mice. Scale bars = 50 µm and 20 µm for insets showing a single crypt. **(C)** RT–qPCR for *Sox9* mRNA from SI crypts of *ΔN* and *IκBα-IEC-KO* mice (n=3/group). The expression of control mice was set to one. Data are means ± SEM of three independent experiments. Statistical analyses were performed by Multiple t-tests with Bonferroni's correction (**:p<0.01) using GraphPad Prism 8. **(D)** Immunofluorescence co-staining using anti-EGFP and -Sox9 antibodies on sections of SI of κ-EGFP reporter mice (n=3/group). Yellow arrowheads point to cellular co-localization of Sox9 expression and NF-κB activity (EGFP expression). Nuclear counterstain: DAPI. Scale bars = 50 µm SI overview and 10 µm insets showing only crypts.

6. DISCUSSION

Part I:

Functional interplay between autophagy and NF-κB signaling in the regulation of inflammation.

6.1 Nuclear LC3 interacts with NF-κB in response to stress-induced inflammation.

NF-κB signaling pathway and autophagy are both implicated in determining cellular fate, influencing each other through positive or negative feedback loops (238). Constitutive activation of the NF-κB pathway and defective autophagy are often associated with different inflammatory diseases and cancer development (117). Recent evidence suggests that autophagy suppresses NF-κB signaling to limit the inflammatory response. For instance, constitutive activation of NF-κB/p65, leading to increased expression of proinflammatory cytokines, was found associated with autophagy suppression either after kidney injury or in intestinal epithelial cell (IEC)-specific *ATG7* KO mice (239,240). By using biochemical analysis and imaging techniques, the current study characterized for the first time the interaction of endogenous autophagic marker LC3 and NF-κB/p65 subunit in response to different stress conditions. Strikingly, accumulation of LC3 within the nucleus strongly co-localized with p65 following NF-κB activation (Fig.5-2), indicating that nuclear LC3 sequesters p65 protein from the nucleus to the cytoplasm to block NF-κB signaling. Previous studies showed that autophagy may degrade nuclear components, but the molecular targets and their molecular process in the nucleus were largely unexplored (178).

Nuclear accumulation of the autophagic marker LC3 has been reported to play a role in different nuclear functions in response to specific types of stress. In this regard, Dou et al., (2015) have shown that nuclear LC3 directly interacts with lamin B1 (LMNB1) to facilitate the autophagic degradation of nuclear lamina upon oncogenic stress (241). Moreover, nuclear LC3 was also described to monitor nucleolar function (242,243), and to be a reservoir of cytosolic LC3 under starvation conditions (244). In addition to LC3, autophagosome proteins ATG5 and ATG7 have also been identified in the nucleus regulating p53 activation (245,246). Similar to p53, ATG5-mediated autophagy was

found to co-localize with p65 in the nucleus in renal epithelial cells in order to alleviate tubular cell inflammation in response to the kidney injury induced by unilateral ureteric obstruction (UUO) or angiotensin II (Ang II) (247). However, the molecular mechanism involved in ATG5-p65 complex formation was not fully elucidated. Based on these previous observations, we hypothesized that p65 may be a target for nuclear autophagic degradation upon stress-induced inflammation. Accordingly, co-localization analysis using immunofluorescence and proximity ligation assay (PLA) showed that the endogenous proteins, LC3 and p65, bound mainly in the cytoplasm in untreated A549 cells and that their interaction increased in the nucleus after stimulation with TNFα or γ-irradiation (Fig. 5-2A and B). In addition, we demonstrate that LC3-p65 interaction is promoted by ubiquitination of the same p65 protein, which is recognized by p62 (Fig. 5-6). p62 is a well-known autophagy cargo receptor recognizing the ubiquitinated proteins for selective degradation via its ubiquitin-binding domain (UBA) and delivering them to autophagosomes via its LC3 interaction region (LIR) (189). Another study demonstrated that the TLR2-dependent signaling from hepatoma tumor cell condition medium mediates cytoplasmic recognition of p65 for lysosomal degradation in macrophages (204). In contrast, immunoprecipitation data from cytoplasmic and nuclear fractions of THP1 cells reveals that p62 is able to bind the p65 subunit not only in the cytoplasm but also in the nucleus after LPS-induced NF-κB activation (Fig. 5-10B). Additionally, immunofluorescence analysis confirms this finding after TNFα or γ-irradiation treatment suggesting that a fraction of nuclear p65 is recognized by p62 after NF-κB activation (Fig.5-6C) and bound to LC3 for autophagic degradation.

p62 has two nuclear localization signals and one nuclear export signal to enable fast nucleo-cytoplasmic shuttling, however, little is known about its possible nuclear roles (188). Recently, Lobb et al. (2021) described a novel function for p62 in trafficking nuclear-ubiquitinated p65 to nucleolar aggresomes in response to aspirin, which induced apoptosis in cancer cells (248). Furthermore, they suggested a competition between the autophagic and nucleolar accumulation of the protein, which might partially explain the difference found in our study. Indeed, PLA analysis using U2OS cells stably expressing GFP-LC3 shows co-localization of p62 and p65 within LC3-positive autophagosome, which further indicates autophagic accumulation of p65 after its activation (Fig.5-6B). Another explanation may be the different stimuli used for NF-κB induction. For instance, the nucleolar trafficking of p65 is restricted to specific stimuli such as aspirin and proteasome inhibitors (249), while nucleolar sequestration of p65 in response to TNFα, LPS or γ-irradiation has not previously reported. Moreover, upon LPS treatment

nucleocytoplasmic shuttling of p62 was further confirmed using a nuclear export inhibitor Leptomycin B (Fig. 5-10C). Although the exact signals that regulate the nuclear-cytoplasmic shuttling of p62-p65 remain to be evaluated in the future, the present study is a direct proof that p62 recognizes nuclear-ubiquitinated p65 and limits the duration of NF-κB activity.

6.2 Ubiquitination of p65 is required for p62-mediated autophagic degradation of nuclear p65.

Adequate control of NF-κB response termination is of fundamental importance to prevent a sustained production of inflammatory mediators and thus immunopathology and cancer. Studies by Saccani et al. (2004) revealed that the termination of NF-κB transcriptional activity occurs even in the absence of IκBα (49). In addition to the robust mechanism of inhibition mediated by IκBα, NF-κB-induced transcription is selectively controlled in a gene-specific manner (49). In this regard, post-translational modifications including ubiquitination are critical in regulating the NF-κB transcriptional response (38). Ubiquitination of p65 occurs predominantly in the nucleus where it appears to control DNA binding of a fraction of nuclear p65 ensuring the limited duration of expression of specific NF-κB target genes (49). Previous studies demonstrated that ubiquitination of NF-κB promotes its nuclear degradation by proteasomes. Accordingly, inhibition of proteasome activity appears to selectively stabilize nuclear p65 with minimal effect on the cytoplasmic fraction (49,250,251). However, inhibition of proteasome activity does not impair dissociation of p65 from all NF-κB target promoters (49), suggesting that additional mechanisms to the proteasomal degradation may occur to remove NF-κB from DNA. We propose that p62 recognizes a specific ubiquitinated fraction of nuclear p65 for autophagic degradation. Interestingly, the inhibition of deubiquitinases was essential for studying the binding between p65 and LC3, indicating that their interaction depends on ubiquitin-conjugation (Fig. 5-4C and D). Additional immunoprecipitation data reveal that p62 recognizes and binds to ubiquitinated p65 via its UBA domain (Fig. 5-6A), which further confirms our hypothesis.

p62 is a multifunctional protein that mediates the delivery and degradation of polyubiquitinated proteins to both, proteasome- and autophagy-dependent pathways (252). In this regard, recent evidence showed that p62 binds to proteosomes via its N-terminal Phox-BEM1 domain (PB1) and to autophagosomes via its LIR domain (189,253). The switch between the proteasomal and autophagic function of p62 remains unknown (254). Jodo et al. (2020) have recently shown that nuclear ubiquitin E3 ligase

PDLIM2-mediated p65 degradation following TLR activation is facilitated by p62, which is bound to both polyubiquitinated PDLIM2 via its UBA domain and to the proteasome via its PB1 domain (255). Although nuclear binding between p62 and p65 was also found in the present study (Fig. 5-10B), we observed that p65 degradation is only partially blocked by proteasome inhibition after TNFα treatment (Fig. 5-9E, upper panel). In contrast, autophagy inhibition is able to completely rescue its protein level (Fig. 5-9E, bottom panel), suggesting the autophagy-lysosome pathway as an alternative mechanism responsible for p65 degradation after NF-κB activation. Accordingly, immunofluorescence analysis confirms that p65 is delivered to the lysosome mainly after activation (Fig. 5-9A). In order to explain the reason for this apparent discrepancy, it is important to note that these two major degradation systems (proteasome and autophagy) are not necessarily mutually exclusive. Several proteins are degraded by both proteasome and autophagy (256,257). It has been proposed that polyubiquitin chains determine the degradation mode. For instance, the protein target with K48-linked chains tends to be degraded by the proteasome, whereas the K63-linked chain or monoubiquitinated substrates are modified by autophagy (258). In addition to K48 linked polyubiquitination, p65 ubiquitination involves a number of other ubiquitin linkages including K63 (53). p65 has also been reported to be regulated by mono-ubiquitination, which promotes nuclear retention of p65 and may negatively regulate its transcriptional activity by inhibiting interaction with the transcription coactivator CBP (259). Interestingly, a recent study identified K63-linked ubiquitination chains at multiple sites of p52/p100 (a non-canonical NF-κB transcription factor; see Introduction 1.2.1), which are essential for the recognition and degradation of p100/p52 by p62-dependent selective autophagy (260). Thus, the search for the potential polyubiquitin chain that promotes p62-mediated autophagic degradation of p65 will continue in the future.

The identification of the p65 ubiquitin ligase(s) acting at the promoter level is required to fully elucidate the possible role of p65 ubiquitination in transcriptional activation. Several E3 ligases are reported to promote the ubiquitination and degradation of nuclear p65 (48). However, the reason why multiple p65 ligases appear to regulate NF-κB transcriptional activity is still unknown. It is possible that these ligases bind to different p65 containing dimers or have prevalent roles depending on the stimulus or cell type (48). Moreover, mass spectrometry studies revealed many ubiquitin acceptor sites on p65, which may reflect the binding specificities of different E3 ligases (53). GST pull-down experiments with truncation mutants of p65 reveal that LC3 interacts with the Rel Homology Domain (RHD) fragments of p65 between amino acids 193 to 306 (Fig. 5-4A).

Congruent with our result, a recent study showed that LRRC25 protein interacts with the RHD domain of p65 to enhance the association between p65 and p62 for subsequent autophagic degradation (198). Future studies including mathematical modelling might be important for unravelling the complexities and dynamics of stress-induced ubiquitination of p65, p62 binding, and nuclear-cytoplasmic translocation to the autophagosome.

6.3 Autophagy mediates termination of the NF-κB inflammatory response

Autophagy plays a critical role in inflammation and immunity (261). Genome-wide association studies suggested a correlation between autophagy-related gene polymorphisms and many inflammatory disorders, including cancer (262–264). For instance, several autophagy-deficient mice models such as myeloid-specific *Atg16L1* KO mice, colonic epithelial cell-specific *Atg7* KO mice, and *Atg4B* null mice all exhibit exacerbated colitis induced by dextran sodium sulfate (DSS) (265–267). All these studies suggest that impaired autophagy promotes a pro-inflammatory condition. However, despite the increasing interest in the role of autophagy in the pathogenesis of several autoimmune and inflammatory disorders, the mechanism by which autophagy prevents exaggerated pro-inflammatory responses needs further investigation.

The crosstalk between NF-κB signaling and autophagy has been suggested to regulate inflammation in different cellular contexts and in response to different stimuli (239,240,268). Here, we observed that both NF-kB induced-inflammatory response and autophagy are induced successively in several cell line models in response to different cellular stresses, such as TNFa, γ-irradiation, and LPS (Fig. 5-1). Most importantly, the mRNA expression of various proinflammatory NF-κB target genes is significantly higher in response to these stimuli when autophagy degradation is impaired (Fig. 5-5B and 5-10A). Interestingly, the reestablishment of the autophagic flux was sufficient to rescue the cytokine expressions at the level of control (Fig. 5-5B and 5-10A). In line with this, luciferase analysis confirms that the modulation of autophagy influences transcriptional NF-κB activity in response to either TNFα or γ-irradiation (Fig.5-5A). Congruent with our results, pharmacological activation of autophagy using rapamycin or other mTOR-inhibitors results in reduction of intestinal inflammation in experimental models of inflammatory bowel disease (IBD; (269)). NF-κB plays important role in sustained inflammatory responses in several chronic inflammatory diseases such as IBD (146,270). Direct inhibition of NF-κB family member p65 abrogates established experimental colitis (271). Therefore, we hypothesize that activation of autophagy might

alleviate the inflammatory response through selective inhibition of NF-κB signaling. A previous study showed that LPS-induced activation of NF-κB was enhanced in IEC-specific *ATG7* KO mice, suggesting that autophagy in IECs controls the inflammatory responses via the NF-κB signaling pathway (240). However, the mechanism through which autophagy affects NF-κB activation in the intestinal epithelium was not fully elucidated.

The current study reveals a novel molecular mechanism modulating the NF-κB inflammatory response through nuclear selective sequestration of the NF-κB/p65 subunit by autophagy proteins. Inhibition of autophagy activity by depletion of an essential autophagy gene *ATG16L1* selectively stabilizes nuclear p65 (Fig. 5-10D and E), which in turn enhanced the expression of several pro-inflammatory cytokines (Fig. 5-5B and 5-10A). The gene *ATG16L1* is one of the most important susceptibility genes associated with the pathogenesis and progression of IBD (264). The gene *NFKBIA* encoding IκBα, the inhibitor of NF-κB, was also identified as a risk locus for IBD, suggesting that both autophagy defects and reduced level of IκBα might contribute to constitutively active NF-κB which correlates with the severity of intestinal inflammation (272,273). Accordingly, Matsuzawa-Ishimoto et al. (2017) recently demonstrated that ATG16L1 in the intestinal epithelium is essential for preventing loss of Paneth cells and reducing TNFα-induced IBD pathology both *in vivo* and *ex-vivo* (274). Similarly, depletion of Paneth cells was also observed in the small intestine of mice with constitutive activation of NF-κB, which induces several hallmarks of IBD including increased apoptosis and mucosal inflammation (146). Moreover, increased proteasomal degradation determines higher rate processing of IκBα protein in the mucosa of IBD patients (275). Here we show that p65 ubiquitination and autophagosomal degradation is a mechanism of post-transcriptional repression to control inflammation-driven NF-κB hyperactivation. However, whether autophagy is a mechanism of transcriptional repression also in the absence of IκBα or if it acts in synergism with resynthesized IκBα to guarantee a timely termination of the response in IECs remains to be evaluated in the future.

Notably, IBD associated-mutations in the *ATG16L1* gene, which cause autophagic dysfunction, play roles in both the epithelial- and immune-driven aspects of IBD (276). Emerging evidence revealed that autophagy intrinsically regulates the immune system function. For example, inhibition of macrophage autophagy promotes inflammatory M1 macrophage polarization which is characterized by increased NF-κB activation (204,267). In addition to epithelial cells, we confirmed that autophagy deficiency also led to increased expression of NF-κB inflammatory target genes in response to LPS in

macrophages depleted of the autophagy gene *ATG16L1* (Fig. 5-10A). However, the mechanism that autophagy plays in NF-κB-induced inflammatory responses in the pathogenesis of intestinal inflammation remains to be addressed in experimental models harboring disease-associated autophagy gene alleles.

Interestingly, we also observed that autophagy affects NF-κB inflammatory response in epithelial cells upon irradiation induced-genotoxic stress (Fig. 5-2, 5-5A and 5-8). Patients with IBD are at an increased risk of developing colorectal cancer later in life (54). Therefore, our data imply that in the subset of IBD patients with missense polymorphisms in the *ATG16L1* gene and thus reduced autophagy, an alternative to the traditional radiation therapy should be considered. Increasing knowledge of the pathways involved in tumor fate decisions due to the activation/inhibition of autophagy will certainly open new insights into tumor biology and potentially provide novel therapeutic targets for cancer therapy.

Part II:

NF-κB in cell fate decisions and stem cell maintenance in the small intestinal epithelium.

6.4 Physiological NF-κB activity in small intestinal crypts is not required for IEC proliferation or survival and does not cause local inflammation.

Loss of NF-κB activity in IKK/NF-κB KO mice leads to embryonic lethality between days E15 and E16 post-coitum, mainly due to strongly increased hepatocyte apoptosis in the liver, in which haematopoiesis is taking place at that time (135,277). In contrast, the *ΔN* mouse model with ubiquitously suppressed NF-κB activity allows 75% of the embryos to survive (136). This helped to discover the postnatal pathophysiological consequences of systemic NF-κB/Rel suppression. Accordingly, NF-κB suppression results in severe defects in the development and morphogenesis of ectodermal appendages such as hair follicles, teeth, mammary glands and of secondary lymph nodes, and in the post-natal self-renewal of hair follicles (136). In the current study, *ΔN* mice were used to study the function of NF-κB in the crypts of the small intestine (SI) in which physiological activation of NF-κB was detected using a NF-κB-responsive reporter mouse line (*κ-EGFP*). High EGFP expression, which is entirely dependent on transcriptional activity of NF-κB, was observed in Paneth cells, in '+4/+5' secretory progenitors and in scattered Lgr5+ crypt base columnar (CBC) stem cells of SI crypts. Previous studies suggested that NF-κB is required for intestinal homeostasis regarding IEC proliferation and apoptosis, as well as for the protection against acute intestinal epithelial inflammation (145). However, ubiquitous suppression of NF-κB (*ΔN*) did not result in intestinal inflammation concomitant with alterations in IEC proliferation or increased apoptosis, which was observed in IEC-specific IKK/NF-κB KOs (146,214). The reason why *ΔN* mice do not recapitulate the IEC-specific phenotype of the IKK/NF-κB KOs is mainly related to the massive inflammation going on in the latter. Generally, the severe chronic intestinal inflammation observed in mice with epithelium-specific IKK/NF-κB KOs originates in the underlying mesenchyme, which is responsible for the recruitment of inflammatory cells and cytokine production, thereby causing IEC apoptosis (143). As expected, IEC-restricted *Villin-ΔN* mice (*Villin-ΔN: loxP-ΔN x villin-Cre*) used in the current study also showed some inflammation at advanced ages, but at 8 weeks of age, the phenotype was

identical to *ΔN* mice (211). The same phenomenon was also observed in mice with epidermis-specific loss of NF-κB activity (278–280).

Recent studies revealed that the IKK complex also regulates other signaling pathways and cellular processes independently from NF-κB, which could additionally explain why the IEC-specific deletion of IKK components does not reflect the NF-κB functions observed in the current study (214,281). It is important to note that inflammatory processes are blocked in *ΔN* mice, as these require NF-κB activity in immune cells, including local dendritic cells and macrophages in the mesenchyme adjacent to the SI epithelium (see Fig. 5-14 and; (136,211)). Thus, these mice represent a unique model to study intrinsic NF-κB functions in tissues independently of any aberrant immune reactions that would affect cell viability.

Although the overall number of Ki67-positive cells was not affected in the small intestines of *ΔN* mice (Fig. 5-13), the Ki67+/Lgr5+ cell ratio was significantly higher when compared to controls, which suggests altered crypt cell composition (Fig. 5-23F). In fact, the crypts of *ΔN* mice appeared mainly filled with highly proliferative transit-amplifying (TA) cells that are normally located adjacent to SI crypts (see Fig. 1-7). Interestingly, a similar phenotype was observed in the absence of Paneth cells in *Atoh1* (Math1) and *Sox9* KO mice (282,283). Under normal conditions, the rapidly cycling TA cells include progenitor cells (Ki67-positive cells) that terminally differentiate into either absorptive or secretory lineages (158). According to our TEM images and PTAB staining results, *ΔN* crypts contained aberrant immature intermediate cells in addition to undifferentiated/TA cells (Fig. 5-21A and 5-22). Together, these cell types might be responsible for a similar proliferation rate and unaltered expression of secretory precursor markers (*Prom1, Msi1 and Ephb3*; see Fig. 5-23C) in crypts of *ΔN and* control mice. Based on these results, a potential role of NF-κB in SI self-renewal and lineage specification was further examined as discussed below.

6.5 NF-κB activity is essential for Paneth versus goblet cell fate decision in the small intestine.

Crypt homeostasis and *ex vivo* organoid growth are ensured by Wnt and Notch ligands, which are mainly produced by Paneth cells (165,230). The current study demonstrates that loss of NF-κB activity in *ΔN* mice strongly reduces Paneth cell numbers in the crypts of the small intestine (Fig. 5-16). Nevertheless, several studies revealed that non-epithelial Wnt ligands in the underlying mesenchyme provide a secondary physiological source of Wnt in the absence of Paneth cells (174,228,284). This would explain why NF-

κB activity is dispensable for maintaining SI epithelial proliferation, but is essential for *ex vivo* organoid growth that requires Paneth cell-derived Wnt3 (Fig. 5-24). Although addition of Wnt3 alone rescues the growth of *ΔN* organoids, it is not sufficient to rescue loss of Paneth cells, which strongly suggests that NF-κB regulates the expression of additional Wnts required for proper Paneth cell differentiation and maturation (see results paragraph 5.14).

Multiple local signaling pathways form an opposing gradient along the crypt axis that are fundamental for correct differentiation processes and for maintenance of intestinal homeostasis. A common secretory precursor cell gives rise to Paneth or goblet cells. The specification of precursors into Paneth cell fate is determined by a local environment of high Wnt/β-catenin and expression of transcription factor Sox9 (see below), whereas low Wnt activity is required for goblet cell formation (285). The exact mechanism of this switch remains unknown. A recent study of Heuberger et al. (2014) proposed that fine-tuning of Wnt signaling might in part be regulated by Shp2/Mek1/MAPK signaling that interferes with Tcf4/β-catenin signaling in goblet/Paneth cell progenitors (170). Accordingly, high Shp2/MAPK activity inhibits Wnt/β-catenin signaling, increasing goblet cell differentiation. On the contrary, MAPK suppression in crypts increases Wnt/β-catenin signaling, which in turn promotes Paneth cell formation (170). Our data suggests that fine-tuning of Wnt activity is disturbed in *ΔN* mice, which increases the expression of goblet cell markers at the expense of Paneth cells. In fact, expression of *Wnt3* and *Wnt10a* mRNA is significantly reduced in SI crypts and in organoids from *ΔN* mice (Fig. 5-29). We hypothesize that NF-κB is required for the Paneth/goblet cell switch in secretory precursors, while a potential connection between Shp2/MAPK signaling and NF-κB activity in SI crypt homeostasis remains to be evaluated in the future.

A previous NF-κB-dependent transcriptome of early primary hair follicle development revealed a number of novel NF-κB target genes (210). Among others, NF-κB-dependent expression of *Wnt10a* was demonstrated to be specifically required for differentiation and morphogenesis in post-mitotic stem cells that have already been primed (286,287). Interestingly, a recent study revealed that *Wnt10a* is also expressed in mature Paneth cells and might control the proliferative capacity of IEC (234). In line with this, in situ hybridization (ISH) analysis confirmed *Wnt10a* mRNA expression in Paneth cells (Fig. 5-29D), suggesting that it might regulate CBC proliferation and maintenance together with Wnt3, but it may additionally control Paneth cell differentiation in the secretory progenitor. Studies have shown that, on one hand, Wnt signals are crucial for maintenance of undifferentiated progenitors. On the other hand, immature Paneth cells,

once specified, use these Wnts to reach full maturity (288,289). Although the exact mechanism remains unknown, *Wnt10a* represents a promising NF-κB-dependent target gene involved in intestinal homeostasis, and future single cell analysis would be crucial to determine its role in cell fate determinations of the small intestine.

In addition to *Wnt10a*, transcription factor *Sox9* was also found as NF-κB target gene in epithelial cells (210). Sox9 plays an important role in SI crypts where it is required for stem/progenitor cell proliferation but also for final differentiation of Paneth cells (237). Interestingly, *Sox9* expression is strongly reduced in SI crypts of *ΔN* mice, while aberrantly upregulated in mice with constitutively elevated NF-κB activity in the intestinal epithelium (*IκBα*$^{IEC\text{-}KO}$; (146)), suggesting that *Sox9* expression is dependent on NF-κB activity in the SI epithelium (Fig. 5-30C). However, while prior studies using IEC-specific *Sox9* KO mice showed loss of Paneth cell differentiation, other secretory lineages like goblet cells remained unaffected in contrast to *ΔN* mice (237,283). Nevertheless, Sox9 was found to repress expression of the goblet cell marker gene *Muc2* in IEC, which would partially explain why in absence of NF-κB activity the expression of goblet cell marker *Muc2* is increased (236). Thus, the molecular and/or physiological changes along with reduced *Sox9* expression in secretory progenitors must cause the increased numbers of goblet cells in *ΔN* mice.

Strong evidence suggests that the Notch ligand Dll1 is strongly up-regulated in a small subset of progenitor cells that are early descendants of Lgr5+ CBC (221,290). These Dll1^{high} progenitor cells differentiate into secretory lineages, and thus into Paneth cells. High expression of Dll1 on mature Paneth cells activates Notch signalling via Notch receptors on adjacent CBCs preventing their differentiation and maintaining their stem cell identity (165). Therefore, loss of Paneth cells would diminish *Dll1* expression in the SI crypts of *ΔN* mice which would lead to reduced local Notch signaling, as verified by decreased expression of Notch target gene *Hes1* (Fig. 5-18A). In accordance with the phenotype that we observed in the SI of *ΔN* mice, loss of Notch signaling within the SI epithelium or IEC-specific *Dll1* KO mice resulted in differentiation of proliferative crypt cells into post-mitotic goblet cells (216,291). Altogether, in the absence of NF-κB activity decreased *Dll1* expression in SI crypts, together with local loss of *Wnt3, Wnt10a* and *Sox9* expression, might incline the fate decisions of secretory progenitors towards goblet cells.

6.6 NF-κB is required for Lgr5+ stem cell maintenance via fine-tuning of Wnt signaling in SI crypts.

The current study demonstrates that, in addition to Paneth/goblet cell fate decision, suppression of NF-κB activity affects Wnt signaling and specifically Lgr5+ CBCs maintenance (see results 5.13 and above, 6.5). Interestingly, crosstalk between Wnt/β-catenin and NF-κB signaling appears to control crypt base columnar stem cell (CBC) expansion during inflammation-induced tumorigenesis (232,233). These studies on tumorigenesis in the intestinal epithelium showed that local aberrant NF-κB signaling enhances Wnt activation and induces dedifferentiation of non-stem cells that acquire stem-cell-like properties. In contrast, IEC-specific ablation of NF-κB *p65/RelA* retarded crypt stem cell expansion (232,233). Furthermore, studies focusing on intrinsic effects of elevated NF-κB activity using organoids of IEC-specific *IκBα* KO mice, which overcome the IBD-like inflammation seen in these mice, revealed increased numbers of misplaced Paneth cells and of CBCs as well as elevated Wnt activity (146). Accordingly, decreased Wnt activity together with reduced number of Lgr5+ CBCs were observed in SI crypts of *ΔN* mice, which may have caused the significantly reduced Wnt-dependent expression of *Lgr5, Ascl2, Ccdn1, Tnfrsf19* and *Edn1* (Fig. 5-23C).

It was demonstrated that Paneth cells express Wnt3 and all essential signals for stem-cell maintenance in culture and genetic removal of Paneth cells *in vivo* resulted in the concomitant loss of Lgr5 stem cells (165). Thus, lack of Paneth cells in absence of NF-κB activity may have driven the reduction of Lgr5+ cells *in vivo*, which was overcome by addition of Wnt3 to support stem cell function in organoid cultures (Fig. 5-24 and 5-25). In fact, *ΔN* organoids derived from either SI crypts or Lgr5+ single cells grown in Wnt3-containing culture medium (WENR) re-express *Lgr5* and *Ascl2* at higher levels than controls (Fig. 5-25A), suggesting that Wnt rather than NF-κB is the major regulator of *Lgr5* and *Ascl2*. Finally, the re-establishment of Ki67/Lgr5+ cell ratio in *ΔN* organoids in WENR medium further confirmed that the Lgr5+ CBC population was restored in the presence of Wnt3 (Fig. 5-25B).

Similar to *ΔN* organoids grown in WENR medium, van Es et al. (2012) showed in their study that early secretory progenitors can revert to Lgr5+ CBCs *in vitro* when provided with exogenous Wnt signals, which might explain how *ΔN* organoids regain stemness (290). These results explain not only why *ΔN* organoids are able to grow exclusively in WENR medium, but also indicates that NF-κB activity is essential for fine-tuning of Wnt signaling in SI crypts. In addition to epithelial Paneth cells, extra-epithelial mesenchymal cells also provide Wnt ligands for maintaining intestinal homeostasis via renewal of the

stem cell pool (292). However, although exogenous Wnt3 alone can restore Lgr5+ CBCs in *ΔN* organoid culture, stromal Wnts may not be sufficient to fully maintain Lgr5+ CBCs in SI crypts of *ΔN* mice. Since Wnt3 is not sufficient to rescue loss of Paneth cells in *ΔN* organoids (Fig. 5-27 and 5-28), NF-κB might regulate the expression of additional Wnts, here Wnt10a secreted by Paneth cells, which are required for stem cell maintenance as well as Paneth cell differentiation. In line with this, mRNA expression of *Wnt3* and *Wnt10a* was strongly downregulated in *ΔN* organoids, independently from Wnt3-containing culture medium (Fig. 5-29C). This suggests that NF-κB activity is crucial for Paneth cell maturation, which in turn is responsible for the expression of these two essential Wnts. According to our hypothesis, an earlier study of the Haller group revealed that Wnt10a - was able to partly rescue intestinal epithelial stemness and proliferation retardation induced by mitochondrial dysfunction (234). Human *Wnt10a* mutations are associated with different ectodermal anomalies and its roles in epithelial regeneration were described recently (286,293). Future studies using genetic mouse models with IEC-specific *Wnt10a* deletion will be important to prove the proper role of Wnt10a in stem cell maintenance in SI crypts.

Dll1- and Dll4-mediated Notch signaling plays an essential role in the homeostasis of intestinal stem cells (216). This study revealed that Dll1 is downregulated in crypts and organoids of *ΔN* mice ((211); Fig. 5-18A), which may be linked to loss of Paneth cells as described above (see paragraph 6.2). Interestingly, while Dll1+ cells were shown to act as a source of Notch signaling to maintain Lgr5+ CBCs (294), inactivation of Dll1 alone in the SI epithelium does not affect the expression of *Olfm4*, a robust marker for Lgr5+ CBCs (212). In contrast, absence of both Dll1 and Dll4 ligands results in the complete loss of Lgr5+ CBCs concomitant with reduced mRNA expression of *Lgr5, Ascl2* and *Olfm4* (216). mRNA expression of *Olfm4* remains unchanged in *ΔN* mice (Fig. 5-23B), which suggests that only a specific subset of stem cell might be affected by suppression of NF-κB activity. Moreover, *Olfm4* was shown to be a Notch target gene (295). Thus, *Dll4* expression in crypts of *ΔN* mice (see Fig. 5-18A) might be sufficient to enable Olfm4 expression. Finally, ISC marker Olfm4 is sensitive to Notch blockade, but not to attenuation of Wnt signaling that affects expression of *Lgr5* and *Ascl2* (295), as observed in *ΔN* mice (Fig. 5-23C).

Among known members of the TNF family, TNF-family member Eda-A1 (Ectodysplasin A1) plays an important role in the physiological activation of NF-κB during fetal skin appendage development and adult hair follicle self-renewal (296,297). However, previous analysis of Eda-A1-mutant mice did not show any altered intestinal phenotype

and Paneth cell numbers remained unchanged compared to control mice (data not shown), suggesting that Eda-A1 signaling is not involved in the intestinal activation of NF-κB. Although the upstream activator of NF-κB that specifically regulates Paneth cell differentiation and Lgr5+ CBC maintenance in the SI epithelium has not been identified yet, TNF Receptor Superfamily Member 19 (Tnfrsf19) represents a potential candidate. *Tnfrsf19* (also called Troy) is a Wnt/β-Catenin target gene expressed in intestinal Lgr5+ CBCs and appears to modulate Wnt signaling in human colorectal cancer cell lines and in intestinal tumors of mice (298). Interestingly, the expression of Troy is downregulated in SI crypts of *ΔN* mice (Fig. 5-23C), which might be due to reduced Wnt ligand expression (see above). Moreover, a recent study showed that Lgr5-Troy interaction is required for activating NF-κB signaling in colon cancer cells and intestinal crypt organoids (299). In summary, the current study demonstrates that NF-κB and Wnt signaling co-regulate important physiological processes in the SI epithelium. This proves yet again that a reciprocal requirement of NF-κB and Wnt signaling is essential for the homeostasis of epithelial tissues, such as the SI or skin appendages (137,211)

7. CONCLUSION

The first part of this research aimed to investigate the functional interplay between autophagy and NF-κB signaling in the regulation of inflammation. By using biochemical analysis and imaging techniques the interaction of endogenous autophagic proteins and NF-κB/p65 subunit was characterized upon stress-induced inflammation. We reveal a novel molecular mechanism modulating the NF-κB inflammatory response through nuclear selective sequestration of p65 by autophagy proteins. Emerging evidence suggests that nuclear accumulation of LC3 plays a role in different nuclear functions in response to specific types of stress (241,242,244). However, this is the first report to show that the activity of a transcription factor can be directly regulated by selective autophagy in the nucleus to prevent exaggerated pro-inflammatory responses. Understanding the exact molecular mechanisms that facilitate proinflammatory responses upon inhibition of autophagic activity could have a great impact on the development of new therapeutic strategies for the treatment of various disorders. Accordingly, constitutive activation of the NF-κB pathway and defective autophagy are often associated with different inflammatory diseases and cancer development (117). For instance, previous genome-wide association studies suggested that both autophagy defects and reduced levels of IκBα, the inhibitor of NF-κB might contribute to constitutively active NF-κB which correlates with the severity of intestinal inflammation (264,272). Therefore, our findings are of great importance for the development of new strategies in prevention and/or treatment of intestinal inflammatory disease.

In addition to its critical role in intestinal inflammation and tumor formation, NF-κB signaling is essential in other biological contexts such as developmental processes (132,136). Establishing 3D organoid culture from the small intestine (SI) and using different mouse lines, we prove in the second part of the thesis that the transcription factor NF-kB plays an important function in cell differentiation and stem cell maintenance *in vivo* and in *ex-vivo*. The self-renewal capacity of the intestinal epithelium is supported by intestinal stem cells that can differentiate into different epithelial cell types, including secretory cells such as Paneth and goblet cells (159). We report for the first time that NF-κB controls Paneth versus goblet cell fate decisions in the mouse SI. Moreover, the expression of *Wnt3, Wnt10A*, and the Wnt target *Sox9* is disrupted in SI crypts and organoids derived from mice with ubiquitous suppression of NF-κB activity (*ΔN* mice). Collectively, these findings uncover a new role for NF-κB in the homeostasis of the small

intestine through cell fate decisions and interaction with the Wnt signaling. Given the critical role of NF-κB in chronic inflammatory diseases (for example Crohn's Disease and Ulcerative Colitis) and cancer (Colorectal Carcinoma), our research improves our understanding of the physiological functions of NF-κB in stem cell biology. This could be essential for future translational studies focusing on the modulation of its activity with great clinical impact.

8. REFERENCES

1. Hayden MS, Ghosh S. Shared Principles in NF-κB Signaling. Cell. 2008 Feb 8;132(3):344–62.

2. Sen R, Baltimore D. Multiple nuclear factors interact with the immunoglobulin enhancer sequences. Cell. 1986 Aug 29;46(5):705–16.

3. Espín-Palazón R, Traver D. The NF-κB family: Key players during embryonic development and HSC emergence. Exp Hematol. 2016 Jul;44(7):519–27.

4. Hinz M, Scheidereit C. The IκB kinase complex in NF-κB regulation and beyond. EMBO Rep. 2014 Jan;15(1):46–61.

5. Coussens LM, Werb Z. Inflammation and cancer. Nature. 2002 Dec;420(6917):860–7.

6. Xia Y, Shen S, Verma IM. NF-κB, an active player in human cancers. Cancer Immunol Res. 2014 Sep;2(9):823–30.

7. Hayden MS, Ghosh S. Regulation of NF-κB by TNF family cytokines. Semin Immunol. 2014 Jun;26(3):253–66.

8. Ghosh G, Wang VY-F, Huang D-B, Fusco A. NF-κB regulation: lessons from structures. Immunol Rev. 2012 Mar;246(1):36–58.

9. Zhong H, May MJ, Jimi E, Ghosh S. The Phosphorylation Status of Nuclear NF-KB Determines Its Association with CBP/p300 or HDAC-1. Mol Cell. 2002 Mar 1;9(3):625–36.

10. Chen FE, Huang DB, Chen YQ, Ghosh G. Crystal structure of p50/p65 heterodimer of transcription factor NF-kappaB bound to DNA. Nature. 1998 Jan 22;391(6665):410–3.

11. Hayden MS, Ghosh S. NF-κB, the first quarter-century: remarkable progress and outstanding questions. Genes Dev. 2012 Feb 1;26(3):203–34.

12. Hoffmann A, Baltimore D. Circuitry of nuclear factor kappaB signaling. Immunol Rev. 2006 Apr;210:171–86.

13. Wertz IE, Dixit VM. Signaling to NF-kappaB: regulation by ubiquitination. Cold Spring Harb Perspect Biol. 2010 Mar;2(3):a003350.

14. Yu H, Lin L, Zhang Z, Zhang H, Hu H. Targeting NF-κB pathway for the therapy of diseases: mechanism and clinical study. Signal Transduct Target Ther. 2020 Sep 21;5(1):1–23.

15. Oeckinghaus A, Ghosh S. The NF-kappaB family of transcription factors and its regulation. Cold Spring Harb Perspect Biol. 2009 Oct;1(4):a000034.

16. Hsu H, Xiong J, Goeddel DV. The TNF receptor 1-associated protein TRADD signals cell death and NF-kappa B activation. Cell. 1995 May 19;81(4):495–504.

17. Hsu H, Huang J, Shu HB, Baichwal V, Goeddel DV. TNF-dependent recruitment of the protein kinase RIP to the TNF receptor-1 signaling complex. Immunity. 1996 Apr;4(4):387–96.

18. Varfolomeev E, Goncharov T, Vucic D. Roles of c-IAP proteins in TNF receptor family activation of NF-κB signaling. Methods Mol Biol. 2015;1280:269–82.

19. Tokunaga F, Sakata S, Saeki Y, Satomi Y, Kirisako T, Kamei K, et al. Involvement of linear polyubiquitylation of NEMO in NF-kappaB activation. Nat Cell Biol. 2009 Feb;11(2):123–32.

20. Devin A, Cook A, Lin Y, Rodriguez Y, Kelliher M, Liu Z. The distinct roles of TRAF2 and RIP in IKK activation by TNF-R1: TRAF2 recruits IKK to TNF-R1 while RIP mediates IKK activation. Immunity. 2000 Apr;12(4):419–29.

21. Zhang J, Clark K, Lawrence T, Peggie MW, Cohen P. An unexpected twist to the activation of IKKβ: TAK1 primes IKKβ for activation by autophosphorylation. Biochem J. 2014 Aug 1;461(Pt 3):531–7.

22. Cao X. Self-regulation and cross-regulation of pattern-recognition receptor signalling in health and disease. Nat Rev Immunol. 2016 Jan;16(1):35–50.

23. Kumar H, Kawai T, Akira S. Toll-like receptors and innate immunity. Biochem Biophys Res Commun. 2009 Oct 30;388(4):621–5.

24. Akira S, Uematsu S, Takeuchi O. Pathogen recognition and innate immunity. Cell. 2006 Feb 24;124(4):783–801.

25. Fitzgerald KA, Rowe DC, Barnes BJ, Caffrey DR, Visintin A, Latz E, et al. LPS-TLR4 signaling to IRF-3/7 and NF-kappaB involves the toll adapters TRAM and TRIF. J Exp Med. 2003 Oct 6;198(7):1043–55.

26. Kawai T, Akira S. The role of pattern-recognition receptors in innate immunity: update on Toll-like receptors. Nat Immunol. 2010 May;11(5):373–84.

27. De Bont R, van Larebeke N. Endogenous DNA damage in humans: a review of quantitative data. Mutagenesis. 2004 May 1;19(3):169–85.

28. Ciccia A, Elledge SJ. The DNA Damage Response: Making it safe to play with knives. Mol Cell. 2010 Oct 22;40(2):179–204.

29. d'Adda di Fagagna F. Living on a break: cellular senescence as a DNA-damage response. Nat Rev Cancer. 2008 Jul;8(7):512–22.

30. McCool KW, Miyamoto S. DNA damage-dependent NF-κB activation: NEMO turns nuclear signaling inside out. Immunol Rev. 2012 Mar;246(1):311–26.

31. Wang W, Mani AM, Wu Z-H. DNA damage-induced nuclear factor-kappa B activation and its roles in cancer progression. J Cancer Metastasis Treat. 2017;3:45–59.

32. Wu Z-H, Miyamoto S. Many faces of NF-kappaB signaling induced by genotoxic stress. J Mol Med Berl Ger. 2007 Nov;85(11):1187–202.

33. Timinszky G, Till S, Hassa PO, Hothorn M, Kustatscher G, Nijmeijer B, et al. A macrodomain-containing histone rearranges chromatin upon sensing PARP1 activation. Nat Struct Mol Biol. 2009 Sep;16(9):923–9.

34. Stilmann M, Hinz M, Arslan SÇ, Zimmer A, Schreiber V, Scheidereit C. A Nuclear Poly(ADP-Ribose)-Dependent Signalosome Confers DNA Damage-Induced IκB Kinase Activation. Mol Cell. 2009 Nov 13;36(3):365–78.

35. Hinz M, Stilmann M, Arslan SÇ, Khanna KK, Dittmar G, Scheidereit C. A cytoplasmic ATM-TRAF6-cIAP1 module links nuclear DNA damage signaling to ubiquitin-mediated NF-κB activation. Mol Cell. 2010 Oct 8;40(1):63–74.

36. Jin H-S, Lee D-H, Kim D-H, Chung J-H, Lee S-J, Lee TH. cIAP1, cIAP2, and XIAP act cooperatively via nonredundant pathways to regulate genotoxic stress-induced nuclear factor-kappaB activation. Cancer Res. 2009 Mar 1;69(5):1782–91.

37. Perkins ND, Gilmore TD. Good cop, bad cop: the different faces of NF-κB. Cell Death Differ. 2006 May;13(5):759–72.

38. Perkins ND. Post-translational modifications regulating the activity and function of the nuclear factor kappa B pathway. Oncogene. 2006 Oct;25(51):6717–30.

39. Vermeulen L, De Wilde G, Van Damme P, Vanden Berghe W, Haegeman G. Transcriptional activation of the NF-kappaB p65 subunit by mitogen- and stress-activated protein kinase-1 (MSK1). EMBO J. 2003 Mar 17;22(6):1313–24.

40. Wang D, Westerheide SD, Hanson JL, Baldwin AS. Tumor necrosis factor alpha-induced phosphorylation of RelA/p65 on Ser529 is controlled by casein kinase II. J Biol Chem. 2000 Oct 20;275(42):32592–7.

41. Sizemore N, Lerner N, Dombrowski N, Sakurai H, Stark GR. Distinct Roles of the IκB Kinase α and β Subunits in Liberating Nuclear Factor κB (NF-κB) from IκB and in Phosphorylating the p65 Subunit of NF-κB *. J Biol Chem. 2002 Feb 8;277(6):3863–9.

42. Buss H, Dörrie A, Schmitz ML, Frank R, Livingstone M, Resch K, et al. Phosphorylation of Serine 468 by GSK-3β Negatively Regulates Basal p65 NF-κB Activity *. J Biol Chem. 2004 Nov 26;279(48):49571–4.

43. Schwabe RF, Sakurai H. IKKbeta phosphorylates p65 at S468 in transactivaton domain 2. FASEB J Off Publ Fed Am Soc Exp Biol. 2005 Oct;19(12):1758–60.

44. Mattioli I, Geng H, Sebald A, Hodel M, Bucher C, Kracht M, et al. Inducible Phosphorylation of NF-κB p65 at Serine 468 by T Cell Costimulation Is Mediated by IKKε *. J Biol Chem. 2006 Mar 10;281(10):6175–83.

45. Zhong H, SuYang H, Erdjument-Bromage H, Tempst P, Ghosh S. The Transcriptional Activity of NF-κB Is Regulated by the IκB-Associated PKAc Subunit through a Cyclic AMP–Independent Mechanism. Cell. 1997 May 2;89(3):413–24.

46. Campbell KJ, Perkins ND. Post-translational modification of RelA(p65) NF-kappaB. Biochem Soc Trans. 2004 Dec;32(Pt 6):1087–9.

47. Chen L-F, Williams SA, Mu Y, Nakano H, Duerr JM, Buckbinder L, et al. NF-kappaB RelA phosphorylation regulates RelA acetylation. Mol Cell Biol. 2005 Sep;25(18):7966–75.

48. Collins PE, Mitxitorena I, Carmody RJ. The Ubiquitination of NF-κB Subunits in the Control of Transcription. Cells [Internet]. 2016 May 12 [cited 2021 Jan 18];5(2). Available from: https://www.ncbi.nlm.nih.gov/pmc/articles/PMC4931672/

49. Saccani S, Marazzi I, Beg AA, Natoli G. Degradation of Promoter-bound p65/RelA Is Essential for the Prompt Termination of the Nuclear Factor κB Response. J Exp Med. 2004 Jul 5;200(1):107–13.

50. Hou Y, Zhang Z, Xu Q, Wang H, Xu Y, Chen K. Inhibitor of growth 4 induces NFκB/p65 ubiquitin-dependent degradation. Oncogene. 2014 Apr;33(15):1997–2003.

51. Hou Y, Moreau F, Chadee K. PPARγ is an E3 ligase that induces the degradation of NFκB/p65. Nat Commun. 2012 Jan;3(1):1300.

52. Zotti T, Uva A, Ferravante A, Vessichelli M, Scudiero I, Ceccarelli M, et al. TRAF7 Protein Promotes Lys-29-linked Polyubiquitination of IκB Kinase (IKKγ)/NF-κB Essential Modulator (NEMO) and p65/RelA Protein and Represses NF-κB Activation. J Biol Chem. 2011 Jul 1;286(26):22924–33.

53. Li H, Wittwer T, Weber A, Schneider H, Moreno R, Maine GN, et al. Regulation of NF-κB activity by competition between RelA acetylation and ubiquitination. Oncogene. 2012 Feb 2;31(5):611–23.

54. Hussain SP, Harris CC. Inflammation and cancer: an ancient link with novel potentials. Int J Cancer. 2007 Dec 1;121(11):2373–80.

55. Tak PP, Firestein GS. NF-κB: a key role in inflammatory diseases. J Clin Invest. 2001 Jan 1;107(1):7–11.

56. Pikarsky E, Porat RM, Stein I, Abramovitch R, Amit S, Kasem S, et al. NF-κB functions as a tumour promoter in inflammation-associated cancer. Nature. 2004 Sep;431(7007):461–6.

57. Greten FR, Eckmann L, Greten TF, Park JM, Li Z-W, Egan LJ, et al. IKKbeta links inflammation and tumorigenesis in a mouse model of colitis-associated cancer. Cell. 2004 Aug 6;118(3):285–96.

58. Pollard JW. Tumour-educated macrophages promote tumour progression and metastasis. Nat Rev Cancer. 2004 Jan;4(1):71–8.

59. Bando H, Toi M. Tumor angiogenesis, macrophages, and cytokines. Adv Exp Med Biol. 2000;476:267–84.

60. Yamamoto Y, Gaynor RB. Therapeutic potential of inhibition of the NF-κB pathway in the treatment of inflammation and cancer. J Clin Invest. 2001 Jan 15;107(2):135–42.

61. Mantovani A, Allavena P, Sica A, Balkwill F. Cancer-related inflammation. Nature. 2008 Jul 24;454(7203):436–44.

62. Biswas SK, Sica A, Lewis CE. Plasticity of Macrophage Function during Tumor Progression: Regulation by Distinct Molecular Mechanisms. J Immunol. 2008 Feb 15;180(4):2011–7.

63. Gordon S, Taylor PR. Monocyte and macrophage heterogeneity. Nat Rev Immunol. 2005 Dec;5(12):953–64.

64. Van Ginderachter JA, Movahedi K, Hassanzadeh Ghassabeh G, Meerschaut S, Beschin A, Raes G, et al. Classical and alternative activation of mononuclear phagocytes: Picking the best of both worlds for tumor promotion. Immunobiology. 2006 Sep 14;211(6):487–501.

65. Mancino A, Lawrence T. Nuclear Factor-κB and Tumor-Associated Macrophages. Clin Cancer Res. 2010 Feb 1;16(3):784–9.

66. Biswas SK, Gangi L, Paul S, Schioppa T, Saccani A, Sironi M, et al. A distinct and unique transcriptional program expressed by tumor-associated macrophages (defective NF-κB and enhanced IRF-3/STAT1 activation). Blood. 2006 Mar 1;107(5):2112–22.

67. Saccani A, Schioppa T, Porta C, Biswas SK, Nebuloni M, Vago L, et al. p50 Nuclear Factor-κB Overexpression in Tumor-Associated Macrophages Inhibits M1 Inflammatory Responses and Antitumor Resistance. Cancer Res. 2006 Dec 1;66(23):11432–40.

68. Hagemann T, Biswas SK, Lawrence T, Sica A, Lewis CE. Regulation of macrophage function in tumors: the multifaceted role of NF-κB. Blood. 2009 Apr 2;113(14):3139–46.

69. Hagemann T, Lawrence T, McNeish I, Charles KA, Kulbe H, Thompson RG, et al. “Re-educating” tumor-associated macrophages by targeting NF-κB. J Exp Med. 2008 Jun 9;205(6):1261–8.

70. Lamb CA, Yoshimori T, Tooze SA. The autophagosome: origins unknown, biogenesis complex. Nat Rev Mol Cell Biol. 2013 Dec;14(12):759–74.

71. Proikas-Cezanne T, Takacs Z, Dönnes P, Kohlbacher O. WIPI proteins: essential PtdIns3P effectors at the nascent autophagosome. J Cell Sci. 2015 Jan 15;128(2):207–17.

72. Mizushima N, Noda T, Yoshimori T, Tanaka Y, Ishii T, George MD, et al. A protein conjugation system essential for autophagy. Nature. 1998 Sep 24;395(6700):395–8.

73. Ichimura Y, Kirisako T, Takao T, Satomi Y, Shimonishi Y, Ishihara N, et al. A ubiquitin-like system mediates protein lipidation. Nature. 2000 Nov 23;408(6811):488–92.

74. Kabeya Y, Mizushima N, Ueno T, Yamamoto A, Kirisako T, Noda T, et al. LC3, a mammalian homologue of yeast Apg8p, is localized in autophagosome membranes after processing. EMBO J. 2000 Nov 1;19(21):5720–8.

75. Wild P, McEwan DG, Dikic I. The LC3 interactome at a glance. J Cell Sci. 2014 Jan 1;127(1):3–9.

76. Tsuboyama K, Koyama-Honda I, Sakamaki Y, Koike M, Morishita H, Mizushima N. The ATG conjugation systems are important for degradation of the inner autophagosomal membrane. Science. 2016 Nov 25;354(6315):1036–41.

77. Antonioli M, Di Rienzo M, Piacentini M, Fimia GM. Emerging Mechanisms in Initiating and Terminating Autophagy. Trends Biochem Sci. 2017 Jan;42(1):28–41.

78. Nazio F, Strappazzon F, Antonioli M, Bielli P, Cianfanelli V, Bordi M, et al. mTOR inhibits autophagy by controlling ULK1 ubiquitylation, self-association and function through AMBRA1 and TRAF6. Nat Cell Biol. 2013 Apr;15(4):406–16.

79. Inoki K, Li Y, Zhu T, Wu J, Guan K-L. TSC2 is phosphorylated and inhibited by Akt and suppresses mTOR signalling. Nat Cell Biol. 2002 Sep;4(9):648–57.

80. Kim J, Kundu M, Viollet B, Guan K-L. AMPK and mTOR regulate autophagy through direct phosphorylation of Ulk1. Nat Cell Biol. 2011 Feb;13(2):132–41.

81. Kim J, Kim YC, Fang C, Russell RC, Kim JH, Fan W, et al. Differential regulation of distinct Vps34 complexes by AMPK in nutrient stress and autophagy. Cell. 2013 Jan 17;152(1–2):290–303.

82. Weidberg H, Shvets E, Elazar Z. Biogenesis and Cargo Selectivity of Autophagosomes. Annu Rev Biochem. 2011;80(1):125–56.

83. Levine B. Cell biology: Autophagy and cancer. Nature. 2007 Apr 11;446:745–7.

84. Kaur J, Debnath J. Autophagy at the crossroads of catabolism and anabolism. Nat Rev Mol Cell Biol. 2015 Aug;16(8):461–72.

85. Rogov V, Dötsch V, Johansen T, Kirkin V. Interactions between Autophagy Receptors and Ubiquitin-like Proteins Form the Molecular Basis for Selective Autophagy. Mol Cell. 2014 Jan 23;53(2):167–78.

86. Geisler S, Holmström KM, Skujat D, Fiesel FC, Rothfuss OC, Kahle PJ, et al. PINK1/Parkin-mediated mitophagy is dependent on VDAC1 and p62/SQSTM1. Nat Cell Biol. 2010 Feb;12(2):119–31.

87. Kirkin V, Lamark T, Sou Y-S, Bjørkøy G, Nunn JL, Bruun J-A, et al. A Role for NBR1 in Autophagosomal Degradation of Ubiquitinated Substrates. Mol Cell. 2009 Feb 27;33(4):505–16.

88. Isakson P, Lystad AH, Breen K, Koster G, Stenmark H, Simonsen A. TRAF6 mediates ubiquitination of KIF23/MKLP1 and is required for midbody ring degradation by selective autophagy. Autophagy. 2013 Dec;9(12):1955–64.

89. Deosaran E, Larsen KB, Hua R, Sargent G, Wang Y, Kim S, et al. NBR1 acts as an autophagy receptor for peroxisomes. J Cell Sci. 2013 Feb 15;126(Pt 4):939–52.

90. Mostowy S, Sancho-Shimizu V, Hamon MA, Simeone R, Brosch R, Johansen T, et al. p62 and NDP52 proteins target intracytosolic Shigella and Listeria to different autophagy pathways. J Biol Chem. 2011 Jul 29;286(30):26987–95.

91. Wild P, Farhan H, McEwan DG, Wagner S, Rogov VV, Brady NR, et al. Phosphorylation of the autophagy receptor optineurin restricts Salmonella growth. Science. 2011 Jul 8;333(6039):228–33.

92. Lazarou M, Sliter DA, Kane LA, Sarraf SA, Wang C, Burman JL, et al. The ubiquitin kinase PINK1 recruits autophagy receptors to induce mitophagy. Nature. 2015 Aug;524(7565):309–14.

93. Gatica D, Lahiri V, Klionsky DJ. Cargo recognition and degradation by selective autophagy. Nat Cell Biol. 2018 Mar;20(3):233–42.

94. Fujiwara Y, Kikuchi H, Aizawa S, Furuta A, Hatanaka Y, Konya C, et al. Direct uptake and degradation of DNA by lysosomes. Autophagy. 2013 Aug;9(8):1167–71.

95. Aizawa S, Fujiwara Y, Contu VR, Hase K, Takahashi M, Kikuchi H, et al. Lysosomal putative RNA transporter SIDT2 mediates direct uptake of RNA by lysosomes. Autophagy. 2016;12(3):565–78.

96. Monkkonen T, Debnath J. Inflammatory signaling cascades and autophagy in cancer. Autophagy. 2018 Feb 1;14(2):190–8.

97. Qi Y, Zhang M, Li H, Frank JA, Dai L, Liu H, et al. Autophagy inhibition by sustained overproduction of IL6 contributes to arsenic carcinogenesis. Cancer Res. 2014 Jul 15;74(14):3740–52.

98. Li P, Du Q, Cao Z, Guo Z, Evankovich J, Yan W, et al. Interferon-γ induces autophagy with growth inhibition and cell death in human hepatocellular carcinoma (HCC) cells through interferon-regulatory factor-1 (IRF-1). Cancer Lett. 2012 Jan 28;314(2):213–22.

99. Netea-Maier RT, Plantinga TS, van de Veerdonk FL, Smit JW, Netea MG. Modulation of inflammation by autophagy: Consequences for human disease. Autophagy. 2015 Jul 29;12(2):245–60.

100. Saitoh T, Fujita N, Jang MH, Uematsu S, Yang B-G, Satoh T, et al. Loss of the autophagy protein Atg16L1 enhances endotoxin-induced IL-1β production. Nature. 2008 Nov;456(7219):264–8.

101. Liu J, Debnath J. The Evolving, Multifaceted Roles of Autophagy in Cancer. Adv Cancer Res. 2016;130:1–53.

102. White E. Deconvoluting the context-dependent role for autophagy in cancer. Nat Rev Cancer. 2012 Jun;12(6):401–10.

103. Karantza-Wadsworth V, Patel S, Kravchuk O, Chen G, Mathew R, Jin S, et al. Autophagy mitigates metabolic stress and genome damage in mammary tumorigenesis. Genes Dev. 2007 Jul 1;21(13):1621–35.

104. Mathew R, Kongara S, Beaudoin B, Karp CM, Bray K, Degenhardt K, et al. Autophagy suppresses tumor progression by limiting chromosomal instability. Genes Dev. 2007 Jun 1;21(11):1367–81.

105. Mathew R, Karp C, Beaudoin B, Vuong N, Chen G, Chen H-Y, et al. Autophagy Suppresses Tumorigenesis Through Elimination of p62. Cell. 2009 Jun 12;137(6):1062–75.

106. Moscat J, Diaz-Meco MT. p62: a versatile multitasker takes on cancer. Trends Biochem Sci. 2012 Jun;37(6):230–6.

107. Yang S, Wang X, Contino G, Liesa M, Sahin E, Ying H, et al. Pancreatic cancers require autophagy for tumor growth. Genes Dev. 2011 Apr 1;25(7):717–29.

108. Guo JY, Chen H-Y, Mathew R, Fan J, Strohecker AM, Karsli-Uzunbas G, et al. Activated Ras requires autophagy to maintain oxidative metabolism and tumorigenesis. Genes Dev. 2011 Mar 1;25(5):460–70.

109. Lock R, Kenific CM, Leidal AM, Salas E, Debnath J. Autophagy-dependent production of secreted factors facilitates oncogenic RAS-driven invasion. Cancer Discov. 2014 Apr;4(4):466–79.

110. Galluzzi L, Bravo-San Pedro JM, Vitale I, Aaronson SA, Abrams JM, Adam D, et al. Essential versus accessory aspects of cell death: recommendations of the NCCD 2015. Cell Death Differ. 2015 Jan;22(1):58–73.

111. Mantovani A, Marchesi F, Malesci A, Laghi L, Allavena P. Tumour-associated macrophages as treatment targets in oncology. Nat Rev Clin Oncol. 2017 Jul;14(7):399–416.

112. Chen P, Cescon M, Bonaldo P. Autophagy-mediated regulation of macrophages and its applications for cancer. Autophagy. 2014 Feb;10(2):192–200.

113. Xu Y, Jagannath C, Liu X-D, Sharafkhaneh A, Kolodziejska KE, Eissa NT. Toll-like receptor 4 is a sensor for autophagy associated with innate immunity. Immunity. 2007 Jul;27(1):135–44.

114. Lin H, Yan J, Wang Z, Hua F, Yu J, Sun W, et al. Loss of immunity-supported senescence enhances susceptibility to hepatocellular carcinogenesis and progression in Toll-like receptor 2-deficient mice. Hepatology. 2013;57(1):171–82.

115. Roca H, Varsos ZS, Sud S, Craig MJ, Ying C, Pienta KJ. CCL2 and Interleukin-6 Promote Survival of Human CD11b+ Peripheral Blood Mononuclear Cells and Induce M2-type Macrophage Polarization*. J Biol Chem. 2009 Dec 4;284(49):34342–54.

116. Chen W, Ma T, Shen X, Xia X, Xu G, Bai X, et al. Macrophage-induced tumor angiogenesis is regulated by the TSC2-mTOR pathway. Cancer Res. 2012 Mar 15;72(6):1363–72.

117. Trocoli A, Djavaheri-Mergny M. The complex interplay between autophagy and NF-κB signaling pathways in cancer cells. Am J Cancer Res. 2011 Apr 26;1(5):629–49.

118. Salminen A, Hyttinen JMT, Kauppinen A, Kaarniranta K. Context-Dependent Regulation of Autophagy by IKK-NF-κB Signaling: Impact on the Aging Process. Int J Cell Biol. 2012;2012:849541.

119. Nivon M, Richet E, Codogno P, Arrigo A-P, Kretz-Remy C. Autophagy activation by NFκB is essential for cell survival after heat shock. Autophagy. 2009 Aug 16;5(6):766–83.

120. Copetti T, Bertoli C, Dalla E, Demarchi F, Schneider C. p65/RelA Modulates BECN1 Transcription and Autophagy. Mol Cell Biol. 2009 May;29(10):2594–608.

121. Comb WC, Cogswell P, Sitcheran R, Baldwin AS. IKK-dependent, NF-κB-independent control of autophagic gene expression. Oncogene. 2011 Apr;30(14):1727–32.

122. Criollo A, Senovilla L, Authier H, Maiuri MC, Morselli E, Vitale I, et al. The IKK complex contributes to the induction of autophagy. EMBO J. 2010 Feb 3;29(3):619–31.

123. Djavaheri-Mergny M, Amelotti M, Mathieu J, Besançon F, Bauvy C, Souquère S, et al. NF-kappaB activation represses tumor necrosis factor-alpha-induced autophagy. J Biol Chem. 2006 Oct 13;281(41):30373–82.

124. Sarkar S, Korolchuk VI, Renna M, Imarisio S, Fleming A, Williams A, et al. Complex Inhibitory Effects of Nitric Oxide on Autophagy. Mol Cell. 2011 Jul 8;43(1):19–32.

125. Verzella D, Pescatore A, Capece D, Vecchiotti D, Ursini MV, Franzoso G, et al. Life, death, and autophagy in cancer: NF-κB turns up everywhere. Cell Death Dis. 2020 Mar 30;11(3):1–14.

126. Kim J-E, You D-J, Lee C, Ahn C, Seong JY, Hwang J-I. Suppression of NF-κB signaling by KEAP1 regulation of IKKβ activity through autophagic degradation and inhibition of phosphorylation. Cell Signal. 2010 Nov 1;22(11):1645–54.

127. Liu K, Zhang L, Zhao Q, Zhao Z, Zhi F, Qin Y, et al. SKP2 attenuates NF-κB signaling by mediating IKKβ degradation through autophagy. J Mol Cell Biol. 2018 Jun 1;10(3):205–15.

128. Qing G, Yan P, Xiao G. Hsp90 inhibition results in autophagy-mediated proteasome-independent degradation of IκB kinase (IKK). Cell Res. 2006 Nov;16(11):895–901.

129. Qing G, Yan P, Qu Z, Liu H, Xiao G. Hsp90 regulates processing of NF-kappa B2 p100 involving protection of NF-kappa B-inducing kinase (NIK) from autophagy-mediated degradation. Cell Res. 2007 Jun;17(6):520–30.

130. Jia L, Gopinathan G, Sukumar JT, Gribben JG. Blocking Autophagy Prevents Bortezomib-Induced NF-κB Activation by Reducing I-κBα Degradation in Lymphoma Cells. PLOS ONE. 2012 Feb 29;7(2):e32584.

131. Duran A, Linares JF, Galvez AS, Wikenheiser K, Flores JM, Diaz-Meco MT, et al. The signaling adaptor p62 is an important NF-kappaB mediator in tumorigenesis. Cancer Cell. 2008 Apr;13(4):343–54.

132. Schmidt-Ullrich R, Memet S, Lilienbaum A, Feuillard J, Raphael M, Israel A. NF-kappaB activity in transgenic mice: developmental regulation and tissue specificity. Development. 1996 Jul 1;122(7):2117–28.

133. Beg AA, Sha WC, Bronson RT, Ghosh S, Baltimore D. Embryonic lethality and liver degeneration in mice lacking the RelA component of NF-kappa B. Nature. 1995 Jul 13;376(6536):167–70.

134. Li Q, Lu Q, Hwang JY, Büscher D, Lee K-F, Izpisua-Belmonte JC, et al. IKK1-deficient mice exhibit abnormal development of skin and skeleton. Genes Dev. 1999 May 15;13(10):1322–8.

135. Tanaka M, Fuentes ME, Yamaguchi K, Durnin MH, Dalrymple SA, Hardy KL, et al. Embryonic lethality, liver degeneration, and impaired NF-kappa B activation in IKK-beta-deficient mice. Immunity. 1999 Apr;10(4):421–9.

136. Schmidt-Ullrich R, Aebischer T, Hülsken J, Birchmeier W, Klemm U, Scheidereit C. Requirement of NF-κB/Rel for the development of hair follicles and other epidermal appendices. Development. 2001 Oct 1;128(19):3843–53.

137. Zhang Y, Tomann P, Andl T, Gallant NM, Huelsken J, Jerchow B, et al. Reciprocal requirements for EDA/EDAR/NF-kappaB and Wnt/beta-catenin signaling pathways in hair follicle induction. Dev Cell. 2009 Jul;17(1):49–61.

138. Takase O, Yoshikawa M, Idei M, Hirahashi J, Fujita T, Takato T, et al. The role of NF-κB signaling in the maintenance of pluripotency of human induced pluripotent stem cells. PloS One. 2013;8(2):e56399.

139. Pasparakis M. Regulation of tissue homeostasis by NF-κB signalling: implications for inflammatory diseases. Nat Rev Immunol. 2009 Nov;9(11):778–88.

140. Ben-Neriah Y, Karin M. Inflammation meets cancer, with NF-κB as the matchmaker. Nat Immunol. 2011 Jul 19;12(8):715–23.

141. Yilmaz ZB, Weih DS, Sivakumar V, Weih F. RelB is required for Peyer's patch development: differential regulation of p52–RelB by lymphotoxin and TNF. EMBO J. 2003 Jan 2;22(1):121–30.

142. Pasparakis M. IKK/NF-kappaB signaling in intestinal epithelial cells controls immune homeostasis in the gut. Mucosal Immunol. 2008 Nov;1 Suppl 1:S54-57.

143. Nenci A, Becker C, Wullaert A, Gareus R, van Loo G, Danese S, et al. Epithelial NEMO links innate immunity to chronic intestinal inflammation. Nature. 2007 Mar 29;446(7135):557–61.

144. Zaph C, Troy AE, Taylor BC, Berman-Booty LD, Guild KJ, Du Y, et al. Epithelial-cell-intrinsic IKK-beta expression regulates intestinal immune homeostasis. Nature. 2007 Mar 29;446(7135):552–6.

145. Steinbrecher KA, Harmel-Laws E, Sitcheran R, Baldwin AS. Loss of epithelial RelA results in deregulated intestinal proliferative/apoptotic homeostasis and susceptibility to inflammation. J Immunol Baltim Md 1950. 2008 Feb 15;180(4):2588–99.

146. Mikuda N, Schmidt-Ullrich R, Kärgel E, Golusda L, Wolf J, Höpken UE, et al. Deficiency in IκBα in the intestinal epithelium leads to spontaneous inflammation and mediates apoptosis in the gut. J Pathol. 2020;251(2):160–74.

147. Shaked H, Hofseth LJ, Chumanevich A, Chumanevich AA, Wang J, Wang Y, et al. Chronic epithelial NF-κB activation accelerates APC loss and intestinal tumor initiation through iNOS up-regulation. Proc Natl Acad Sci U S A. 2012 Aug 28;109(35):14007–12.

148. Clevers H. The Intestinal Crypt, A Prototype Stem Cell Compartment. Cell. 2013 Jul 18;154(2):274–84.

149. Specian RD, Oliver MG. Functional biology of intestinal goblet cells. Am J Physiol. 1991 Feb;260:C183-193.

150. Sato A. Tuft cells. Anat Sci Int. 2007 Dec 1;82(4):187.

151. Clevers HC, Bevins CL. Paneth cells: maestros of the small intestinal crypts. Annu Rev Physiol. 2013;75:289–311.

152. Allaire JM, Crowley SM, Law HT, Chang S-Y, Ko H-J, Vallance BA. The Intestinal Epithelium: Central Coordinator of Mucosal Immunity. Trends Immunol. 2018 Sep 1;39(9):677–96.

153. Barker N, van Es JH, Kuipers J, Kujala P, van den Born M, Cozijnsen M, et al. Identification of stem cells in small intestine and colon by marker gene Lgr5. Nature. 2007 Oct;449(7165):1003–7.

154. Sangiorgi E, Capecchi MR. Bmi1 is expressed in vivo in intestinal stem cells. Nat Genet. 2008 Jul;40(7):915–20.

155. Montgomery RK, Carlone DL, Richmond CA, Farilla L, Kranendonk MEG, Henderson DE, et al. Mouse telomerase reverse transcriptase (mTert) expression marks slowly cycling intestinal stem cells. Proc Natl Acad Sci. 2011 Jan 4;108(1):179–84.

156. Takeda N, Jain R, LeBoeuf MR, Wang Q, Lu MM, Epstein JA. Interconversion Between Intestinal Stem Cell Populations in Distinct Niches. Science. 2011 Dec 9;334(6061):1420–4.

157. Powell AE, Wang Y, Li Y, Poulin EJ, Means AL, Washington MK, et al. The Pan-ErbB Negative Regulator Lrig1 Is an Intestinal Stem Cell Marker that Functions as a Tumor Suppressor. Cell. 2012 Mar 30;149(1):146–58.

158. Tetteh PW, Farin HF, Clevers H. Plasticity within stem cell hierarchies in mammalian epithelia. Trends Cell Biol. 2015 Feb;25(2):100–8.

159. Gehart H, Clevers H. Tales from the crypt: new insights into intestinal stem cells. Nat Rev Gastroenterol Hepatol. 2019 Jan;16(1):19–34.

160. Korinek V, Barker N, Moerer P, van Donselaar E, Huls G, Peters PJ, et al. Depletion of epithelial stem-cell compartments in the small intestine of mice lacking Tcf-4. Nat Genet. 1998 Aug;19(4):379–83.

161. Pinto D, Gregorieff A, Begthel H, Clevers H. Canonical Wnt signals are essential for homeostasis of the intestinal epithelium. Genes Dev. 2003 Jul 15;17(14):1709–13.

162. Barker N, Ridgway RA, van Es JH, van de Wetering M, Begthel H, van den Born M, et al. Crypt stem cells as the cells-of-origin of intestinal cancer. Nature. 2009 Jan;457(7229):608–11.

163. Moser AR, Luongo C, Gould KA, McNeley MK, Shoemaker AR, Dove WF. ApcMin: A mouse model for intestinal and mammary tumorigenesis. Eur J Cancer. 1995 Jul 1;31(7):1061–4.

164. Sancho R, Cremona CA, Behrens A. Stem cell and progenitor fate in the mammalian intestine: Notch and lateral inhibition in homeostasis and disease. EMBO Rep. 2015 May;16(5):571–81.

165. Sato T, Es JH van, Snippert HJ, Stange DE, Vries RG, Born M van den, et al. Paneth cells constitute the niche for Lgr5 stem cells in intestinal crypts. Nature. 2011 Jan;469(7330):415–8.

166. van Es JH, Sato T, van de Wetering M, Lyubimova A, Yee Nee AN, Gregorieff A, et al. Dll1+ secretory progenitor cells revert to stem cells upon crypt damage. Nat Cell Biol. 2012 Oct;14(10):1099–104.

167. Li HJ, Kapoor A, Giel-Moloney M, Rindi G, Leiter AB. Notch signaling differentially regulates the cell fate of early endocrine precursor cells and their maturing descendants in the mouse pancreas and intestine. Dev Biol. 2012 Nov 15;371(2):156–69.

168. Snippert HJ, Schepers AG, van Es JH, Simons BD, Clevers H. Biased competition between Lgr5 intestinal stem cells driven by oncogenic mutation induces clonal expansion. EMBO Rep. 2014 Jan;15(1):62–9.

169. Grumati P, Morozzi G, Hölper S, Mari M, Harwardt M-LI, Yan R, et al. Full length RTN3 regulates turnover of tubular endoplasmic reticulum via selective autophagy. Zhang H, editor. eLife. 2017 Jun 15;6:e25555.

170. Heuberger J, Kosel F, Qi J, Grossmann KS, Rajewsky K, Birchmeier W. Shp2/MAPK signaling controls goblet/paneth cell fate decisions in the intestine. Proc Natl Acad Sci. 2014 Mar 4;111(9):3472–7.

171. Tsai Y-H, VanDussen KL, Sawey ET, Wade AW, Kasper C, Rakshit S, et al. ADAM10 regulates Notch function in intestinal stem cells of mice. Gastroenterology. 2014 Oct;147(4):822-834.e13.

172. Al Alam D, Danopoulos S, Schall K, Sala FG, Almohazey D, Fernandez GE, et al. Fibroblast growth factor 10 alters the balance between goblet and Paneth cells in the adult mouse small intestine. Am J Physiol Gastrointest Liver Physiol. 2015 Apr 15;308(8):G678-690.

173. Zhang X, Liu S, Wang Y, Hu H, Li L, Wu Y, et al. Interleukin-22 regulates the homeostasis of the intestinal epithelium during inflammation. Int J Mol Med. 2019 Apr;43(4):1657–68.

174. Farin HF, Van Es JH, Clevers H. Redundant Sources of Wnt Regulate Intestinal Stem Cells and Promote Formation of Paneth Cells. Gastroenterology. 2012 Dec;143(6):1518-1529.e7.

175. Sato T, Clevers H. Primary mouse small intestinal epithelial cell cultures. Methods Mol Biol. 2013;945:319–28.

176. Moolenbeek C, Ruitenberg EJ. The 'Swiss roll': a simple technique for histological studies of the rodent intestine. Lab Anim. 1981 Jan;15(1):57–60.

177. Mizushima N, Yoshimori T, Levine B. Methods in Mammalian Autophagy Research. Cell. 2010 Feb 5;140(3):313–26.

178. Luo M, Zhao X, Song Y, Cheng H, Zhou R. Nuclear autophagy: An evolutionarily conserved mechanism of nuclear degradation in the cytoplasm. Autophagy. 2016;12(11):1973–83.

179. Pietrocola F, Izzo V, Niso-Santano M, Vacchelli E, Galluzzi L, Maiuri MC, et al. Regulation of autophagy by stress-responsive transcription factors. Semin Cancer Biol. 2013 Oct 1;23(5):310–22.

180. Mayr-Buro C, Schlereth E, Beuerlein K, Tenekeci U, Meier-Soelch J, Schmitz ML, et al. Single-Cell Analysis of Multiple Steps of Dynamic NF-κB Regulation in Interleukin-1α-Triggered Tumor Cells Using Proximity Ligation Assays. Cancers. 2019 Aug;11(8):1199.

181. Rogov VV, Stolz A, Ravichandran AC, Rios-Szwed DO, Suzuki H, Kniss A, et al. Structural and functional analysis of the GABARAP interaction motif (GIM). EMBO Rep. 2017 Aug 1;18(8):1382–96.

182. Jacomin A-C, Samavedam S, Promponas V, Nezis IP. iLIR database: A web resource for LIR motif-containing proteins in eukaryotes. Autophagy. 2016 Aug 2;12(10):1945–53.

183. Rozenknop A, Rogov VV, Rogova NYu, Löhr F, Güntert P, Dikic I, et al. Characterization of the Interaction of GABARAPL-1 with the LIR Motif of NBR1. J Mol Biol. 2011 Jul 15;410(3):477–87.

184. Zaffagnini G, Martens S. Mechanisms of Selective Autophagy. J Mol Biol. 2016 May 8;428:1714–24.

185. Suzuki K, Ohsumi Y. Molecular machinery of autophagosome formation in yeast, Saccharomyces cerevisiae. FEBS Lett. 2007;581(11):2156–61.

186. Fujita N, Itoh T, Omori H, Fukuda M, Noda T, Yoshimori T. The Atg16L complex specifies the site of LC3 lipidation for membrane biogenesis in autophagy. Mol Biol Cell. 2008 May;19(5):2092–100.

187. Lystad AH, Carlsson SR, de la Ballina LR, Kauffman KJ, Nag S, Yoshimori T, et al. Distinct functions of ATG16L1 isoforms in membrane binding and LC3B lipidation in autophagy-related processes. Nat Cell Biol. 2019 Mar;21(3):372–83.

188. Pankiv S, Lamark T, Bruun J-A, Øvervatn A, Bjørkøy G, Johansen T. Nucleocytoplasmic Shuttling of p62/SQSTM1 and Its Role in Recruitment of

Nuclear Polyubiquitinated Proteins to Promyelocytic Leukemia Bodies. J Biol Chem. 2010 Feb 19;285(8):5941–53.

189. Pankiv S, Clausen TH, Lamark T, Brech A, Bruun J-A, Outzen H, et al. p62/SQSTM1 Binds Directly to Atg8/LC3 to Facilitate Degradation of Ubiquitinated Protein Aggregates by Autophagy. J Biol Chem. 2007 Aug 17;282(33):24131–45.

190. Moscat J, Diaz-Meco MT, Wooten MW. Signal integration and diversification through the p62 scaffold protein. Trends Biochem Sci. 2007 Feb 1;32(2):95–100.

191. Zotti T, Scudiero I, Settembre P, Ferravante A, Mazzone P, D'Andrea L, et al. TRAF6-mediated ubiquitination of NEMO requires p62/sequestosome-1. Mol Immunol. 2014 Mar 1;58(1):27–31.

192. Wang Y, Zhang N, Zhang L, Li R, Fu W, Ma K, et al. Autophagy Regulates Chromatin Ubiquitination in DNA Damage Response through Elimination of SQSTM1/p62. Mol Cell. 2016 Jul 7;63(1):34–48.

193. Durán A, Serrano M, Leitges M, Flores JM, Picard S, Brown JP, et al. The Atypical PKC-Interacting Protein p62 Is an Important Mediator of RANK-Activated Osteoclastogenesis. Dev Cell. 2004 Feb 1;6(2):303–9.

194. Sanz L, Diaz-Meco MT, Nakano H, Moscat J. The atypical PKC-interacting protein p62 channels NF-kappaB activation by the IL-1-TRAF6 pathway. EMBO J. 2000 Apr 3;19(7):1576–86.

195. Moscat J, Diaz-Meco MT. p62 at the Crossroads of Autophagy, Apoptosis, and Cancer. Cell. 2009 Jun 12;137(6):1001–4.

196. Yang S, Qiang L, Sample A, Shah P, He Y-Y. NF-κB Signaling Activation Induced by Chloroquine Requires Autophagosome, p62 Protein, and c-Jun N-terminal Kinase (JNK) Signaling and Promotes Tumor Cell Resistance. J Biol Chem. 2017 Feb 24;292(8):3379–88.

197. Chang C-P, Su Y-C, Lee P-H, Lei H-Y. Targeting NFKB by autophagy to polarize hepatoma-associated macrophage differentiation. Autophagy. 2013 Apr 4;9(4):619–21.

198. Feng Y, Duan T, Du Y, Jin S, Wang M, Cui J, et al. LRRC25 Functions as an Inhibitor of NF-κB Signaling Pathway by Promoting p65/RelA for Autophagic Degradation. Sci Rep. 2017 Oct 18;7(1):13448.

199. Tang J, Zhan M-N, Yin Q-Q, Zhou C-X, Wang C-L, Wo L-L, et al. Impaired p65 degradation by decreased chaperone-mediated autophagy activity facilitates epithelial-to-mesenchymal transition. Oncogenesis. 2017 Oct;6(10):e387–e387.

200. Schröder B, Wrocklage C, Pan C, Jäger R, Kösters B, Schäfer H, et al. Integral and Associated Lysosomal Membrane Proteins. Traffic. 2007;8(12):1676–86.

201. Fornasiero EF, Mandad S, Wildhagen H, Alevra M, Rammner B, Keihani S, et al. Precisely measured protein lifetimes in the mouse brain reveal differences across tissues and subcellular fractions. Nat Commun. 2018 Oct 12;9(1):4230.

202. Mantovani A, Sica A, Sozzani S, Allavena P, Vecchi A, Locati M. The chemokine system in diverse forms of macrophage activation and polarization. Trends Immunol. 2004 Dec;25(12):677–86.

203. Biswas SK, Lewis CE. NF-κB as a central regulator of macrophage function in tumors. J Leukoc Biol. 2010;88(5):877–84.

204. Chang C-P, Su Y-C, Hu C-W, Lei H-Y. TLR2-dependent selective autophagy regulates NF-κB lysosomal degradation in hepatoma-derived M2 macrophage differentiation. Cell Death Differ. 2013 Mar;20(3):515–23.

205. Bryant CE, Spring DR, Gangloff M, Gay NJ. The molecular basis of the host response to lipopolysaccharide. Nat Rev Microbiol. 2010 Jan;8(1):8–14.

206. Sakai J, Cammarota E, Wright JA, Cicuta P, Gottschalk RA, Li N, et al. Lipopolysaccharide-induced NF-κB nuclear translocation is primarily dependent on MyD88, but TNFα expression requires TRIF and MyD88. Sci Rep. 2017 May 3;7:1428.

207. Kudo N, Wolff B, Sekimoto T, Schreiner EP, Yoneda Y, Yanagida M, et al. Leptomycin B Inhibition of Signal-Mediated Nuclear Export by Direct Binding to CRM1. Exp Cell Res. 1998 Aug;242(2):540–7.

208. Taniguchi K, Karin M. NF-κB, inflammation, immunity and cancer: coming of age. Nat Rev Immunol. 2018 May;18(5):309–24.

209. Vlantis K, Wullaert A, Sasaki Y, Schmidt-Supprian M, Rajewsky K, Roskams T, et al. Constitutive IKK2 activation in intestinal epithelial cells induces intestinal tumors in mice. J Clin Invest. 2011 Jul 1;121(7):2781–93.

210. Tomann P, Paus R, Millar SE, Scheidereit C, Schmidt-Ullrich R. Lhx2 is a direct NF-κB target gene that promotes primary hair follicle placode down-growth. Development. 2016 May 1;143(9):1512–22.

211. Brischetto C, Krieger K, Klotz C, Krahn I, Kunz S, Kolesnichenko M, et al. NF-κB determines Paneth versus goblet cell fate decision in the small intestine. Development. 2021 Nov 9;148(21):dev199683.

212. van der Flier LG, Haegebarth A, Stange DE, van de Wetering M, Clevers H. OLFM4 Is a Robust Marker for Stem Cells in Human Intestine and Marks a Subset of Colorectal Cancer Cells. Gastroenterology. 2009 Jul;137(1):15–7.

213. Karin M, Lin A. NF-κB at the crossroads of life and death. Nat Immunol. 2002 Mar;3(3):221–7.

214. Vlantis K, Wullaert A, Polykratis A, Kondylis V, Dannappel M, Schwarzer R, et al. NEMO Prevents RIP Kinase 1-Mediated Epithelial Cell Death and Chronic Intestinal Inflammation by NF-κB-Dependent and -Independent Functions. Immunity. 2016 Mar 15;44(3):553–67.

215. STEEDMAN HF. Alcian Blue 8GS: A New Stain for Mucin. J Cell Sci. 1950 Dicembre;s3-91(16):477–9.

216. Pellegrinet L, Rodilla V, Liu Z, Chen S, Koch U, Espinosa L, et al. Dll1- and Dll4-mediated Notch signaling is required for homeostasis of intestinal stem cells. Gastroenterology. 2011 Apr;140(4):1230-1240.e7.

217. Garg P, Ravi A, Patel NR, Roman J, Gewirtz AT, Merlin D, et al. Matrix metalloproteinase-9 regulates MUC-2 expression through its effect on goblet cell differentiation. Gastroenterology. 2007 May;132(5):1877–89.

218. Lueschow SR, McElroy SJ. The Paneth Cell: The Curator and Defender of the Immature Small Intestine. Front Immunol. 2020;11:587.

219. Gregorieff A, Stange DE, Kujala P, Begthel H, van den Born M, Korving J, et al. The ets-domain transcription factor Spdef promotes maturation of goblet and paneth cells in the intestinal epithelium. Gastroenterology. 2009 Oct;137(4):1333-1345.e1-3.

220. Shroyer NF, Wallis D, Venken KJT, Bellen HJ, Zoghbi HY. Gfi1 functions downstream of Math1 to control intestinal secretory cell subtype allocation and differentiation. Genes Dev. 2005 Oct 15;19(20):2412–7.

221. Stamataki D, Holder M, Hodgetts C, Jeffery R, Nye E, Spencer-Dene B, et al. Delta1 Expression, Cell Cycle Exit, and Commitment to a Specific Secretory Fate Coincide within a Few Hours in the Mouse Intestinal Stem Cell System. PLOS ONE. 2011 set;6(9):e24484.

222. Shimizu H, Okamoto R, Ito G, Fujii S, Nakata T, Suzuki K, et al. Distinct expression patterns of Notch ligands, Dll1 and Dll4, in normal and inflamed mice intestine. PeerJ. 2014 May 1;2:e370.

223. Noah TK, Kazanjian A, Whitsett J, Shroyer NF. SAM pointed domain ETS factor (SPDEF) regulates terminal differentiation and maturation of intestinal goblet cells. Exp Cell Res. 2010 Feb 1;316(3):452–65.

224. Bry L, Falk P, Huttner K, Ouellette A, Midtvedt T, Gordon JI. Paneth Cell Differentiation in the Developing Intestine of Normal and Transgenic Mice. Proc Natl Acad Sci U S A. 1994;91(22):10335–9.

225. Garabedian EM, Roberts LJJ, McNevin MS, Gordon JI. Examining the Role of Paneth Cells in the Small Intestine by Lineage Ablation in Transgenic Mice *. J Biol Chem. 1997 Sep 19;272(38):23729–40.

226. Mah AT, Yan KS, Kuo CJ. Wnt pathway regulation of intestinal stem cells. J Physiol. 2016 Sep 1;594(17):4837–47.

227. Kim HS, Lee C, Kim WH, Maeng YH, Jang BG. Expression profile of intestinal stem cell markers in colitis-associated carcinogenesis. Sci Rep. 2017 Jul 26;7(1):6533.

228. Shoshkes-Carmel M, Wang YJ, Wangensteen KJ, Tóth B, Kondo A, Massassa EE, et al. Subepithelial telocytes are an important source of Wnts that supports intestinal crypts. Nature. 2018 May;557(7704):242–6.

229. Aoki R, Shoshkes-Carmel M, Gao N, Shin S, May CL, Golson ML, et al. Foxl1-expressing mesenchymal cells constitute the intestinal stem cell niche. Cell Mol Gastroenterol Hepatol. 2016 Feb 1;2(2):175–88.

230. Sato T, Vries RG, Snippert HJ, Wetering M van de, Barker N, Stange DE, et al. Single Lgr5 stem cells build crypt-villus structures in vitro without a mesenchymal niche. Nature. 2009 May;459(7244):262–5.

231. Merenda A, Fenderico N, Maurice MM. Wnt Signaling in 3D: Recent Advances in the Applications of Intestinal Organoids. Trends Cell Biol. 2020 Jan 1;30(1):60–73.

232. Zhao X, Ma L, Dai L, Zuo D, Li X, Zhu H, et al. TNF-α promotes the malignant transformation of intestinal stem cells through the NF-κB and Wnt/β-catenin signaling pathways. Oncol Rep. 2020 Aug;44(2):577–88.

233. Schwitalla S, Fingerle AA, Cammareri P, Nebelsiek T, Göktuna SI, Ziegler PK, et al. Intestinal Tumorigenesis Initiated by Dedifferentiation and Acquisition of Stem-Cell-like Properties. Cell. 2013 Jan 17;152(1):25–38.

234. Berger E, Rath E, Yuan D, Waldschmitt N, Khaloian S, Allgäuer M, et al. Mitochondrial function controls intestinal epithelial stemness and proliferation. Nat Commun. 2016 Oct 27;7(1):13171.

235. Krappmann D, Wegener E, Sunami Y, Esen M, Thiel A, Mordmuller B, et al. The IkappaB kinase complex and NF-kappaB act as master regulators of lipopolysaccharide-induced gene expression and control subordinate activation of AP-1. Mol Cell Biol. 2004 Jul;24(14):6488–500.

236. Blache P, van de Wetering M, Duluc I, Domon C, Berta P, Freund J-N, et al. SOX9 is an intestine crypt transcription factor, is regulated by the Wnt pathway, and represses the CDX2 and MUC2 genes. J Cell Biol. 2004 Jul 5;166(1):37–47.

237. Bastide P, Darido C, Pannequin J, Kist R, Robine S, Marty-Double C, et al. Sox9 regulates cell proliferation and is required for Paneth cell differentiation in the intestinal epithelium. J Cell Biol. 2007 Aug 13;178(4):635–48.

238. Xiao G. Autophagy and NF-κB fight for fate. Cytokine Growth Factor Rev. 2007;18(3–4):233–43.

239. Peng X, Wang Y, Li H, Fan J, Shen J, Yu X, et al. ATG5-mediated autophagy suppresses NF-κB signaling to limit epithelial inflammatory response to kidney injury. Cell Death Dis. 2019 Mar 15;10(4).

240. Fujishima Y, Nishiumi S, Masuda A, Inoue J, Nguyen NMT, Irino Y, et al. Autophagy in the intestinal epithelium reduces endotoxin-induced inflammatory responses by inhibiting NF-κB activation. Arch Biochem Biophys. 2011 Feb 15;506(2):223–35.

241. Dou Z, Xu C, Donahue G, Shimi T, Pan J-A, Zhu J, et al. Autophagy mediates degradation of nuclear lamina. Nature. 2015 Nov 5;527(7576):105–9.

242. Kraft LJ, Manral P, Dowler J, Kenworthy AK. Nuclear LC3 associates with slowly diffusing complexes that survey the nucleolus. Traffic. 2016 Apr;17(4):369–99.

243. Shim MS, Nettesheim A, Hirt J, Liton PB. The autophagic protein LC3 translocates to the nucleus and localizes in the nucleolus associated to NUFIP1 in response to cyclic mechanical stress. Autophagy. 2020 Jul;16(7):1248–61.

244. Huang R, Xu Y, Wan W, Shou X, Qian J, You Z, et al. Deacetylation of nuclear LC3 drives autophagy initiation under starvation. Mol Cell. 2015 Feb 5;57(3):456–66.

245. Simon HU, Yousefi S, Schmid I, Friis R. ATG5 can regulate p53 expression and activation. Cell Death Dis. 2014 Jul;5(7):e1339.

246. Lee IH, Kawai Y, Fergusson MM, Rovira II, Bishop AJR, Motoyama N, et al. Atg7 Modulates p53 Activity to Regulate Cell Cycle and Survival During Metabolic Stress. Science. 2012 Apr 13;336(6078):225–8.

247. Peng X, Wang Y, Li H, Fan J, Shen J, Yu X, et al. ATG5-mediated autophagy suppresses NF-κB signaling to limit epithelial inflammatory response to kidney injury. Cell Death Dis. 2019 Mar 15;10(4):1–16.

248. Lobb IT, Morin P, Martin K, Thoms HC, Wills JC, Lleshi X, et al. A Role for the Autophagic Receptor, SQSTM1/p62, in Trafficking NF-κB/RelA to Nucleolar Aggresomes. Mol Cancer Res MCR. 2021 Feb;19(2):274–87.

249. Stark LA, Dunlop MG. Nucleolar Sequestration of RelA (p65) Regulates NF-κB-Driven Transcription and Apoptosis. Mol Cell Biol. 2005 Jul;25(14):5985–6004.

250. Tanaka T, Grusby MJ, Kaisho T. PDLIM2-mediated termination of transcription factor NF-kappaB activation by intranuclear sequestration and degradation of the p65 subunit. Nat Immunol. 2007 Jun;8(6):584–91.

251. Maine GN, Mao X, Komarck CM, Burstein E. COMMD1 promotes the ubiquitination of NF-kappaB subunits through a cullin-containing ubiquitin ligase. EMBO J. 2007 Jan 24;26(2):436–47.

252. Myeku N, Figueiredo-Pereira ME. Dynamics of the Degradation of Ubiquitinated Proteins by Proteasomes and Autophagy: ASSOCIATION WITH SEQUESTOSOME 1/p62 *. J Biol Chem. 2011 Jun 24;286(25):22426–40.

253. Seibenhener ML, Babu JR, Geetha T, Wong HC, Krishna NR, Wooten MW. Sequestosome 1/p62 is a polyubiquitin chain binding protein involved in ubiquitin proteasome degradation. Mol Cell Biol. 2004 Sep;24(18):8055–68.

254. Liu WJ, Ye L, Huang WF, Guo LJ, Xu ZG, Wu HL, et al. p62 links the autophagy pathway and the ubiqutin–proteasome system upon ubiquitinated protein degradation. Cell Mol Biol Lett. 2016 Dec 13;21(1):29.

255. Jodo A, Shibazaki A, Onuma A, Kaisho T, Tanaka T. PDLIM7 Synergizes With PDLIM2 and p62/Sqstm1 to Inhibit Inflammatory Signaling by Promoting Degradation of the p65 Subunit of NF-κB. Front Immunol. 2020;11:1559.

256. Webb JL, Ravikumar B, Atkins J, Skepper JN, Rubinsztein DC. α-Synuclein Is Degraded by Both Autophagy and the Proteasome *. J Biol Chem. 2003 Jul 4;278(27):25009–13.

257. Isakson P, Bjørås M, Bøe SO, Simonsen A. Autophagy contributes to therapy-induced degradation of the PML/RARA oncoprotein. Blood. 2010 Sep 30;116(13):2324–31.

258. Kwon YT, Ciechanover A. The Ubiquitin Code in the Ubiquitin-Proteasome System and Autophagy. Trends Biochem Sci. 2017 Nov;42(11):873–86.

259. Hochrainer K, Racchumi G, Zhang S, Iadecola C, Anrather J. Monoubiquitination of nuclear RelA negatively regulates NF-κB activity independent of proteasomal degradation. Cell Mol Life Sci CMLS. 2012 Jun;69(12):2057–73.

260. Chen M, Zhao Z, Meng Q, Liang P, Su Z, Wu Y, et al. TRIM14 Promotes Noncanonical NF-κB Activation by Modulating p100/p52 Stability via Selective Autophagy. Adv Sci. 2020;7(1):1901261.

261. Levine B, Mizushima N, Virgin HW. Autophagy in immunity and inflammation. Nature. 2011;469(7330):323–35.

262. Yin H, Wu H, Chen Y, Zhang J, Zheng M, Chen G, et al. The Therapeutic and Pathogenic Role of Autophagy in Autoimmune Diseases. Front Immunol. 2018 Jul 31;9:1512.

263. Shao Y, Chen F, Chen Y, Zhang W, Lin Y, Cai Y, et al. Association between genetic polymorphisms in the autophagy-related 5 gene promoter and the risk of sepsis. Sci Rep. 2017 Aug 24;7(1):9399.

264. Rioux JD, Xavier RJ, Taylor KD, Silverberg MS, Goyette P, Huett A, et al. Genome-wide association study identifies new susceptibility loci for Crohn disease and implicates autophagy in disease pathogenesis. Nat Genet. 2007 May;39(5):596–604.

265. Cabrera S, Fernández AF, Mariño G, Aguirre A, Suárez MF, Español Y, et al. ATG4B/autophagin-1 regulates intestinal homeostasis and protects mice from experimental colitis. Autophagy. 2013 Aug;9(8):1188–200.

266. Tsuboi K, Nishitani M, Takakura A, Imai Y, Komatsu M, Kawashima H. Autophagy Protects against Colitis by the Maintenance of Normal Gut Microflora and Secretion of Mucus. J Biol Chem. 2015 Aug 14;290(33):20511–26.

267. Zhang H, Zheng L, McGovern DPB, Hamill AM, Ichikawa R, Kanazawa Y, et al. Myeloid ATG16L1 Facilitates Host-Bacteria Interactions in Maintaining Intestinal Homeostasis. J Immunol. 2017 Mar 1;198(5):2133–46.

268. Ye Y, Lin P, Zhang W, Tan S, Zhou X, Li R, et al. DNA Repair Interacts with Autophagy To Regulate Inflammatory Responses to Pulmonary Hyperoxia. J Immunol. 2017 Apr 1;198(7):2844–53.

269. Massey DCO, Bredin F, Parkes M. Use of sirolimus (rapamycin) to treat refractory Crohn's disease. Gut. 2008 Sep;57(9):1294–6.

270. Atreya I, Atreya R, Neurath MF. NF-kappaB in inflammatory bowel disease. J Intern Med. 2008 Jun;263(6):591–6.

271. Neurath MF, Pettersson S, Meyer zum Büschenfelde KH, Strober W. Local administration of antisense phosphorothioate oligonucleotides to the p65 subunit of NF-kappa B abrogates established experimental colitis in mice. Nat Med. 1996 Sep;2(9):998–1004.

272. Hong SN, Park C, Park SJ, Lee CK, Ye BD, Kim YS, et al. Deep resequencing of 131 Crohn's disease associated genes in pooled DNA confirmed three reported variants and identified eight novel variants. Gut. 2016 May;65(5):788–96.

273. Klein W, Tromm A, Folwaczny C, Hagedorn M, Duerig N, Epplen JT, et al. A polymorphism of the NFKBIA gene is associated with Crohn's disease patients lacking a predisposing allele of the CARD15 gene. Int J Colorectal Dis. 2004 Mar;19(2):153–6.

274. Matsuzawa-Ishimoto Y, Shono Y, Gomez LE, Hubbard-Lucey VM, Cammer M, Neil J, et al. Autophagy protein ATG16L1 prevents necroptosis in the intestinal epithelium. J Exp Med. 2017 Oct 31;214(12):3687–705.

275. Visekruna A, Joeris T, Seidel D, Kroesen A, Loddenkemper C, Zeitz M, et al. Proteasome-mediated degradation of IkappaBalpha and processing of p105 in Crohn disease and ulcerative colitis. J Clin Invest. 2006 Dec;116(12):3195–203.

276. Haq S, Grondin J, Banskota S, Khan WI. Autophagy: roles in intestinal mucosal homeostasis and inflammation. J Biomed Sci. 2019 Dec;26(1):19.

277. Gerondakis S, Grossmann M, Nakamura Y, Pohl T, Grumont R. Genetic approaches in mice to understand Rel/NF-kappaB and IkappaB function: transgenics and knockouts. Oncogene. 1999 Nov 22;18(49):6888–95.

278. Rebholz B, Haase I, Eckelt B, Paxian S, Flaig MJ, Ghoreschi K, et al. Crosstalk between keratinocytes and adaptive immune cells in an IkappaBalpha protein-mediated inflammatory disease of the skin. Immunity. 2007 Aug;27(2):296–307.

279. Stratis A, Pasparakis M, Markur D, Knaup R, Pofahl R, Metzger D, et al. Localized inflammatory skin disease following inducible ablation of I kappa B kinase 2 in murine epidermis. J Invest Dermatol. 2006 Mar;126(3):614–20.

280. Stratis A, Pasparakis M, Rupec RA, Markur D, Hartmann K, Scharffetter-Kochanek K, et al. Pathogenic role for skin macrophages in a mouse model of keratinocyte-induced psoriasis-like skin inflammation. J Clin Invest. 2006 Aug;116(8):2094–104.

281. Mikuda N, Kolesnichenko M, Beaudette P, Popp O, Uyar B, Sun W, et al. The IκB kinase complex is a regulator of mRNA stability. EMBO J. 2018 Dec 14;37(24):e98658.

282. Durand A, Donahue B, Peignon G, Letourneur F, Cagnard N, Slomianny C, et al. Functional intestinal stem cells after Paneth cell ablation induced by the loss of transcription factor Math1 (Atoh1). Proc Natl Acad Sci. 2012 Jun 5;109(23):8965–70.

283. Mori-Akiyama Y, van den Born M, van Es JH, Hamilton SR, Adams HP, Zhang J, et al. SOX9 is required for the differentiation of paneth cells in the intestinal epithelium. Gastroenterology. 2007 Aug;133(2):539–46.

284. Kim T-H, Escudero S, Shivdasani RA. Intact function of Lgr5 receptor-expressing intestinal stem cells in the absence of Paneth cells. Proc Natl Acad Sci U S A. 2012 Mar 6;109(10):3932–7.

285. Buske P, Galle J, Barker N, Aust G, Clevers H, Loeffler M. A Comprehensive Model of the Spatio-Temporal Stem Cell and Tissue Organisation in the Intestinal Crypt. PLOS Comput Biol. 2011 Jen;7(1):e1001045.

286. Xu M, Horrell J, Snitow M, Cui J, Gochnauer H, Syrett CM, et al. WNT10A mutation causes ectodermal dysplasia by impairing progenitor cell proliferation and KLF4-mediated differentiation. Nat Commun. 2017 Jun 7;8:15397.

287. Krieger K, Millar SE, Mikuda N, Krahn I, Kloepper JE, Bertolini M, et al. NF-κB Participates in Mouse Hair Cycle Control and Plays Distinct Roles in the Various Pelage Hair Follicle Types. J Invest Dermatol. 2018 Feb;138(2):256–64.

288. van Es JH, Jay P, Gregorieff A, van Gijn ME, Jonkheer S, Hatzis P, et al. Wnt signalling induces maturation of Paneth cells in intestinal crypts. Nat Cell Biol. 2005 Apr;7(4):381–6.

289. Andreu P, Colnot S, Godard C, Gad S, Chafey P, Niwa-Kawakita M, et al. Crypt-restricted proliferation and commitment to the Paneth cell lineage following Apc loss in the mouse intestine. Development. 2005 Mar 15;132(6):1443–51.

290. van Es JH, Sato T, van de Wetering M, Lyubimova A, Gregorieff A, Zeinstra L, et al. Dll1 marks early secretory progenitors in gut crypts that can revert to stem cells upon tissue damage. Nat Cell Biol. 2012 Oct;14(10):1099–104.

291. van Es JH, van Gijn ME, Riccio O, van den Born M, Vooijs M, Begthel H, et al. Notch/γ-secretase inhibition turns proliferative cells in intestinal crypts and adenomas into goblet cells. Nature. 2005 Jun;435(7044):959–63.

292. Valenta T, Degirmenci B, Moor AE, Herr P, Zimmerli D, Moor MB, et al. Wnt Ligands Secreted by Subepithelial Mesenchymal Cells Are Essential for the Survival of Intestinal Stem Cells and Gut Homeostasis. Cell Rep. 2016 May 3;15(5):911–8.

293. Adaimy L, Chouery E, Mégarbané H, Mroueh S, Delague V, Nicolas E, et al. Mutation in WNT10A Is Associated with an Autosomal Recessive Ectodermal Dysplasia: The Odonto-onycho-dermal Dysplasia. Am J Hum Genet. 2007 Oct;81(4):821–8.

294. Es JH van, Wiebrands K, López-Iglesias C, Wetering M van de, Zeinstra L, Born M van den, et al. Enteroendocrine and tuft cells support Lgr5 stem cells on Paneth cell depletion. Proc Natl Acad Sci. 2019 Dec 26;116(52):26599–605.

295. VanDussen KL, Carulli AJ, Keeley TM, Patel SR, Puthoff BJ, Magness ST, et al. Notch signaling modulates proliferation and differentiation of intestinal crypt base columnar stem cells. Development. 2012 Feb 1;139(3):488–97.

296. Kumar A, Eby MT, Sinha S, Jasmin A, Chaudhary PM. The ectodermal dysplasia receptor activates the nuclear factor-kappaB, JNK, and cell death pathways and binds to ectodysplasin A. J Biol Chem. 2001 Jan 26;276(4):2668–77.

297. Schmidt-Ullrich R, Tobin DJ, Lenhard D, Schneider P, Paus R, Scheidereit C. NF-κB transmits Eda A1/EdaR signalling to activate Shh and cyclin D1 expression, and controls post-initiation hair placode down growth. Development. 2006 Mar 15;133(6):1045–57.

298. Fafilek B, Krausova M, Vojtechova M, Pospichalova V, Tumova L, Sloncova E, et al. Troy, a Tumor Necrosis Factor Receptor Family Member, Interacts With Lgr5 to Inhibit Wnt Signaling in Intestinal Stem Cells. Gastroenterology. 2013 Feb 1;144(2):381–91.

299. Lai S, Cheng R, Gao D, Chen Y-G, Deng C. LGR5 constitutively activates NF-κB signaling to regulate the growth of intestinal crypts. FASEB J. 2020;34(11):15605–20.

9. ABBREVIATIONS

AMPK	AMP-activated protein kinase
Ang II	angiotensin II
ANK	ankyrin
Ascl2	Achaete-scute family bHLH transcription factor 2
ATG16L	Autophagy Related 16 Like 1
Atoh1/Math1	atonal homolog 1
bHLH	Basic helix-loop-helix
BNIP3	BCL-2 interacting protein 3
BrdU	5-Bromo-2'-deoxyuridine
CAC	colitis-associated colorectal cancer
CBC	Crypt Base Columnar
CCL20	C-C Motif Chemokine Ligand 20
Ccnd1	Cyclin D1
ChromoA	Chromogranin A
CHX	Cycloheximide
CK2	Casein kinase 2
CMA	chaperon-mediated autophagy
CQ	chloroquine
Cxcl20	C-X-C Motif Chemokine Ligand 12

DCs	dendritic cells
DD	death domain
DDR	DNA damage response
DiD	dimerization domain
Dll1	Delta-like 1
Dll4	Delta-like 4
DSB	DNA double-strand breaks
DSS	dextran sulfate sodium
Eda-A1	Ectodysplasin A1
Edn1	Endothelin-1
EdU	5-ethynyl-2′-deoxyuridine
EEC	enteroendocrine cells
EGF	epidermal growth factor
Ephb3	Ephrin type B Receptor 3
ER	endoplasmic reticulum
FIP200	FAK family kinase interacting protein of 200 kDa
FL	full length
GALT	gut associated lymphoid tissue
Gfi1	Growth factor independent-1
GFP	green fluorescent protein
Gob5/Clca1	Chloride channel accessory 1
GRR	glycine-rich region
HCC	hepatocellular carcinoma
Hes1	hairy and enhancer-of-split 1
Hopx	homeobox protein
Hsp90	heat shock protein 90
IBD	inflammatory bowel disease
Icam1	Intercellular Adhesion Molecule 1
IEC	intestinal epithelial cell
IHC	immunohistochemistry
IKK	IκB kinase
IL-1	interleukin 1
IL-1R	IL-1 receptor
IL1α	Interleukin 1 Alpha
IL1β	Interleukin 1 Beta

IL6	Interleukin 6
IL8	Interleukin 8
iNOS	nitric oxide
IR	ionizing radiation
IRAK	IL-1 receptor-associated kinase
ISC	intestinal stem cells
ISH	In situ hybridization
KEAP1	Kelch-like ECH-associated protein 1
Klf4	Krüppel-like factor 4
KO	knock-out
LAMP1	lysosome-associated membrane glycoprotein
LC3	Microtubule-associated protein light chain 3
LDHA	Lactate Dehydrogenase A
Lgr1	Leucine-rich repeat-containing G protein-coupled receptor 1
Lgr5	Leucine-Rich Repeat Containing G Protein-Coupled Receptor 5
LIR	LC3 Interacting Region
LMB	Leptomycin B
LMNB1	lamin B1
LPS	lipopolysaccharide
LUBAC	linear ubiquitin chain assembly
LZ	leucine zipper
Msi1	Musashi RNA Binding Protein 1
mTORC1	mammalian target of rapamycin complex 1
Muc2	mucin-2
NEM	N-ethylmaleimide
NF-κB	nuclear factor-κB
NGF	nerve growth factor
NIK	NF-kappa B-inducing kinase
NLS	nuclear localization signal
NTD	amino-terminal domain
Olfm4	Olfactomedin 4
OMM	outer mitochondrial membrane
OPTN	optineurin
P1	postnatal day 1
P15	postnatal day 15

P9	postnatal day 8
PAR	poly-ADP-ribosylation
PARP1	Poly(ADP-Ribose) Polymerase 1
PAS	phagophore assembly site
PB1	Phox-BEM1 domain
PDB	Paget's disease of the bone
PE	phosphatidylethanolamine
PIASy	protein inhibitor of activated STATy
PINK1	PTEN-induced kinase 1
PKAc	protein kinase A
PLA	Proximity Ligation Assay
Prom1	Prominin 1
PRR	pattern recognition receptor
PSI	proximal small intestine
PTAB	phloxine/tartrazine /Alcian Blue
PTEN	phosphatase and tensin homolog
PTM	post-translational modification
RANKL	RANK ligand
RHD	Rel homology domain
RIP1	receptor-interacting protein 1
RNI	reactive nitrogen intermediates
ROS	reactive oxygen species
SI	small intestinal
SKP2	S-phase kinase-associated protein 2
Smoc2	SPARC Related Modular Calcium Binding 2
Sox9	SRY-box containing gene 9
Spdef	Sam-Pointed Domain Ets Transcription Factor
SQSTM1	Sequestosome 1
SST	Somatostatin
SUMO	small ubiquitin modifier
TA	transit-amplifying
TAB	TAK1 binding protein
TAD	transactivation domain
TAK1	TGF-β-activated kinase 1
TAMs	tumor-associated macrophages

TEM	transmission electron microscopy
Tert	Telomerase Reverse Transcriptase
TGFα	transforming growth factor-α
TIRAP	Toll/interleukin-1 (IL-1) receptor adaptor protein
TLR4	Toll-like receptor 4
TLRs	toll-like receptors
TNFR	TNF receptor
Tnfrsf19	TNF Receptor Superfamily Member 19
TNFα	tumor necrosis factor-alpha
TRAF6	TNF Receptor Associated Factor 6
TRAM	TRIF-related adaptor molecule
UBA	Ubiquitin-associated domain
UBD	ubiquitin-binding domain
ULK	UNC51-like kinase
UT	unstimulated
UUO	unilateral ureteric obstruction
UV	ultraviolet
VPS15	vacuolar protein sorting 15
WB	Western blot
Wnt10a	Wnt Family Member 10A
WT	wild-type

10. APPENDIX

10.1. Eidesstattliche Erklärung zur Selbstständigkeit

Hiermit erkläre ich, dass ich die vorliegende Arbeit selbstständig und nur unter der Verwendung der angegebenen Quellen und Hilfsmittel angefertigt habe. Alle Materialien oder Zuarbeiten, die ich von Dritten erhalten habe, sind als solche gekennzeichnet. Ich versichere, dass ich mich nicht anderweitig um einen Doktorgrad beworben habe oder einen entsprechenden Doktortitel bereits besitze. Die Promotionsordnung der MathematischNaturwissenschaftlichen Fakultät I der Humboldt-Universität zu Berlin habe ich gelesen und verstanden.

Ort, Datum Unterschrift

10.2. Acknowledgements

First of all, I would like to thank Claus for giving me the chance to be part of his laboratory. Thank you for believing in me and teaching me how to become a strong independent scientist. I would like to also thank you for all the amazing opportunities that you gave me including being part of SignGene, going to international conferences, and the additional training obtained in Frankfurt. You always support my ideas and push me to never give up.

I would like to thank Yinon Ben-Neriah for agreeing to be my SignGene co-mentor, to welcome me to his laboratory in Jerusalem, and for his valuable suggestions on my research project.

Special thanks to Thomas Sommer for being my University Supervisor. Thank you for the support received during my Ph.D. and for pushing me to believe always in my dreams.

I would like to thank Michael Naumann, Achim Leutz, and Marc Erhardt for agreeing to be my Ph.D. thesis committee members. Thanks very much also to Gaetano Gargiulo as a member of my committee meeting for his valuable comments and insights.

Thank you very much to Ruth Schmidt-Ullrich for introducing me to the “mouse world”. Thank you for giving me the chance to work together on such a challenging project, to support me, and for listening to me. Thanks for the amazing time spent together also outside of the lab. I will always be grateful to have met you during this journey.

Thanks to all my previous and current lab colleagues: Ahmet, Patrick, Inbal, Marina, Linda, Nadine, Michael, Hinz, and Barto. Everyone gave me the chance to improve myself as a valuable team member. Special thanks to Eva, Inge, and Sabine: you are the most brilliant and lovely soul of this lab. You made me feel at home and never alone. Thank you for all!

Thanks to all the MDC and SignGene Ph.D. and Scientist members: You are the proof that Science is a collaborative effort. I will always be grateful for all the help I received during my Ph.D., especially from Gargiulo and DiVirgilio’s labs. Thanks to Christian Klotz for teaching me everything about organoids.

Daniela Keyner (tua piccola cipolla), Sandra Krull and Hanna Singer, thank you for helping me every time I need and for your constant support.

I would like to thank Paolo Grumati to welcome me to Dikic's lab and for sharing insights, tips, and tools. You have been an inspiration to me when I needed the most.

Thank you to all my friends from all around the world. Thank you for all the craziness, enthusiasm, joy, and love (HippieJohnnys, NYE, trote e trotine). Special thanks to my "The George" family: Jules and Matteo, you rescued me, giving me the most beautiful flatmate experience I could ever imagine. Thanks DiFra and Ruzzi for introducing me to the real life in Berlin (concerts, exhibitions, clubs, etc) and for the always Italian Aperitivo together. Thanks to Alexa for your true love and the amazing time spent together.

Thank you Patrick, my forever LOVE. I couldn't have made it to the end without you. I will always be greatful for your help, suggestions and discussions.

Last but not the least, thank you to my FAMILY. Grazie Mammina per aver creduto sempre in me e per avermi sempre spinto ad affrontare con coraggio qualsiasi opportunita´della vita. Grazie Sissy e Mario per essermi stati vicini e per fare sempre il tifo per me. Vi amo infinitamente.